UNIVERSITAT POLITÈCNICA
DE CATALUNYA
BARCELONATECH

Design and optimization of metro-access networks supporting 5g services

Samael Sarmiento Hernández

Universitat Politècnica de Catalunya
(UPC)

Signal Theory and Communications Department (TSC)

Optical Communications Group (GCO)

Ph. D. Thesis

DESIGN AND OPTIMIZATION OF METRO-ACCESS NETWORKS SUPPORTING 5G SERVICES

Author:

Samael Sarmiento Hernández

Advisors:

José Antonio Lázaro Villa

Salvatore Spadaro

2 February 2020

ISBN:

Reg:

Optical Communications Group (GCO)

Universitat Politècnica de Catalunya (UPC)

C/ Jordi Girona, 1-3

Campus Nord, D4-S107

08034 Barcelona, Spain

UNIVERSITAT POLITÈCNICA DE CATALUNYA
BARCELONATECH
Escola de Doctorat

Acta de qualificació de tesi doctoral

Curs acadèmic:

Nom i cognoms

Programa de doctorat

Unitat estructural responsable del programa

Resolució del Tribunal

Reunit el Tribunal designat a l'efecte, el doctorand / la doctoranda exposa el tema de la seva tesi doctoral titulada _____

_____.

Acabada la lectura i després de donar resposta a les qüestions formulades pels membres titulars del tribunal, aquest atorga la qualificació:

☐ NO APTE ☐ APROVAT ☐ NOTABLE ☐ EXCEL·LENT

(Nom, cognoms i signatura) President/a	(Nom, cognoms i signatura) Secretari/ària

(Nom, cognoms i signatura) Vocal	(Nom, cognoms i signatura) Vocal	(Nom, cognoms i signatura) Vocal

_____, _____ d'/de _____ de _____

El resultat de l'escrutini dels vots emesos pels membres titulars del tribunal, efectuat per l'Escola de Doctorat, a instància de la Comissió de Doctorat de la UPC, atorga la MENCIÓ CUM LAUDE:

☐ SÍ ☐ NO

(Nom, cognoms i signatura) President de la Comissió Permanent de l'Escola de Doctorat	(Nom, cognoms i signatura) Secretari de la Comissió Permanent de l'Escola de Doctorat

Barcelona, _____ d'/de _____ de _____

"The ultimate measure of a man is not where he stands in moments of comfort and convenience, but where he stands at times of challenge and controversy."

—Martin Luther King

Contents

List of Figures

List of Tables

Abstract

The Internet data traffic constant growth caused by the popularization of cloud services, mobile and social networks, demand changes to the networks in order to enable scalable growth in traffic volume, while supporting a high level of dynamic connectivity, full flexibility, reduced end-to-end latency and increased energy-efficiency. Cost-effective and energy efficient solutions for flexible network subsystems are also required to provide future sustainable networks. This thesis is focused on pushing the current state of the art of metro and access networks to provide a new flexible infrastructure supporting 5G services. To achieve that objective, it is presented cost-effective and flexible all-optical commutation nodes—reconfigurable add/drop multiplexer (ROADM) and optical cross-connect (OXC)—and transceivers that can be remotely managed by a software defined networking (SDN) controller, able to satisfy the requirements of future converged metro-access networks. Network simulations are conducted to prove the capabilities of presented solutions as network elements for different traffic conditions. Benefits of proposed solutions are the usage of off-the-shelf components, reduced cost, pay-as-you-grow, low response time, reduced power consumption and coexistence with legacy systems.

This thesis also investigates experimentally new modulation formats that can triple the current transmission data rate in both metro and access networks, while simultaneously reducing the total power consumption, using low-cost commercial devices. Thanks to that, the use of investigated modulation can also be extended to mobile fronthaul and data center (DC) networks, where cost and power consumption are key parameters as well. Specifically, alternative 5G multicarrier modulation formats—filter bank multicarrier (FBMC), universal filtered multicarrier (UFMC) and generalised frequency division multiplexing (GFDM)—and orthogonal frequency division multiplexing (OFDM) are assessed and compared for a high-layer split fronthaul scenario. Non-orthogonal multiple access (NOMA) combined with multi-band carrierless amplitude phase modulation (MB-CAP) is proposed and evaluated for high-capacity passive optical networks (PONs) and DC optical interconnects. Finally, it is also demonstrated the convergence of wireless NOMA-CAP waveform and PAM-4 wired signal in a PON scenario.

It shall be mentioned that this thesis has been mainly carried out in the framework of the projects SUNSET and ALLIANCE founded by the Spanish Ministry of Economy and Competitiveness under contracts TEC2017-90034-C2-1-R and TEC2017-90034-C2-2-R,

respectively.

Acknowledgements

First, I would like to thank to my advisors Dr. José A. Lázaro and Dr. Salvatore Spadaro for all their technical support and guidance in the realization of this thesis. JAL has set an example of excellence as a researcher, mentor, instructor, and role model.

I would like to thank Dr. José A. Altabás, Dr. José Manuel Delgado Mendinueta and Dr. Juan José Vegas Olmos. JAA for his important scientific assistance and discussions during the whole thesis, Mendi for his invaluable guidance during and after my research stay in NICT, and JJ, for opening doors and showing opportunities. Thanks also to all my co-authors around the world, without whom little of this would have been possible.

Thanks to the Spanish Science Ministry for the funding of my Ph. D. studies (FPI-BES-2015-074302).

Finally, the biggest thank to my family and friends, within and outside the Lab D4-S107. Thank to my fiancée, Alejandra Azpúrua Cardenas, for being always there.

Chapter 1. Introduction

1.1 Evolution of optical communication networks

Over the last three decades, optical communication networks (OCNs) have gone through an extensive and rapid evolution [1], [2], [3], [4], [5]. Fig. 1.1 summarizes the evolution of OCNs through the years, highlighting the main traits of each evolutionary step with respect to link capacity, network topology and functionality.

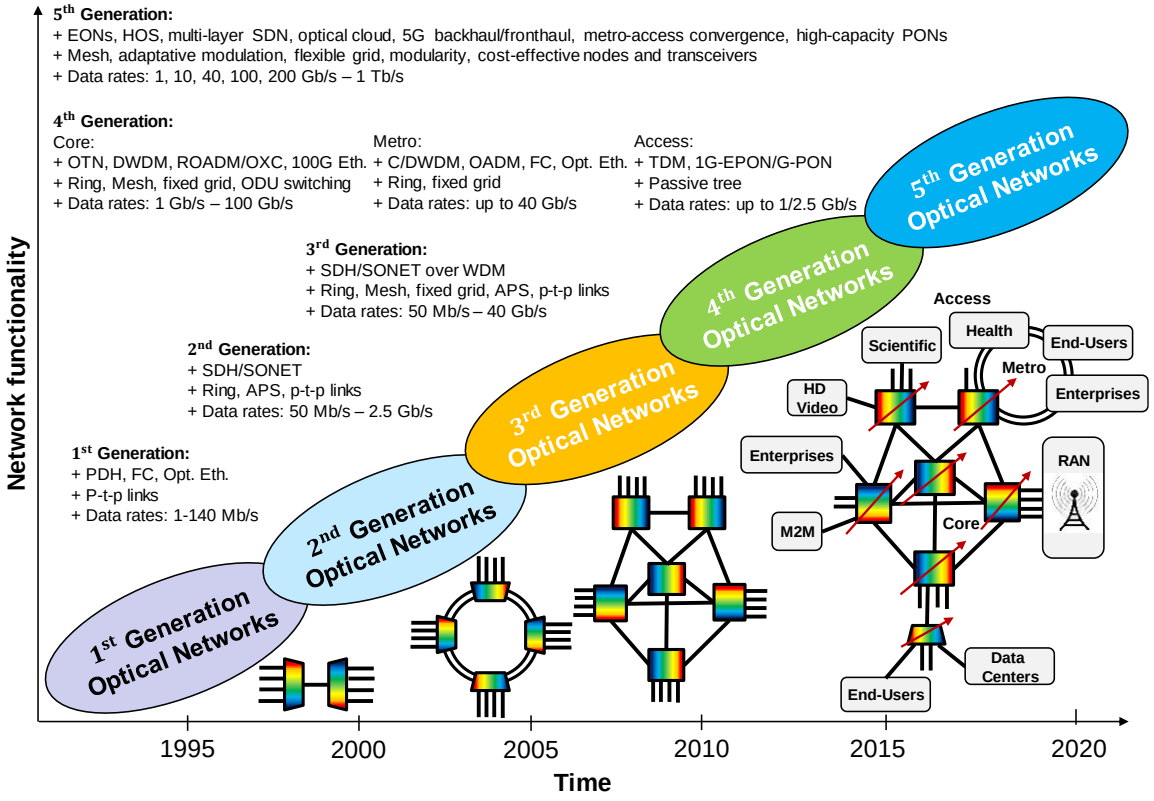

Fig. 1.1. Evolution of optical communication networks (OCNs) thorough the years, highlighting the main traits of each evolutionary step with respect to link capacity, network topology and functionality.

1st Generation (1G) OCNs, showing low functionality, were based on point-to-point (p-t-p) optical links connecting optical nodes mainly present in major cities. In this generation, the used transmission technologies were plesiochronous digital hierarchy (PDH) [6], fiber channel (FC) [7] and first implementations of optical Ethernet [8], providing transmission bit rates up to 140 Mb/s. Although these transmission technologies using optical fibers signified a great progress compared to legacy systems using co-axial or in general coper wire cables, the lack of standards and switching technologies along with strict

synchronization requirements limited their use for rapid service provisioning demanded by network's vendors. In order to overcome those limitations, synchronous digital hierarchy and synchronous optical network (SDH/SONET) were proposed and standardized in the 1990's [9], setting the 2nd Generation (2G) OCNs. These standards considered mainly p-t-p and ring topologies including automatic protection switching (APS) technologies to increase network resilience to failures. Unlike previous transmission technologies, SDH/SONET could provide a vendor independent and sophisticated network structure, resulting into the development of new applications, new network equipment and more management flexibility. Additional services were supported as high/low speed data (from 50 Mb/s to 2.5 Gb/s), local area network (LAN) interconnections, voice, high definition TV (HDTV) and broadband integrated services digital network (ISDN), therefore extending the use of the optical fiber up to the end-users, often replacing copper-pair/coaxial-based links.

3rd Generation (3G) OCNs were characterized by providing high transmission capacities—from 50 Mb/s to 40 Gb/s—thanks to the emergence of wavelength division multiplexing (WDM) technologies [10], which enabled the multiplexing of multiple wavelength channels into the same fiber link through a fixed grid, enhancing the utilization of the optical spectrum. This increased the network functionally and flexibility compared to the previous generation. SDH/SONET, well developed and standardized, were the used transmission technologies working over p-t-p, ring and mesh topologies, all of them using APS technology.

Until the 3G OCNs, although the transmission between end-points were performed through optical fibers, the whole end-to-end link was not exempt of multiple electrical interfaces. Indeed, all the traffic incoming to a node had to undergo an optical-electrical-optical (O-E-O) conversion for control functionalities, therefore, increasing substantially the cost and the power consumption of nodal equipment. Furthermore, as the optical fiber solutions were evolving to higher bit rates, the electronic processing was starting to become an important bottleneck in terms of network scalability. To overcome that situation, all-optical solutions were developed, remaining in the optical domain the whole end-to-end link between the source and destination nodes. One of the key elements to enable such functionality was the optical add/drop multiplexer (OADM) [11], [12]. OADMs allow for the insertion/extraction of certain wavelength channels to/from the network, while letting the remaining wavelength channels to optically pass through the node. This reduced end-to-end latency connections since E-O and O-E conversion just needed to be done at the

end-points of the connections. Similar to OADMs, optical cross-connects (OXCs) allow for a totally optical commutation of the signals coming from any incoming port to any outgoing port, thus eliminating costly electronic processing. This commutation node was particularly interesting for mesh topologies, enabling a better optical resource utilization and resilience schemes.

Nowadays, a 4th Generation (4G) OCN is divided into three main segments as is depicted in Fig. 1.2 [13]. The segments are backbone (or core) network which is used for long-distance transport (>1000 km), metro/regional network that is responsible for traffic grooming and multiplexing functions (<100 km), and access network which provides end-user connectivity (<20 km).

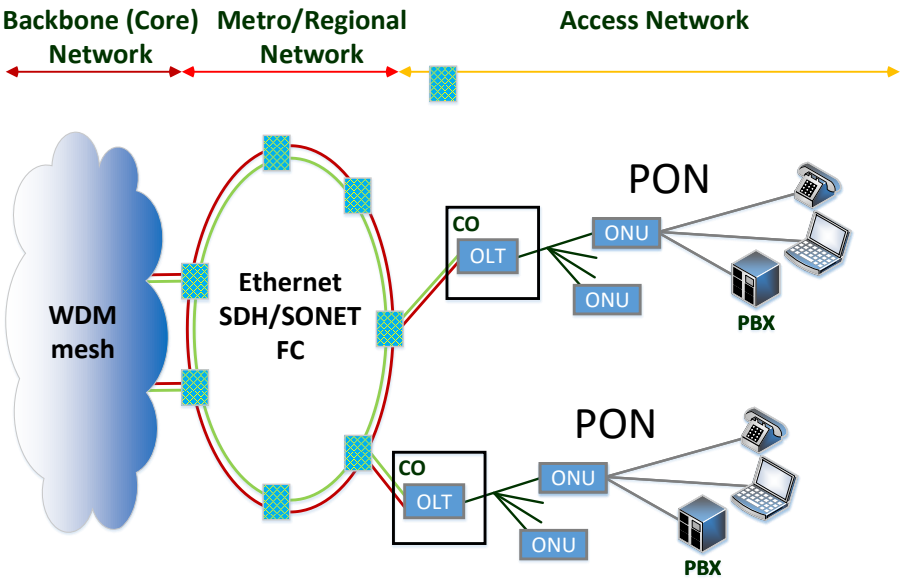

Fig. 1.2. Generic structure of a 4th Generation optical communication network (OCN).

The backbone network, using a mesh topology and dense WDM (DWDM)-based technology including reconfigurable OADMs (ROADMs) and OXCs, is the segment of the network which shows the highest functionality. It makes used of optical transport networks (OTN) concept and optical data unit (ODU) switching technology [14]. Here, the optical spectrum is typically divided into fixed channels of 50 GHz and the transmission technology is 100G [15], providing transmission bit rate up to 100 Gb/s. Similar to the backbone network, metro network uses DWDM-based technology with the difference that fixed channels are typically of 100/200 GHz, although higher bandwidths are also considered to reduce costs [16]. In this segment, the topology is typically a dual ring where the channels can be added/dropped using OADMs. Optical Ethernet, SDH/SONET and FC are the most common transmission technologies, reaching a maximum transmission bit rate

of 40 Gb/s. Finally, the access network is the segment that connect the central office (CO), placed at the edge of a metro network, with the end-users. In this case, passive optical networks (PONs) have been considered as the best solution, where non-active multiplexing devices are used and a single optical fiber is serving multiple end-points, keeping the complexity at the terminals [17]. In PONs, multiplexing can be performed in time domain (TDM), in frequency domain (WDM) or in both domains (TWDM). The common transmission technologies are 1 gigabit Ethernet PON (1G-EPON) and gigabit-capable PON (G-PON) since their supports compatibility with legacy systems [18], [19]. The maximum bit rates supported in 1G-EPON and G-PON are 1 Gb/s and 2.5 Gb/s, respectively. Other more recent transmission technologies are NG-PON1 [20] and 10G-EPON [21], providing bit rates up to 10 Gb/s, and 25G-EPON [22] and NG-PON2 [23], providing up to 25 Gb/s and 40 Gb/s, respectively.

In the last years, the Internet data traffic has grown exponentially and is expected to continue this trend, up to the point that over 10,000 million handsets are expected by 2022 [24], [25]. Such an enormous number of terminals connected to the Internet, all of them running a wide and heterogeneous set of data applications will push current OCNs capacity and flexibility far beyond their limits. Therefore, a new generation of OCNs, providing a high-capacity and futureproof backhaul/fronthaul for 5th Generation (5G) wireless networks, is demanded. In this context, the main target to be accomplished by designing new 5G OCNs is to develop technologies for fast and efficient provisioning of high data rate optical connections [1], [26], [27], [28]. According to [1], [26], [27], [28], [29], this target can be possible by developing and optimally utilizing flexible, bandwidth-variable and software-controllable optical systems and sub-systems, as well as, by using advanced network concepts such as elastic optical networking (EON) and hybrid optical switching (HOS). Additionally, the introduction of the software-defined networking (SDN) concept in the optical domain will be key for high-performance OCNs. Recent efforts and achievements in several research areas have pointed out the way towards 5G OCNs, especially through:

- Increasing capacity, performance, flexibility and energy efficiency.
- Defining, standardizing and implementing optical SDN.
- Extending the reach of optical access networks and integrating metro and access segments.
- Developing strategies for optical-wireless convergence in support of 5G wireless networks.

In the following, the main enabling technologies for 5G OCNs and recent efforts in the above-mentioned fields are briefly outlined.

1.2 Enabling technologies for 5G optical communication networks

There has been recently a lot of research effort focused on developing new components and methods for increasing capacity and performance of optical transmission systems and networks, while making the optical infrastructure more flexible and energy efficient.

1.2.1 Bandwidth-variable and software-controllable optical transceivers

Bandwidth-variable optical transceivers (BVOTs) controlled by software are considered as key enabling components for 5G OCNs. Therefore, it is expected that BVOTs can operate on flexible-wavelength grid (FlexGrid) with new and demanding small spectral granularity as low as 12.5 GHz or 6.25 GHz, while being able to accommodate flexible traffic needs by varying bit rate, reach and spectral efficiency [1], [29], [30], [31], [32]. New-generation optical transceivers with digital signal processing already provide a high level of adaptability to support trade-offs between bit rate, spectral efficiency and reach. They can also provide different modulation formats such as on-off keying (OOK), 4-level pulse amplitude modulation (PAM-4), binary phase shift keying (BPSK), quadrature phase shift keying (QPSK) and quadrature amplitude modulation (QAM). Recently, other more advanced modulation formats as orthogonal frequency division multiplexing (OFDM) and Nyquist frequency division multiplexing (NFDM) [33] are also supported.

Several approaches for a flexible variation of the three key parameters of a transceiver (bit rate, reach and spectral efficiency) have been proposed in [32], [34], [35], [36], [37], [38], [39], [40], [41], [42], [43], [44]. All of them targeted to achieve a trade-off between complexity of the implementation in electrical and optical domains and realizing format-flexible digital signal processing (DSP) in a resource-efficient manner.

1.2.2 Flexible and elastic optical network nodes

Nodes for 5G OCNs should provide a high level of flexibility in various multiplexing domains, supporting elastic switching over a FlexGrid. Other key requirements are adaptability, scalability and resilience. Thus, there is a need for new node architectures providing flexibility and adaptability through a reconfigurable and on-demand structure [45], [46], [47], [48], [49], [50]. Components such as FlexGrid wavelength selective switches (WSSs) [51], [52], multiplexers/demultiplexers [53], [54], optical amplifiers, fast

optical and/or electronic switches [53], [54] and transponders are part of a flexible architecture to best cope with changing traffic demands [55]. Therefore, a modular architecture should enable scalability and an easy extension of the node functionality through adding new functional modules or replacing the old ones in order to optimally support future services. Furthermore, inactive modules can be switched off, thereby reducing the energy consumption and increasing energy efficiency.

1.2.3 Software-defined networking

The software-defined networking (SDN) concept is based on the complete decoupling between the data plane (physical layer) and a logically-centralized programmable control plane so as to enable the abstraction of network resources to develop new applications [56]. A centralized network intelligence makes possible, e.g., to inspect all the network concurrently to determine a path and transport technology that best suites to carry traffic. The SDN controller can also evaluate the performance of the network to dynamically reroute traffic or add more bandwidth to avoid congestions, finding optimal (or sub-optimal) solutions in milliseconds. The SDN, thus, opens the way for dynamic network optimization as well as for automated congestion control and cost management. Therefore, the main role of the control plane is to provide a common set of basic services that all applications can leverage.

Current SDN implementations are focused mainly on Ethernet networks for data centers (DCs) [56], [57]. It is essential to extend and apply the SDN concept to OCNs where there is currently a lack of standards and products providing automated provisioning. Modern OCNs already provide a relatively high level of flexibility and controllable attributes, so an SDN controller can control them. Moreover, many optical systems available on the market implement the path computation element (PCE), which is standardized in IETF RFC 4655 as a control protocol for MPLS and GMPLS networks [58]. PCE engine can be implemented in an SDN controller as a software module to provide path computation across several layers. Topology management and virtual routing modules are also available. However, additional standardization is required to allow the SDN controllers to directly manage optical transmission components such as BVOTs, ROADMs and OXCs. Within the network, the available spectrum can also be flexibly handled by allocating one, two or more spectral slices to a data flow. Some realizations of ROADMs and OXCs are very flexible and allow the control of the wavelength channel without restrictions [59], [60], [61], [62], [63], [64], [65]. Fig. 1.3 shows examples of components that can be used to

implement SDN-based 5G OCNs together with parameters that could potentially be controlled by software.

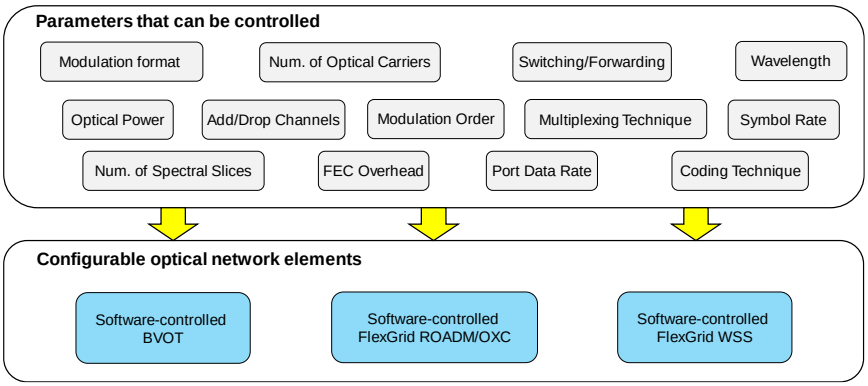

Fig. 1.3. Examples of parameters and network elements that could potentially be software-controlled in optical software-defined networks.

1.2.4 Coherent ultra-dense WDM technology for PONs

Time division multiplexing (TDM) technique offers a cost-effective solution for PONs. Nevertheless, this technique requires transceivers with electrical bandwidths being orders of magnitude higher than the bandwidth accessible by each individual end-user, making it unfeasible for the provisioning of multi-gigabit/s per end-user [66]. Alternatively, DWDM technologies are being considered by network's vendors due to their high level of bit rate scalability [67], [68].

To enable flexible network operation by allowing filterless operation, coherent receivers have been proposed for PONs, as recently done for backbone and metro networks. Coherent receivers can select a wavelength channel simply by tuning the local oscillator (LO) laser to the wavelength of the channel of interest. Filterless operation is desirable to make receivers cost-effective in volume production due to its standardized design, and more manageable for network's vendors by expediting its operation and maintenance [69]. Besides, fine wavelength selectivity in coherent DWDM-PONs enables also the use of ultra-dense wavelength spacing (<25 GHz) while avoiding the requirement for sophisticated optical wavelength filtering. Recent demonstrations include both unidirectional and bidirectional coherent u-DWDM transmissions [38], [44] [70], [71], [72], [73], , [74], providing a maximum bit rate per channel of 10 Gb/s for a 5 GHz grid.

In addition to this key advantage, coherent receivers offer significantly higher receiver sensitivities and higher chromatic dispersion (CD) tolerance compared to direct detection (DD) receivers [75], [72]. These are the major advantages for future PONs, operating at

multi-gigabit/s per end-user, and offering higher power budgets, enabling higher split ratios (i.e., increased number of end-users) and longer reach.

1.2.5 50-100 Gb/s PON-based access networks

PAM-4 providing 50 Gb/s per lane has already been standardized by IEEE 802.3bs for 200 and 400 gigabit Ethernet and are expected to displace 100 Gb/s per lane in DCs from 2020 [76]. An obvious choice therefore would be to adopt IEEE 802.3bs proposed solution for the next generation 50G TDM-PON. Nevertheless, high costs and reduced available power budgets (PBs) make this solution unfeasible for PON-based access networks, where the required PB is typically higher than 20 dB for a maximum reach of around 20 km. Therefore, the biggest technical challenges that must be successfully addressed when increasing the bit rate to 50-100 Gb/s for PONs are the reduction in PB, reduced fiber reach and decreased CD tolerance. To increase PB and reach, the most promising solution is semiconductor optical amplifiers (SOAs) [76], [77], [78], due to their low cost and large optical bandwidth as well as their small size and ability to be integrated with other optical devices. Other solution is to use more powerful FEC techniques, such as low-density parity-check used in 25G-EPON [22], but increasing the de/coder complexity. In terms of enhancing CD tolerance, optical duobinary or cyclic-prefix (CP) OFDM can be used, although they might require a top-performance Mach-Zehnder modulator (MZM) at the transmitter side. Alternatively, CD pre-compensation methods can also be used but at the cost of increasing digital signal processing (DSP) complexity [79].

Finally, u-DWDM deployment, where each connected end-user can be assigned a unique wavelength, plus coherent technology can also be considered as a potential alternative solution to intensity modulation direct detection (IM-DD) TDM-PON implementations to reach bit rates between 50 and 100 Gb/s [76]. This solution increases both PB and CD tolerance.

1.2.6 Metro-access convergence

As mentioned previously, current metro and access are two completely distinct networks that differ in terms of technology and protocols, see Fig. 1.2. Maintaining these two different networks is complex and expensive and the node that interconnects both networks must perform O-E-O conversions of the data traversing from one network to the other, so as to produce coexisting signals. This means that it must be able to handle the different technologies and protocols employed in both networks, making these interconnection nodes rather costly. Therefore, new network architectures and technologies for metro-

access networks convergence, given their potential for additional cost savings, are required. The converged metro-access network needs high capacity at the links traversed by the traffic to/from all of the subscribers. Different cost-effective and scalable solutions to increase this transmission capacity, avoiding the deployment of more optical fibers, have been proposed in the literature [80], [81]. For example, the SARDANA network transparently merges single-fiber TDM-PONs with a main double-fiber WDM ring using remote nodes (RN), as shown in Fig. 1.4(a) [80]. The 100 km WDM ring transports up to 32 wavelengths for >1000 users, allowing a maximum TDM-PON splitting ratio of 1:32 and only one wavelength per TDM-PON. Fig. 1.4(b) shows the DISCUS end-to-end network [81], comprising a flat optical core and a long-range PON (LR-PON) that combines metro and access networks. DISCUS approach can offer a physical split up to 512 (logical split up to 1024) and a maximum range of 125 km. In this architecture, 10 Gb/s time-division multiplexing dense wavelength-division multiplexing (TDWDM) LR-PONs can coexist with business 100 Gb/s dedicated channels.

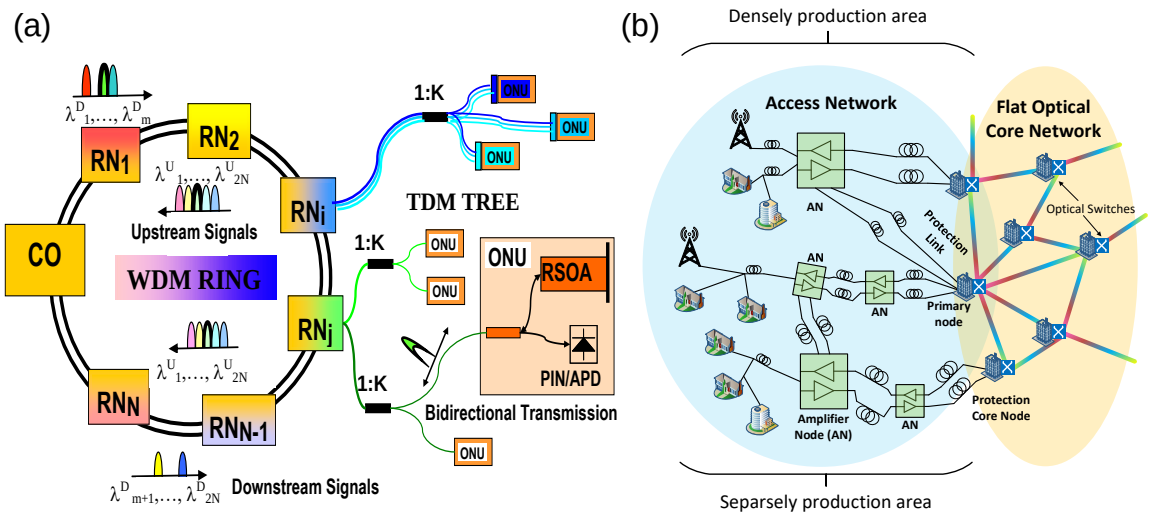

Fig. 1.4. Examples of converged metro-access network architectures: (a) SARDANA network and (b) DISCUS network.

On the other hand, since receivers' sensitivity and frequency selectivity are higher, coherent optical systems has been proposed as an excellent solution to enable cost-effective u-DWDM-PON-based metro-access scenarios [38], [44], [71], [72], [73], [74]. In this context, systems with wavelength spacing of 12 GHz, can improve highly the spectral efficiency regarding TDM and enabling heterogeneous traffic demands scenarios [71], [82].

1.2.7 5G wireless modulation formats

In radio access networks (RANs), the design of the access to the medium is essential to improve the system capacity and to dynamically allocate the available resources. OFDM has been adopted in fourth generation (4G) wireless networks, brought to the fact that it brings about numerous benefits, such as immunity to interferences, high resilience to frequency selective fading and efficient/flexible resource management [83], [84], [85]. However, traditional OFDM is unable to accomplish several of the requirements for future wireless networks, such as reduced out-of-band (OOB) noise and, high power and spectral efficiency. In order to address these new challenges, filter bank multicarrier (FBMC), universal filtered multicarrier (UFMC) and generalised frequency division multiplexing (GFDM), all considered as feasible alternatives for implementing 5G orthogonal multicarrier modulation formats, have recently been proposed as promising candidate technologies [86]. Alternatively, carrierless amplitude phase modulation (CAP) has gained more attention for future wireless networks since it allows less complex transceivers than OFDM [87] and has shown better results as well [88], [89]. Finally, to support a massive number of and dramatically different classes of users and applications, non-orthogonal multiple access (NOMA) schemes, for example, multiplexing various users in power/amplitude domain, have been also considered [86], [89], [90].

1.2.8 Optical fronthaul and wire-wireless convergence

It is expected that modern macrocell wireless networks will reach their limits in terms of capacity, flexibility, reliability and latency very soon [24]. To overcome that situation, small-cell-based mobile networks are considered as the most promising solution. However, in that network solution, a large number of small cells must be deployed to provide wide coverage. This makes it particularly important to simplify remote cell sites to reduce cost and increase energy efficiency. In this context, cloud radio access networks (C-RANs) have recently been proposed as a hopeful network architecture solution [91], [92]. That solution considers the division of the traditional base station, which integrated all the functionalities of radio and baseband processing, into several only-transmitting simple and cheap remote radio heads (RRHs) and a single cloud-hub base band unit (BBU) located at the central office (CO), where complex processing is centralised. As a consequence of that, a new connectivity segment called fronthaul is deployed between the multiple distributed RRHs and the centralised BBU.

On the one hand, the most common standard, used by fronthaul's vendors, is known as common public radio interface (CPRI) [93]. That standard uses the digitized baseband signal transmission over fiber (DBBoF) technique, where the base band IQ samples are digitised and serially transmitted at a constant bit rate. As a result, CPRI transmission needs huge bandwidth. For example, for 100 MHz radio bandwidth and multiple-input multiple-output (MIMO) degree of 8, the data rate per sector of the fronthaul transmission system should be of 49.3 Gb/s [94], [95]. To overcome this issue, alternatively, radio-over-fiber (RoF) technology has recently gained more and more attention [96], [97], [98], [99], not only for simplifying the interfaces of both BBUs and RRHs (digitisation and format conversion are not required), but also for saving bandwidth. Thus, for the aforementioned scenario, the RoF-based fronthaul just needs 2.4 GHz of bandwidth [99]. That means a reduction of the required bandwidth of 30 times regarding to CPRI when the OOK modulation format is used. On the other hand, massive small cell deployment requires a huge number of optical fibers. To solve that issue, high-layer split DWDM-PON-based fronthaul architecture has been proposed in [20]. In this architecture, transmission techniques based on u-DWDM are a promising solution.

Finally, in order to minimize both the capital expenditure (CAPEX) and the operation expenditure (OPEX) [100], operators expect to provide both broadband wireline and wireless access for end-users through the existing access network infrastructures. In this context, deployed PONs are already the most competitive solution to serve as mobile fronthaul, since high capacity, low latency and high level of flexibility can be achieved [91]. Wire-wireless convergence has been widely studied before in [101], [102], [103], [104], for long-term evolution (LTE) signals, basically OFDM, but mentioned convergence for 5G wireless signals have been little studied. In [105], the convergence of wire and wireless services was studied in a PON scenario for UFMC and GFDM.

1.2.9 Optical interconnects for data centers

Data centers (DCs) are considered as an important part of future networks. Most of the applications hosted in the DC servers such as cloud computing and search engines are data-intensive and require high interaction between the servers in the DC [106]. This interaction demands more efficient interconnection schemes providing high bandwidth and reduced latency while keeping the total power consumption inside the racks as low as possible due to thermal constraints [107]. In order to overcome this situation, optical interconnects have gained more and more attention as a key building block to ensure end-to-end energy

efficient solutions, offering high throughput, low latency and reduced energy consumption compared to current networks based on active optical cables. An efficient way to perform such optical interconnects is to make use of multi-core fibers (MCFs), which multiplex several channels in space domain through the use of different cores inside the same cladding [108], [109]. This technique allows for increasing the system capacity far beyond the Shannon limit of standard single-mode fibers (SSMF). However, the main drawback of MCFs is the inter-core crosstalk which reduces the transmission reach of signals. Recently, the design and fabrication of several types of MCFs have been reported in [110], [111], [112], showing low loss and low crosstalk. Moreover, MCF has been experimentally demonstrated for ultra-high-capacity transmission archiving up to 100 Tb/s [113]. All this pushes MCFs as a promising technology for communications inside DCs since no complex signal processing is required to reduce crosstalk effects as well as minimizing the CAPEX and OPEX costs of the network [111], [114], [115], [116], [117], [118], [119].

1.3 Objectives of the thesis

Fig. 1.5 shows the flexible 5G metro-access network scenario considered in this thesis. It provides the infrastructure to establish connectivity services among heterogeneous actors such as 5G-based radio stations, business, home users and data centers (DCs). Bringing DCs close to end-users allows low-latency services. An SDN-based controller is considered to achieve programmatic control over the network devices, allowing for a dynamic and flexible configuration of the whole network. The objectives of this thesis are various:

- Design, implementation, characterization and modelling of optical nodes that can be managed by a centralized SDN controller for future metro-access networks based on u-DWMD transmission technologies. This objective is mainly focused on the design of ROADMs and OXCs. In the design and implementation of these nodes, a trade-off between flexibility, complexity and economical costs must be achieved. The characterization of those nodes must be done in terms of insertion losses, power consumption and commutation time. Once the nodes have been characterized, they can be modelled for the SDN controller understanding.
- Development of algorithms and strategies for optical resource allocation that maximize the performances of converged u-DWDM metro-access networks based on proposed ROADM and OXC nodes in terms of the throughput or bandwidth blocking probability.

- Study the suitability of alternative 5G wireless modulation formats in optical domain for different applications such as mobile fronthaul, 50-100 Gb/s PONs and MCF-based optical interconnects inside of DCs, as well as the potential convergence of wired and wireless services in a heterogeneous access network.

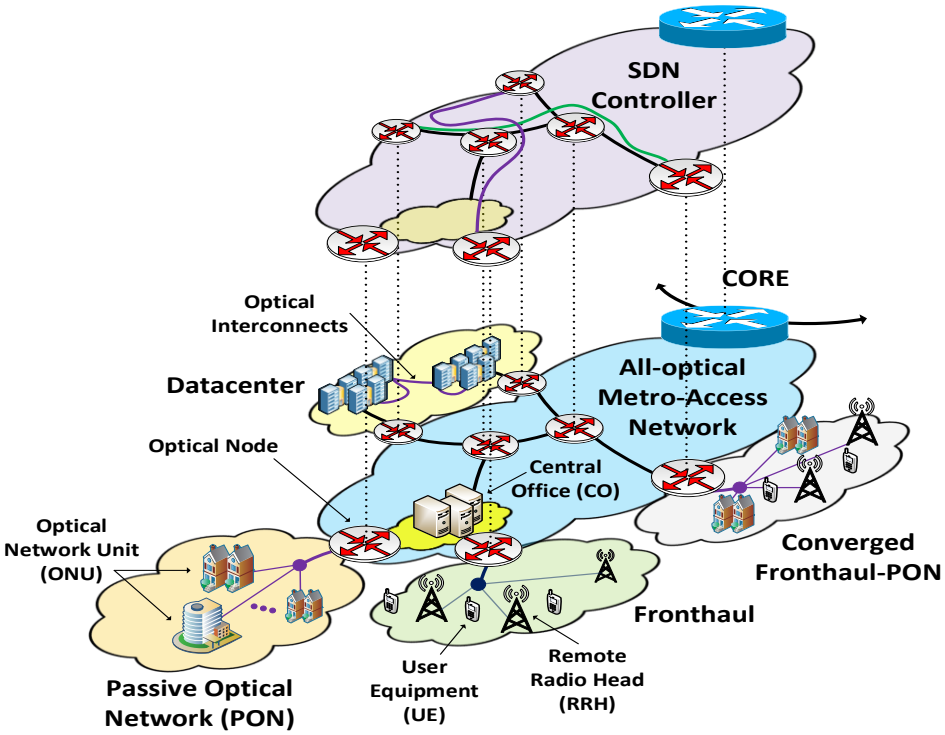

Fig. 1.5. Flexible 5G metro-access network scenario considered in the thesis.

1.4 Organization of the thesis

This thesis is organized as follows. Chapter 2 presents the design of cost-effective and flexible optical nodes (ROADM and OXC) and transceivers, remotely managed by an SDN controller, as essential building blocks for metro-access networks supporting 5G services. In particular, the overall architecture including both the novel data plane nodes and the SDN control plane is discussed.

Chapter 3 studies through simulations the performance of the proposed cost-effective ROADM as a metro-access ring network element for both online and offline cases in a u-DWDM scenario. For both cases, different heuristics are proposed to determine the best node design which maximizes the network capacity.

Chapter 4 demonstrates that proposed cost-effective OXC enables the migration from a ring-based u-DWDM metro-access network with cost-effective ROADMs to a reconfigurable mesh topology. A heuristic based on an iterative process is presented for determining the best design of proposed cost-effective OXC and ROADM nodes to offer maximum network throughput while the node cost is minimized.

Chapter 5 experimentally assesses and compares alternative 5G multicarrier waveforms (FBMC, UFMC and GFDM) and OFDM in terms of the system performance in a high-layer split u-DWDM-PON-based fronthaul scenario using the RoF technique with direct and quasi-coherent detection.

Chapter 6 experimentally assesses NOMA-CAP modulation for high-capacity PONs (50-100 Gb/s) and DC optical interconnects with cost-effective intensity modulation and direct detection (IM-DD). For PONs, SOA-based amplification is considered to increase available power budget, while for DC optical interconnects, multi-core fiber (MCF) is deemed to increase link capacity.

Chapter 7 demonstrates the downlink transmission of wireless NOMA-CAP waveform converged with a single-carrier wired signal in a PON scenario using a cost-effective IM-DD-based system.

Finally, chapter 8 concludes this thesis with general conclusions and also offers the reader some future work suggestions.

Chapter 2. SDN-Enabled Optical Node Designs and Transceivers for Flexible Sustainable u-DWDM Metro-Access Networks Convergence

2.1 Introduction

The current exponential growth of internet data traffic due to the popularization of cloud and new multimedia streaming services, the deployment of the Internet of Things (IoT) and the convergence between optical and wireless communications at the 5G paradigm and beyond [24], [25], demand changes to the networks so as to enable scalable growth in traffic volume, while supporting a high level of dynamic connectivity, full flexibility, reduced end-to-end latency and increased energy-efficiency. These features can be achieved by considering the cooperation between the network control and data planes. On the one hand, the management and control of networks are evolving towards an SDN centralized architecture (see Fig. 2.1). On the other hand, conventional ring-based metro networks are been migrated to a partially or fully reconfigurable mesh topology solution by adding new fiber links and new nodes to the network with new functionalities [49], [50], [62], as shown in Fig. 2.1. Moreover, metro networks are converging with access networks and evolving towards all-optical solutions [81], [80]. In this context, transmission techniques based on u-DWDM are a promising alternative to time division multiplexing (TDM) solutions due to their high spectral efficiency [72], which is accomplished by the division of a DWDM channel of 100(200) GHz into smaller channels called frequency slots (FS) wherein the uplink (U) and the downlink (D) for each end-user can be established (see Fig. 2.1) [38], [44]. Finally, in order to reduce network costs, the access networks are based on PON solutions as depicted in Fig. 2.1.

According to the scenario shown in Fig. 2.1, the metro-access network relies on different node elements such as the optical metro-core node (OMCN), the optical aggregation node (OAN), the optical network unit (ONU), the reconfigurable optical add-drop multiplexer (ROADM) and the optical cross-connect (OXC). The ROADM and the OXC are the all-optical nodes of the network. In particular, the ROADM is the node that connects the metro to the access networks while the OXC is responsible of conveying information through the

metro network, adding extra flexibility and resilience. The OMCN, OAN and ONU, still performing O-E-O conversion for their functions, are the nodes that allow the transfer of information between the metro and core network, the metro network and a DC or a 5G fronthaul, and the access network and end-users, respectively. In this chapter, it is presented the design of flexible optical nodes and transceivers, remotely managed by an SDN controller, as essential building blocks for metro-access networks supporting 5G services. In particular, the overall architecture including both the novel data plane nodes and the SDN control plane is discussed.

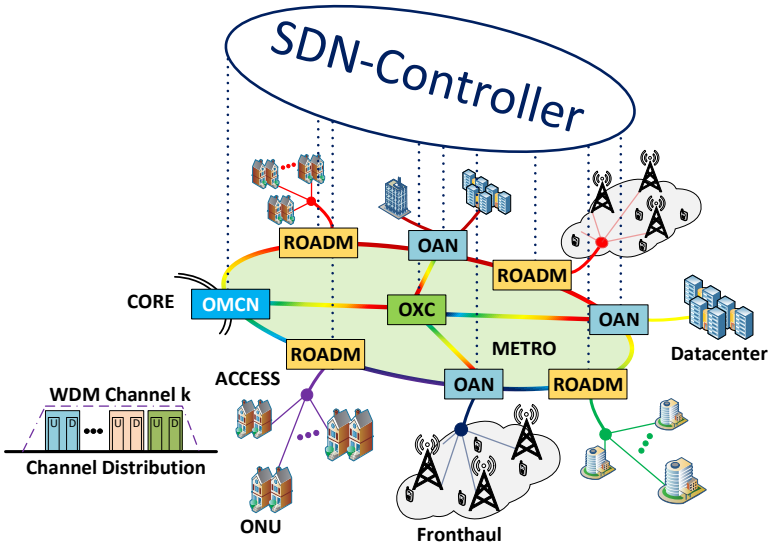

Fig. 2.1. Flexible 5G metro-access network scenario. (Inset) Proposed flexible ultra-dense WDM full-duplex frequency slot division.

The remainder of this chapter is organized as follows. Section 2.2 shows different transmitter and receiver technologies available in the literature that can be used for the implementation of the OMCN, OAN and ONU supporting u-DWDM feature. In this section, it is also summarized the most representative attributes of considered transmitters and receivers. Section 2.3 presents two possible node designs for the ROADM and the OXC. The first design, presenting top performance but high implementation cost, is based on WSSs and it shall be considered as the ideal architecture to compare in this thesis. The second design, based on cost-effective devices, shall be the technology considered for the implementation of the ROADM and OXC for future converged metro-access networks. Section 2.4 collects the main advantages of the proposed cost-effective ROADM and OXC. Section 2.5 presents the experimental characterization of proposed cost-effective ROADM and OXC in terms of the insertion loss, sensitivity and crosstalk as well as the experimental setup used for their characterization. Section 2.6 discusses a possible implementation of the

SDN control plane that can interact with the data plane based on presented optical nodes and transceivers. Finally, section 2.7 completes the chapter with the main conclusions.

2.2 Cost-effective optical transceivers for OMCN, OAN and ONU implementation

The OMCN, OAN and ONU, being the interface between different network segments with different transmission techniques, must be able to: add/remove specific channels to/from the network segments to which they are connected without affecting the other channels; aggregate and de-aggregate traffic tributaries; implement conversion of modulation formats, etc. To perform all these functionalities, it is necessary to conduct an O-E-O conversion using cost-effective optical transceivers. Fig. 2.2 shows the proposed node architecture for the OMCN, OAN and ONU. While the ONU is a simple node based on a transmitter and a received connected by a low-cost device, e.g., a power splitter, the OMCN and the OAN are more complex devices. The OAN consists of N stacked cards where each card represents a port of the node. A card is composed of different optical transceivers that are connected to a single fiber port through a DWDM multiplexer (MUX). The OMCN node architecture can be divided into two parts. The first one presents a similar architecture to the OAN and the second one, is the part of the node which is connected with the core network. This node second part implementation shall not be discussed in this thesis.

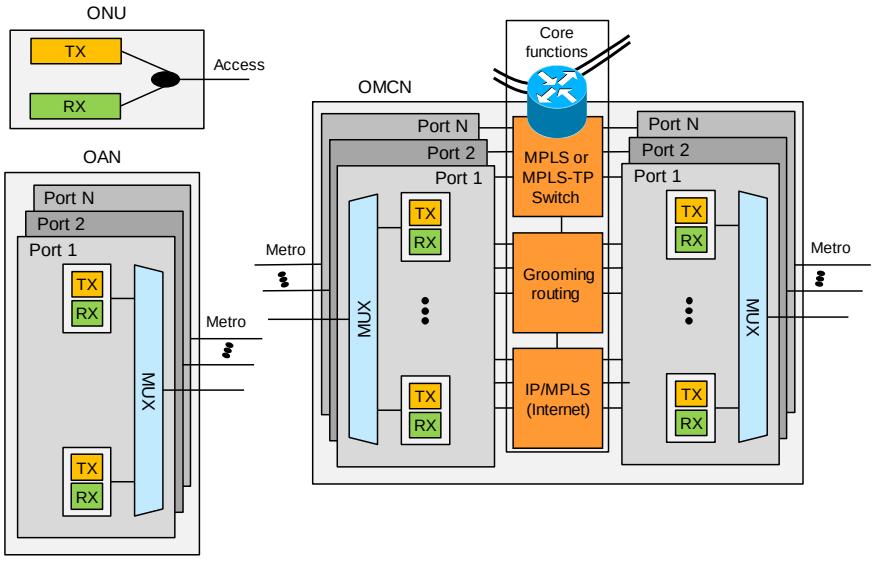

Fig. 2.2. OMCN, OAN, ONU node architecture.

Table 2.1 and Table 2.2 show respectively the most representative attributes of different cost-effective solutions proposed in the literature for transmitters (TX) and receivers (RX), that may be part of each of the mentioned nodes requiring O-E-O conversions for their

functionalities. The proposed transmitters are based on: *i)* a Mach-Zehnder modulator (MZM) plus a tuneable laser potentially covering C and L bands; *ii)* a distributed feedback laser (DFB), whose emission wavelength can be tuned thermally within a range of 4-5 nm; *iii)* a continuous-emitting vertical cavity surface emitting laser (VCSEL) plus a phase-modulated reflective semiconductor optical amplifier (RSOA) with a range of use of 5 nm; and *iv)* a VCSEL that can be employed within a range of 5 nm. For each of these transmitters, it is indicated the modulation format, the baud rate and the transmission power that can be implemented or obtained. A set of transmitters are proposed as a selection of the most appropriate O-E-O node for each case.

Table 2.1. Cost-effective transmitter for ONU, OAN, OMCN.

Transmitter based on	O-E-O Node	Wavelength Range (nm)	Modulation Format	Baud Rate (GBd)	Tx Power (dBm)	Refs.
MZM	OAN & OMCN	(C+L)~120	OOK	1-10	-6 to 0	[44]
			DPSK	1-10		
			QPSK	0.5-5		
			8-PSK	0.25-2.5		
			8-QAM	0.25-2.5		
			16-QAM	0.125-1.25		
			M-QAM	0.125-40		
DFB	ONU, OAN & OMCN	4-5	OOK	1-10	-6 to 0	[44]
			DPSK	1-10		
			QPSK	0.5-5		
			8-PSK	0.25-2.5		
			8-QAM	0.25-2.5		
			16-QAM	0.125-1.25		
VCSEL-RSOA	ONU, OAN & OMCN	5	OOK	1-10	-3	[38]
			DPSK	1-10		
			QPSK	0.5-5		
			8-PSK	0.25-2.5		
			8-QAM	0.25-2.5		
			16-QAM	0.125-1.25		
VCSEL	ONU, OAN & OMCN	5	OOK	1-5	-3 to 0.6	[38], [40]
			DPSK	0.125-2.5	-2 to 0	[43]

The proposed receivers are based on: *i)* direct detection (DD), *ii)* a coherent receiver in which the detected signal is mixed with a local oscillator based on a DFB (Coh. DFB), *iii)* a coherent receiver in which the local oscillator is a VCSEL (Coh. VCSEL), and *iv)* a colorless coherent integrated receiver that uses a 120º hybrid. For all these receptors, the receiver sensitivity, defined as the minimum received power to ensure a BER of $2.2 \cdot 10^{-3}$, corresponding to 7% overhead (OH) for forward error corrections (FEC) [120], is presented as a function of the modulation format and baud rate. Polarisation dependency is also

indicated so that for those receivers, where frequency selectivity is possible, double the number of channels that could be received. All these proposed transmitters and receivers can be adapted to implement transmission techniques based on u-DWDM, in which each WDM channel is divided into FS wherein the U and the D for each end-user can be established (see Fig. 2.1), offering different bit rates as required.

Table 2.2. Cost-effective receivers for ONU, OAN, OMCN.

Receiver	Wav. Range (nm)	Modulation Format	Baud Rate (GBd)	Rx Sens. (dBm)	Pol. Dep.	Wav. Select.	Refs.
DD	(C+L)~120	OOK	1-10	-26	NO	NO	[23]
Coh. DFB	4	OOK	1-10	-48.5	YES	YES	[38], [121], [122]
		DPSK	1-10	-52			
		QPSK	0.5-2.5	-48.8			
		8-PSK	0.125-1.25	-43.3			
		8-QAM	0.125-1.25	-43.7			
		16-QAM	0.0625-0.625	-40.9			
Coh. VCSEL	5	OOK	1-10	-45.5	YES	YES	[40], [121], [122]
		DPSK	1-10	-49			
		QPSK	0.5-2.5	-45.8			
		8-PSK	0.125-1.25	-40.3			
		8-QAM	0.125-1.25	-40.7			
		16-QAM	0.0625-0.625	-37.9			
Coh. Integrated	C~40	DPSK	1-10	-39.1 to -34.1	YES	YES	[41], [42], [122]
		QPSK	0.5-2.5	-35.9 to -30.9			
		8-PSK	0.125-1.25	-30.4 to -25.4			
		8-QAM	0.125-1.25	-30.8 to -25.8			
		16-QAM	0.0625-0.625	-28 to -23*			

*For acceptable optical signal-to-noise ratio (OSNR) penalty of 1.5 dB

2.3 ROADM and OXC node architecture design

In general, ROADMs and OXCs are considered as key elements for future metro-access networks because they can help to overcome the strict limitations of conventional DWDM-based metro networks with fixed OADMs [123]. The four main features considered as essential in the design of ROADMs and OXCs are: directionless, colorless, contentionless, FlexGrid and bidirectionality [59], [60], [61], [62], [63], [64], [65]. These features are defined as follows.

- *Colorless* means that any port of the node is not wavelength channel selective; that is, any wavelength channel can be switched from one port to any of the other ports of the node.
- *Directionless* means that any port of the node can be connected with any of the other ports of the node.

- *Contentionless* means that there is no wavelength channel blocking, allowing the switching of two channels with the same wavelength from different input ports to the same output port. Thanks to this characteristic, wavelengths can be more easily reused multiple times without any manual configuration.
- *FlexGrid* refers to the node feature to operate over a flexible grid.
- *Bidirectionality* determines if the data can be transmitted in both directions, allowing full-duplex communications. It can be implemented through different fibers or using a WDM technique.

Nowadays, ROADMs and OXCs with colorless, directionless, contentionless, FlexGrid and bidirectional features are solutions designed exclusively for core networks due to their high cost, making them prohibitive for converged metro-access networks [124]. Therefore, new sub-optimal solutions are required, e.g., removing contentionless and relaxing the FlexGrid feature. This substantially reduces the cost of the node [125], [126].

Only few works have been reported in the literature focused on the design of cost-effective ROADMs and OXCs for metro-access networks. In [45], the authors present a hybrid coarse WDM and dense WDM (C/DWDM) ROADM node architecture, which can be used for developing scalable metro/access networks that initially use CWDM wavelengths and allow vendors to add new DWDM channels as demand grows. Although, the CWDM ROADM can be migrated to a hybrid C/DWDM system by simply connecting a DWDM multiplexer (MUX) to the given CWDM module as demand grows, it uses WSSs for it switching functionalities, keeping a high cost of the node. In [46], authors propose a stackable ROADM (S-ROADM) node architecture for single-fiber coarse wavelength division multiplexing (CWDM) ring networks. The S-ROADM consists of some modules with different wavelengths filters and optical switches that are reconfigured manually to perform low-cost commutation nodes. In [48], authors present an OXC architecture based on semiconductor optical amplifiers (SOAs) that allows switching data signals in wavelength and time for fully exploiting statistical multiplexing. Hereunder, cost-effective DWDM ROADM and OXC node are proposed for future converged metro-access networks.

2.3.1 WSS-based node solutions

ROADMs and OXCs are conventionally based on WSSs, consisting of micro electro-mechanical systems (MEMS) and liquid crystal on silicon (LCoS) technologies [55]. Although technologically mature and providing high switching performances, both MEMS

and LCoS technologies are not scalable enough to be applied to metro and access networks where cost, volumes, power consumption, and reliability are extremely significant features [80], [81]. Therefore, this WSS technology is considered as the ideal case for the ROADM and OXC implementation, and it is compared with the investigated solutions in this thesis.

Fig. 2.3(a) and Fig. 2.3(b) show respectively an example of architecture of a bidirectional ROADM and OXC with colorless and directionless features based on WSSs that can be used in the proposed scenario shown in Fig. 2.1. Both metro network and access network transmission systems are based on single bidirectional fiber links and the considered multiplexing technique is u-DWDM, characterized by dividing each DWDM channel into FSs. The ROADM is based on three 1x2 WSSs which allow implementing add/drop and pass-through functions for each wavelength channel individually. In this way, when add/drop function is selected for a specific wavelength channel, it can be routed to/from the West (W) or East (E) ports in the metro part of the network from/to the Add/Drop (A/D) port where the access part of the network is connected, see Fig. 2.3(a). On the other hand, when the pass-through function is chosen, the selected wavelength channel can be routed from/to W/E port to/from E/W port. The OXC is composed of four 1x3 WSSs, which allow the implementation of the switching functions between any pair of ports of the OXC over each channel individually, see Fig. 2.3(b). Both nodes architecture can be implemented to work with a FS granularity of 12.5 GHz using nowadays commercial WSSs [51], [52], and it is expected to supports 6.25 GHz granularity and even lower in the near future. These WSS-based nodes, providing a high performance colorless and directionless functionality at the FS level, though at relatively high cost due to the WSS modules [126], are specifically the reference node architectures for comparison in this thesis. In order to reach a trade-off solution between performance and costs, a cost-effective DWDM node architecture for the ROADM and OXC are proposed below.

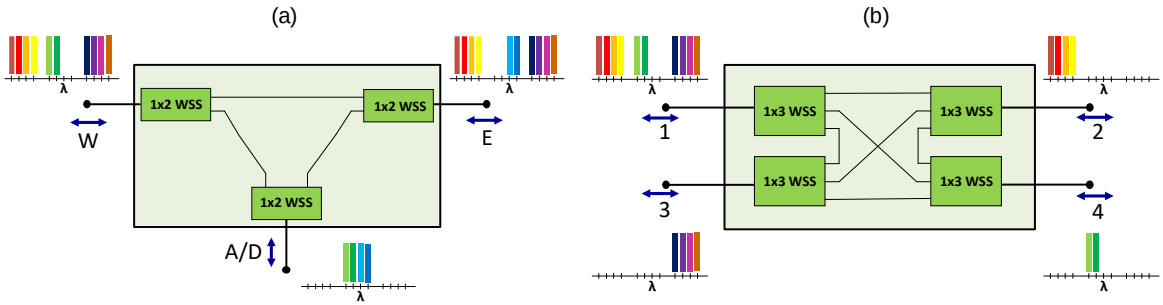

Fig. 2.3. WSS-based reference node architecture setup with colorless and directionless features for: (a) ROADM and (b) OXC.

2.3.2 Cost-effective DWDM-based node solutions

The ROADM and OXC node design for future converged metro-access networks are basically driven by new network-level requirements, such as full flexibility, adaptability, scalability (pay-as-you-grow), resilience and increased energy-efficiency [1], [29]. To offer all those features, it is here proposed a cost-effective DWDM-based node architecture design for the ROADM and the OXC.

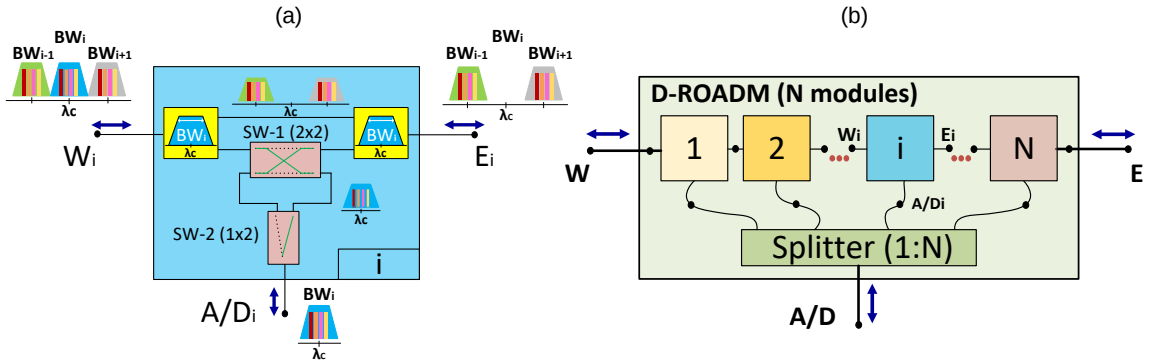

Fig. 2.4. (a) Setup of a basic module of the cost-effective DWDM ROADM (D-ROADM). (b) Cost-effective ROADM design for N modules.

Fig. 2.4(a) shows the basic module of the bidirectional cost-effective ROADM that can switch a group of frequency slots of the same WDM channel. The basic module of the ROADM consists of two three-port DWDM-fixed filters that are characterized by their 3 dB bandwidth (BW_i) and two latched switches (SWs). The filtered WDM channel may pass through the module or can be added/dropped from/to the access network depending on the 2x2 SW configuration. The 1x2 SW determines over which port, E_i or W_i, the connection is established. For a group of FSs outside of the DWDM channel managed by the ROADM module, it is transparent for them. This ROADM design can be scaled to manage other channels through the addition of similar modules to that shown in Fig. 2.4(a) as it is indicated in Fig. 2.4(b), where a 1 to N power splitter (1:N) can be used for this purpose, thus reducing the cost of the proposed ROADM. However, the losses of the ROADM increase significantly when the number of modules of the ROADM (N) improves due to the splitter. In this way, an optical insertion loss (IL) study of the cost-effective ROADM depending on the N must be made. Section 2.5.1 shall provide that study, proposing an IL model for the DWDM ROADM with N modules. In addition, for cases where the number of modules could be high, a wavelength division multiplexer (WDM) can be used instead of the power splitter for reducing losses. Therefore, it enables the coverage of both C and L bands. In that case, the cost-effective ROADM works as a

colorless directionless all-optical node at DWDM channel level, while the WSS-based reference ROADM, Fig. 2.3(a), is a colorless directionless ROADM at FS level.

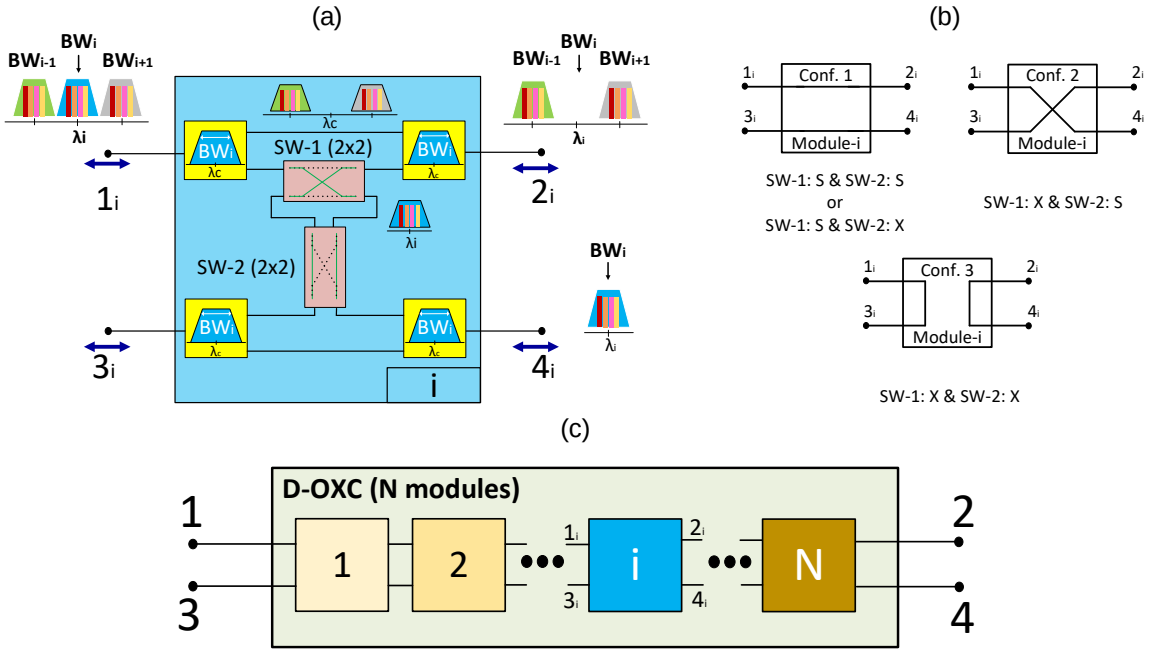

Fig. 2.5. (a) Setup of a basic module of the DWDM OXC (D-OXC). (b) Possible ports configurations of the basic module of the D-OXC for the different switches (SWs) states: straight (S) and cross (X). (c) D-OXC design for N modules.

Fig. 2.5(a) exhibits the basic module of the cost-effective OXC that can switch a group of FSs of the same DWDM channel bidirectionally. The module is based on two 2x2 SWs and four three-port DWDM-fixed filters (BW_i) that determine the DWDM channel which is added/dropped. Then, the filters are used for the A/D of a group of FSs, whereas the SWs are used for guiding those FSs between any pairs of ports of the OXC. Each of the SWs has two states: straight (S) and cross (X). Therefore, a total of 2^2=4 combinations of the switches states are available in one OXC module, but just three of them generate different ports configurations to the module, as it is shown in Fig. 2.5(b). Specifically, the module configuration 1 (Conf. 1) defined in Fig. 2.5(b), corresponding to the connection between ports 1_i and 2_i and, 3_i and 4_i, has two possible switches combinations. In this case, it is chosen the SWs combination in which both SWs are in S state. Moreover, note that for other different groups of FSs from those supported by the DWDM channel of the OXC module, it is transparent for them. In other words, if a group of FSs are out of range of the module's bandwidth, it leaves through the module by ports 2_i and 4_i when the input ports are 1_i and 3_i, respectively, see Fig. 2.5(a). Finally, the cost-effective OXC design can also be scaled to manage more DWDM channels as shown in Fig. 2.5(c). Thus, the DWDM

OXC through the addition of more modules can switch any channel of the C and L bands. In that case, the proposed cost-effective OXC (N) works as a colorless directionless all-optical node, thought at the DWDM channel level, differing from the reference WSS-based reference OXC that switches at FS level, see Fig. 2.3(b). In section 2.5.1, it shall be proposed an IL model for the cost-effective OXC with N modules as well.

2.4 Advantages of cost-effective DWDM ROADM and OXC

Taking into account the proposed cost-effective DWDM ROADM and OXC node architecture, the major advantages that vendors can enjoy are:

- *Off-the-shelf components*. Both proposed cost-effective all-optical nodes, Fig. 2.4 and Fig. 2.5, consist mainly of three-port fixed filters and latched switches (1x2 and 2x2). On the one hand, there is a huge choice of switches in the niche market that can operate over C and L bands at lower cost [53], [54]. On the other hand, the prize of the fixed filters depends on their bandwidth, being highly available those whose bandwidth is between 2 THz and 50 GHz [53], [54]. Therefore, the proposed cost-effective all-optical nodes can be easily adapted to work with coarse or dense WDM channels relying upon the requirements of vendors. For lower node granularities, it is necessary to change the used technology to MUXs based on arrayed waveguide grating or WSSs. These technologies increase the implementation cost of the proposed nodes [51], [52], [55], [127], while obtaining a commutation bandwidth granularity of 12.5 GHz.
- *Bidirectionality and reconfigurability*. Current metro networks use two different fibers to provide full-duplex communications while just one fiber is generally used in access networks. This increases the complexity of the node that connects both networks. Since the proposed cost-effective ROADM and OXC are bidirectional, full-duplex communications can be stablished through one fiber using a WDM technique. Thanks to that, less complex and homogenous single-fiber metro-access networks can be provided by the proposed cost-effective ROADM and OXC. Regarding reconfigurability, the cost-effective ROADM and OXC also offer different protection schemes to the network.
- *Reduced cost*. The proposed cost-effective ROADM and OXC are based on the so-called first-generation of all-optical commutation nodes of type I [128], [129]. They employ different demux-switch-mux approaches to enforce their functionalities. Those approaches are characterized by presenting low-cost, scalable implementation. Table

2.3 and Table 2.4 allow to benchmark the cost implementation of the WSS-based ROADM and OXC and, the cost-effective DWDM ROADM and OXC. In particular, Table 2.3 shows the unit cost values (in arbitraries units) of different components required for both nodes and for both considered node implementations. Those values have been normalized to the cost of a 200 GHz spacing single channel DWDM multiplexer, e.g., DWDM-200-47 whose price is 175 $ as it is indicated in [130]. Table 2.4 shows the required components number and the total unit cost (TUC) for: *i)* a WSS-based reference ROADM and OXC node at FS level, Fig. 2.3; *ii)* a WSS-based ROADM and OXC at DWDM channel level; and *iii)* the proposed cost-effective ROADM and OXC design, Fig. 2.4 and Fig. 2.5; all of them covering the whole C band. So, for the WSS-based ROADM and OXC, two different granularities have been considered. The first one is 12.5 GHz, which corresponds with the considered frequency slot granularity. The second one is 100 GHz that is a granularity close to the proposed cost-effective ROADM and OXC of 125 GHz. That value for the cost-effective ROADM and OXC granularity shall be demonstrated in section 2.5.1. Due to the fact that for both ROADM and OXC architectures all the components are off-the-shelf, factors such as the maturity, production volume and components' performance have been taken into account to calculate the TUCs of the different ROADM and OXC implementations proposed. Finally, the considered configuration of the proposed cost-effective ROADM and OXC design covering the whole C band, with N=20, Fig. 2.4(b) and Fig. 2.5(c), can be considered the worst case, while in general $1 \leq N \leq 20$, and for many cases a single module ROADM and OXC, N=1, as in Fig. 2.4(a) and Fig. 2.5(a), is enough, as it shall be study in chapters 3 and 4. From Table 2.4, it can be noticed that the proposed cost-effective DWDM ROADM TUC is, for the case of N=20(N=1), 10.6(190.2) times lower than the TUC of the WSS-based ROADM with a FS granularity of 12.5 GHz, and 8.1(146.3) times lower than the TUC of the WSS-based ROADM with a 100 GHz granularity. In the case of the cost-effective DWDM OXC, for N=20(N=1), the TUC is of 101.6(5.08), as reported in Table 2.4. That value is 7.2(143.3) times lower than the total TUC of the WSS-based OXC working with a commutation granularity of 100 GHz. In the case of a WSS-based OXC with a commutation granularity of 12.5 GHz, the TUC is 9.1(181.1) times higher than the TUC of the cos-effective DWDM OXC with N=20(N=1).

Table 2.3. Normalized unit cost for proposed components.

Component	Normalized unit cost	Refs.
1x32 splitter	0.34	[131]
Dual 1x2 SW	0.40	[132]
Dual 2x2 SW	0.54	[133]
1x2 WDM MUX (175 GHz)	1	[130]
1x2 WSS (12.5 GHz)	208	[51], [126]
1x4 WSS (12.5 GHz)	230	[51], [126]
1x2 WSS (100 GHz)	160	[51]
1x4 WSS (100 GHz)	182	[51]

- *Pay-as-you-grown*. The proposed cost-effective ROADM and OXC are excellent low-cost solutions for growing metro-access networks. If the number of demands increases, the number of channels can be increased, as one module handles one channel. Adding one new channel at a time allows on-demand service introduction with minimal initial investment. However, the proposed architecture for the cost-effective ROADM and OXC shown respectively in Fig. 2.4 and Fig. 2.5 have to be upgraded so as to avoid that the ongoing traffic could be interrupted because of adding new modules.
- *Low commutation time.* The commutation time of the proposed cost-effective ROADM and OXC only depends on the commutation speed of a switch. In that case, the potentially switching speed of these proposed cost-effective nodes is lower than 8 ms [132], [133]. That value is within the same order of magnitude of the switching speed of the WSS-based node whose switching speed is of a few milliseconds [51], [52].

Table 2.4. Components number list for WSS-based ROADM and OXC for different granularities and for the cost-effective DWDM ROADM and OXC and, their total unit cost (TUC).

Node		Granularity (GHz)	Number of Components								Total unit cost (TUC)
			1x32 splitter	Dual 1x2 SW	Dual 2x2 SW	1x2 WDM (125 GHz)	1x2 WSS (12.5 GHz)	1x4 WSS (12.5 GHz)	1x2 WSS (100 GHz)	1x4 WSS (100 GHz)	
ROADM	WSS-based	12.5					3				624
		100							3		480
	Cost-effective	125	1	20	20	40					59.14
OXC	WSS-based	12.5						4			920
		100								4	728
	Cost-effective	125			40	80					101.6

- *Reduced power consumption*. Table 2.5 shows the worst case of power consumption of both WSS-based and cost-effective node implementations for the ROADM and OXC

when they work for the whole C band. For the cost-effective ROADM and OXC, the worst-case power consumption corresponds to N=20 when it is considered that each module presents an effective bandwidth of 125 GHz. From Table 2.5, it can be noticed that the power consumption of the cost-effective ROADM is 3.5 times lower than the WSS-based ROADM, while for the cost-effective OXC is 4.7 lower than WSS-based OXC. That node power consumption reduction is because of the proposed cost-effective ROADM and OXC uses latched switches [132], [133] which maintain their state after being commuted, allowing keeping the power consumption reduced. This makes the cost-effective ROADM and OXC to be a good solution for future sustainable networks. Furthermore, cost-effective ROADM and OXC reduce the instances of O-E-O conversions by setting all-optical links between metro and access nodes. That helps to reduce the power consumption of the network.

- *Coexistence with legacy systems.* The proposed granularity for the cost-effective DWDM ROADM and OXC permits that they can be compatible with various technology transmission systems such as NG-PON which requires channels with 100 GHz of bandwidth [23] and u-DWDM [38], [39], [44]. Regarding the compatibility with existing metro networks, the present solution is fully compatible, provided there are enough free spectral resources. Furthermore, it should be noted that this solution employs a wavelength division duplexing and it does not require any additional fiber to this end.

Table 2.5. Power consumption of the WSS-based and cost-effective ROADM and OXC.

Node		Power Consumption (W)
ROADM	WSS-based	25.2
	Cost-effective	7.2
OXC	WSS-based	33.6
	Cost-effective	7.2

2.5 Experimental characterization of the cost-effective DWDM ROADM and OXC

In order to characterize the basic module of the proposed cost-effective ROADM and OXC, three types of measurements have been realized: *i)* spectral characterization which permits to determine the effective bandwidth, the insertion loss (IL) and the isolation among node ports; *ii)* single channel data transmission sensitivity for checking potential distortions in the received signal; and *iii)* multiple channel data transmission sensitivity for checking

potential crosstalk due to lack of full isolation between proposed cost-effective node ports. Since both cost-effective ROADM and OXC have similar architectures and use the same technology to implement their functionalities, all mentioned measurements have only been performed for a single module ROADM based on two fixed filters with a bandwidth of 175 GHz and centered at 1539.77 nm (JDS Uniphase [130]), and two commercial opto-mechanical latched switches [132], [133], controlled by a prototype current source and a micro-PC.

2.5.1 Insertion loses measurement

Fig. 2.6 shows the ROADM effective bandwidth (at −3 dB cut-off frequencies), BW_{eff}=125 GHz, and its 37.5 GHz guard bands (GB). The out-band and in-band insertion losses for the pass-through configuration (PT IL line in Fig. 2.6, measured W↔E and switch 2x2 in Fig. 2.4(a) in straight state) are: IL_{o-band}^{PT}=0.6 dB and $IL_{i-band,PT}^{PT}$=2 dB, respectively. And the in-band IL for the add/drop configuration (A/D IL line in Fig. 2.6, measured from W/E↔A/D and switch 2x2 in Fig. 2.4(a) in cross state) is $IL_{i-band,A/D}^{A/D}$ =2 dB. The in-band add/drop isolation, equivalent to an IL between pass-through ports, but when the channel is added/dropped, is $IL_{i-band,A/D}^{PT}$=35 dB (A/D isolation line, measured W↔E and switch 2x2 in Fig. 2.4(a) in cross state). On the other hand, the in-band pass-through isolation, equivalent to an IL between W/E and A/D ports when the channel pass-through the module, is $IL_{i-band,PT}^{A/D}$>60 dB (PT isolation line, measured W/E↔A/D and switch 2x2 in Fig. 2.4(a) in straight state). Those measurements were obtained with a BOSA high resolution optical complex spectrum analyser (HROCSA) from Aragon Photonics Labs.

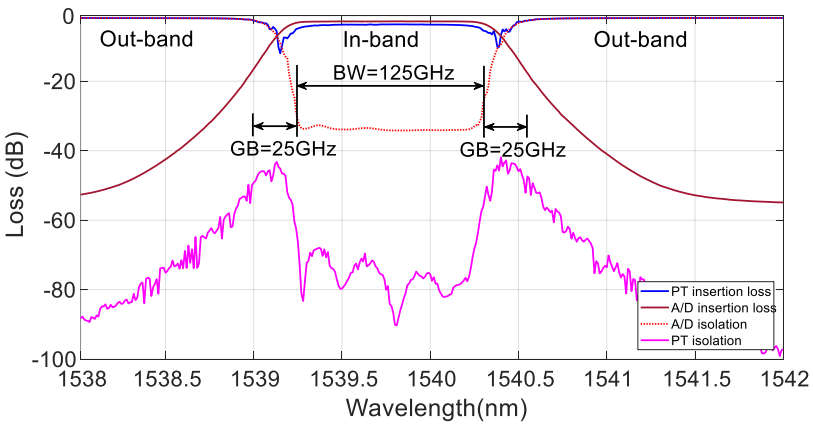

Fig. 2.6. Single module cost-effective ROADM insertion loss for pass-through (PT) and add/drop (A/D); and isolation: add/drop (A/D) and pass-through (PT).

Once characterized the insertion losses of a single ROADM module, the optical IL for a ROADM based on N modules can be calculated as it is indicated in Eqs. (2.1)-(2.4), where i and BW_{eff-i} are the module position in the ROADM and the range of wavelengths inside the effective bandwidth of the i-module, respectively. Eq. (2.1) represents the ROADM insertion loss between W and E ports, expressed in dB, for wavelengths out of the range of operation of all ROADM modules, $\lambda \notin BW_{eff-i}$ ($1 \leq i \leq N$), $IL^{W \leftrightarrow E}_{\lambda \notin BW_{eff-i}}$, while in Eq. (2.2) is indicated the losses between W and E ports for wavelengths in the range of operation of the ROADM i-module ($1 \leq i \leq N$), $IL^{W \leftrightarrow E}_{\lambda \in BW_{eff-i}}$, in PT configuration. As it can be seen in both $IL^{W \leftrightarrow E}_{\lambda \notin BW_{eff-i}}$ and $IL^{W \leftrightarrow E}_{\lambda \in BW_{eff-i}}$ equations, they scale linearly with the number modules of the ROADM. Eqs. (2.3) and (2.4) express the insertion loss between W and A/D ports and E and A/D ports, respectively, for the add/drop configuration. In both cases, the third term includes the insertion loss of a real 1:N power splitter. As commented, also a WDM MUX can be used instead of the power splitter for reducing losses in case of high N. Thus, for $N \geq 4$, an arrayed-waveguide grating-based MUX, whose typical insertion loss of 5 dB independent of the number of wavelength channels, can be used. In this thesis, it is considered a 1:N power splitter since it covers the worst-case node implementation. Taking into account Eqs. (2.1)-(2.4), the worst-case insertion loss (IL_{WC}) of the cost-effective ROADM working for the whole C band, N=20 using 200 GHz spaced filters, is 30.9 dB while the WSS-based ROADM is of 10 dB [51]. Nevertheless, the IL_{WC} of cost-effective ROADM can be reduced to 18.4 dB when an arrayed-waveguide grating-based MUX [134] is used instead of the power splitter. Furthermore, in many cases, a single module cost-effective ROADM (N=1, Fig. 2.4) could be enough to provide service to the users of a PON, as it shall be demonstrate in chapters 3 and 4. In that case, the IL_{WC} of the cost-effective ROADM is just of 2 dB.

$$IL^{W \leftrightarrow E}_{\lambda \notin BW_{eff-i}}(dB) = IL^{PT}_{o-band} \cdot N = 0.6 \cdot N \tag{2.1}$$

$$IL^{W \leftrightarrow E}_{\lambda \in BW_{eff-i}}(dB) = IL^{PT}_{o-band} \cdot (N-1) + IL^{PT}_{i-band,PT} = 0.6 \cdot (N-1) + 2 \tag{2.2}$$

$$\begin{aligned} IL^{W \leftrightarrow A/D}_{\lambda \in BW_{eff-i}}(d) &= IL^{PT}_{o-band} \cdot (i-1) + IL^{A/D}_{i-band,A/D} + 3.5 \cdot ceil(\log_2(N)) \\ &= 0.6 \cdot (i-1) + 2 + 3.5 \cdot ceil(\log_2(N)) \end{aligned} \tag{2.3}$$

$$IL^{E\leftrightarrow A/D}_{\lambda\in BW_{eff-i}}(dB) = IL^{PT}_{o-band}\cdot(N-i) + IL^{A/D}_{i-band,A/D} + 3.5\cdot ceil(\log_2(N)) = 0.6\cdot(N-i) + 2 + 3.5\cdot ceil(\log_2(N)) \quad (2.4)$$

From previous spectral characterization of the basic module of the cost-effective ROADM, it can also be deduced the ILs for the different port configurations of the cost-effective OXC module (see Fig. 2.5(b)) that works with a given BW_{eff} determined by the combination of considered fixed filters (see Fig. 2.6). Those ILs, in dB, are indicated in Eqs. (2.5)-(2.9), where IL^{S}_{SW}, IL^{X}_{SW}, $\mathrm{IL}^{\mathrm{PT}}_{\mathrm{WDM}}$, $\mathrm{IL}^{\mathrm{A/D}}_{\mathrm{WDM}}$, are the typical insertion losses for the S and X states of the considered 2x2 latched switches and the IL of the 1x2 WDM MUX for PT and A/D modes, respectively; $IL^{1_i\leftrightarrow 2_i|3_i\leftrightarrow 4_i}_{o-band}$ is the out-band ($\lambda \notin BW_{eff}$) insertion losses for the connection between ports 1_i and 2_i and, 3_i and 4_i; $IL^{1_i\leftrightarrow 2_i}_{i-band,Conf1}$ and $IL^{3_i\leftrightarrow 4_i}_{i-band,Conf1}$ are respectively the in-band ($\lambda \in BW_{eff}$) insertion losses for the connection between ports 1_i and 2_i and, 3_i and 4_i for the first module ports configuration (Cong. 1) defined in Fig. 2.5(b); $IL^{1_i\leftrightarrow 4_i|2_i\leftrightarrow 3_i}_{i-band,Conf2}$ is the in-band ($\lambda \in BW_{eff}$) IL for the connection between ports 1_i and 4_i and, 2_i and 3_i, corresponding to the second configuration of the module ports (Conf. 2) defined in Fig. 2.5(b); and, $IL^{1_i\leftrightarrow 3_i|2_i\leftrightarrow 4_i}_{i-band,Conf3}$ is the in-band ($\lambda \in BW_{eff}$) IL for connections between ports 1_i and 4_i, 2_i and 3_i for the third ports configuration (Conf. 3) of the D-OXC module defined in Fig. 2.5(b).

$$IL^{1_i\leftrightarrow 2_i|3_i\leftrightarrow 4_i}_{o-band} = 2\cdot IL^{PT}_{WDM} = 0.6\ dB \quad (2.5)$$

$$IL^{1_i\leftrightarrow 2_i}_{i-band,Conf1} = 2\cdot IL^{A/D}_{WDM} + IL^{S}_{SW-1} = 2.1\ dB \quad (2.6)$$

$$IL^{3_i\leftrightarrow 4_i}_{i-band,Conf1} = 2\cdot IL^{A/D}_{WDM} + IL^{S}_{SW-1} + IL^{S}_{SW-2} = 2.2\ dB \quad (2.7)$$

$$IL^{1_i\leftrightarrow 4_i|2_i\leftrightarrow 3_i}_{i-band,Conf2} = 2\cdot IL^{A/D}_{WDM} + IL^{X}_{SW-1} + IL^{S}_{SW-2} = 2.6\ dB \quad (2.8)$$

$$IL^{1_i\leftrightarrow 3_i|2_i\leftrightarrow 4_i}_{i-band,Conf3} = 2\cdot IL^{A/D}_{WDM} + IL^{X}_{SW-1} + IL^{X}_{SW-2} = 3\ dB \quad (2.9)$$

Once the ILs of a cost-effective OXC module are determined, the optical ILs for a cost-effective OXC based on N modules can be calculated as it is shown in Eqs. (2.10)-(2.15),

where i, and BW_{eff-i} are the module position in the cost-effective OXC and the range of wavelengths inside the effective bandwidth of the i-module, respectively. Eq. (2.10) represents the cost-effective OXC insertion loss between the ports 1 and 2 and, 3 and 4 for wavelengths out of the range of operation of all cost-effective OXC modules, $\lambda \notin BW_{eff-i}$ ($1 \leq i \leq N$), $IL^{1\leftrightarrow 2|3\leftrightarrow 4}_{\lambda \notin BW_{eff-i}}$. Meanwhile, in Eqs.(2.11) and (2.12) are respectively expressed the losses between the ports 1 and 2 and, 3 and 4 for wavelengths in the range of operation of the cost-effective OXC i-module, $\lambda \in BW_{eff-i}$ ($1 \leq i \leq N$), $IL^{1\leftrightarrow 2}_{\lambda \in BW_{eff-i},Conf1}$ and $IL^{3\leftrightarrow 4}_{\lambda \in BW_{eff-i},Conf1}$, for the first module ports configuration (Conf. 1) shown in Fig. 2.5(b). The Eq. (2.13), expresses the IL between ports 1 and 4 and, 2 and 3, $IL^{1\leftrightarrow 4|2\leftrightarrow 3}_{\lambda \in BW_{eff-i},Conf2}$, for the second module ports configuration (Conf. 2) defined in Fig. 2.5(b). Finally, Eqs. (2.14) and (2.15) respectively represent the IL between ports 1 and 3, $IL^{1\leftrightarrow 3}_{\lambda \in BW_{eff-i},Conf3}$, and, 2 and 4, $IL^{2\leftrightarrow 4}_{\lambda \in BW_{eff-i},Conf3}$, for the third module ports configuration (Conf. 3) defined in Fig. 2.5(b). Taking into account Eqs. (2.10)-(2.15), the IL_{WC} of the cost-effective OXC working for the whole C band, N=20, is 25.8 dB, while for the WSS-based OXC is 10 dB [51]. Nevertheless, finding out an optimal design of the cost-effective OXC for a considered network example, the IL_{WC} can be significantly reduced, as it shall be shown chapter 4.

$$IL^{1\leftrightarrow 2|3\leftrightarrow 4}_{\lambda \notin BW_{eff-i}}(dB) = IL^{1_i\leftrightarrow 2_i|3_i\leftrightarrow 4_i}_{o-band} \cdot N = 0.6 \cdot N \tag{2.10}$$

$$\begin{aligned} IL^{1\leftrightarrow 2}_{\lambda \in BW_{eff-i},Conf1}(dB) &= IL^{1_i\leftrightarrow 2_i|3_i\leftrightarrow 4_i}_{o-band} \cdot (N-1) + IL^{1_i\leftrightarrow 2_i}_{i-band,Conf1} \\ &= 0.6 \cdot (N-1) + 2.1 \end{aligned} \tag{2.11}$$

$$\begin{aligned} IL^{3\leftrightarrow 4}_{\lambda \in BW_{eff-i},Conf1}(dB) &= IL^{1_i\leftrightarrow 2_i|3_i\leftrightarrow 4_i}_{o-band} \cdot (N-1) + IL^{3_i\leftrightarrow 4_i}_{i-band,Conf1} \\ &= 0.6 \cdot (N-1) + 2.2 \end{aligned} \tag{2.12}$$

$$\begin{aligned} IL^{1\leftrightarrow 4|2\leftrightarrow 3}_{\lambda \in BW_{eff-i},Conf2}(dB) &= IL^{1_i\leftrightarrow 2_i|3_i\leftrightarrow 4_i}_{o-band} \cdot (N-1) + IL^{1_i\leftrightarrow 4_i|2_i\leftrightarrow 3_i}_{i-band,Conf2} \\ &= 0.6 \cdot (N-1) + 2.6 \end{aligned} \tag{2.13}$$

$$\begin{aligned} IL^{1\leftrightarrow 3}_{\lambda \in BW_{eff-i},Conf3}(dB) &= 2 \cdot IL^{1_i\leftrightarrow 2_i|3_i\leftrightarrow 4_i}_{o-band} \cdot (i-1) + IL^{1_i\leftrightarrow 3_i|2_i\leftrightarrow 4_i}_{i-band,Conf3} \\ &= 1.2 \cdot (i-1) + 3 \end{aligned} \tag{2.14}$$

$$IL^{2\leftrightarrow 4}_{\lambda\in BW_{eff-i},Conf3}(dB) = 2\cdot IL^{1_i\leftrightarrow 2_i|3_i\leftrightarrow 4_i}_{o-band}\cdot(N-i) + IL^{1_i\leftrightarrow 3_i|2_i\leftrightarrow 4_i}_{i-band,Conf3}$$
$$= 1.2\cdot(N-i)+3 \qquad (2.15)$$

2.5.2 Sensitivity and crosstalk measurements

The experimental setup for sensitivity and crosstalk measurements are shown in Fig. 2.7. The transmitter (TX) was based on an external cavity, 100 kHz linewidth, tunable laser source (TLS), modulated by a Mach-Zehnder modulator (MZM). The TLS was used to adjust its wavelength inside the frequency slot for these measurements. The MZM was set at the minimum transmission point of the MZM for phase modulation and it was thermally controlled to ensure its stability. The optical transmitter used a digital transmitter (DTX) unit, where a total of 2^{18} bits were randomly generated. The data were differentially encoded and shaped to achieve maximum performance for a 1 Gb/s data-stream. The transmitted symbols in the digital transmitter (DTX) were filtered using a Nyquist pulse shaper filter with a length of 12 symbols and a roll off factor value of zero. The DTX was implemented in MATLAB™ and the electrical signals were generated by a 12 GSa/s arbitrary waveform generator (AWG) [38], [39], [44].

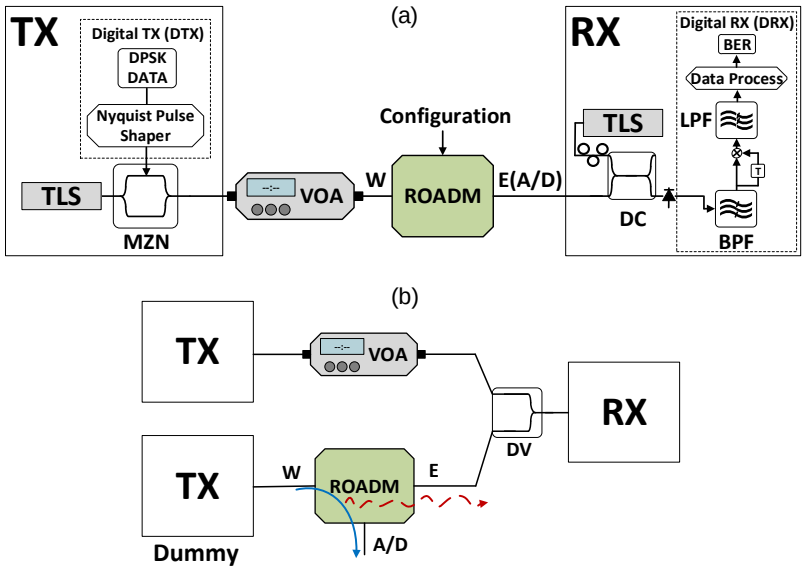

Fig. 2.7. Experimental setup for: (a) sensitivity and (b) crosstalk measurements.

The receiver (RX) was based on a single photodetector heterodyne detection. The local oscillator (LO) was also an external cavity TLS. In the proposed setup, the LO and the signal were coupled at the photodiode using an optical coupler and a polarization controller, though this heterodyne receiver can be easily upgradeable to a polarization insensible heterodyne receiver as it is indicated in [75], [135]. After the heterodyne detector, the

received signal was optically down-converted to an intermediate frequency (IF) equal to 2 GHz. The IF signal passed through a DC block and it was digitized with a 40 GSa/s digital oscilloscope [38], [39], [44]. The first step in the digital processing was the bandpass filtering of the digitized signal with a finite impulse response (FIR) filter in order to reduce the noise. Then, to demodulate the DPSK format, the signal was multiplied with itself delayed one symbol and lowpass filtered with a FIR filter. Finally, the BER was calculated comparing the detected data-stream with the original one. A variable optical attenuator (VOA) was used to modify the received power.

The sensitivity for a FEC limit of 7% OH [120] has been evaluated for a 1 Gb/s data-stream over a 12.5 GHz FS. Nevertheless, the proposed network scenario shown Fig. 2.1 considers that the D and U for an end-user are in the same FS. It has been demonstrated in [38], [39], [44] that the penalty when both U and D are established in the same FS is negligible for a similar transmission as the system shown in Fig. 2.7(a). Therefore, any possible penalty in the sensitivity is just due to the proposed cost-effective nodes and it can be evaluated using only one channel in the FS.

The sensitivity measurement is taken in five different cases. The sensitivity for back-to-back (B2B) transmission is -48 dBm, as shown in Fig. 2.8(a). No sensitivity penalties were observed for a single channel located out-band and in-band for pass-through configuration and also for in-band for the add/drop configuration, at the single module ROADM characterized in Fig. 2.6. Hence, neither the used latched switches nor the band filters do add any observable penalties.

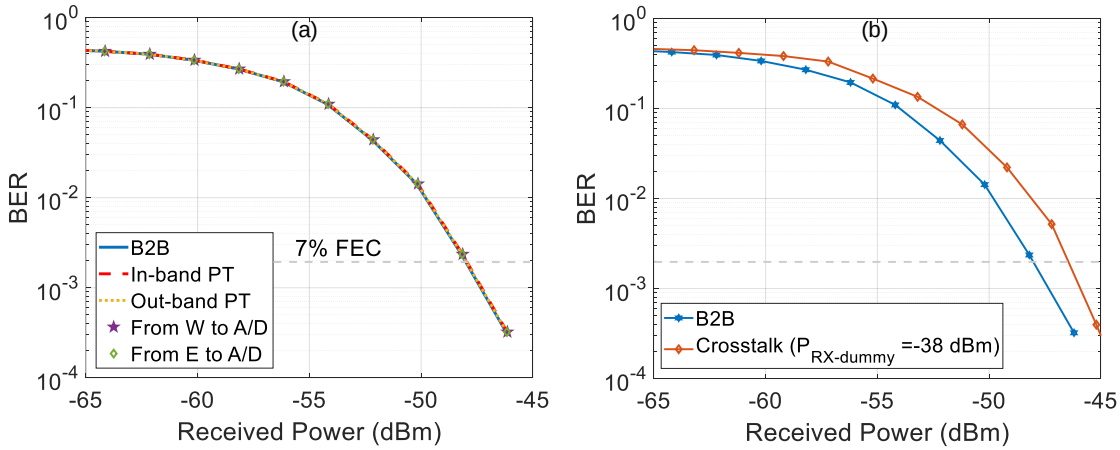

Fig. 2.8. (a) BER versus received power for a 1Gb/s over a 12.5 GHz frequency slot for back-to-back (B2B), pass-through (PT) and add/drop (A/D) configurations. (b) BER versus received power for a 1 Gb/s data-stream over a 12.5 GHz frequency slot when a similar channel is dropped at the ROADM A/D port.

In order to measure the impact of the limited pass-through isolation between W and E ports (35 dB, Fig. 2.6), the following crosstalk measurement has been done (Fig. 2.7(b)): a dummy 1 Gb/s data-stream over a 12.5 GHz FS is dropped at the ROADM A/D port, while the BER of another similar 1 Gb/s channel at the same wavelength is measured. For a dummy channel received power of -38 dBm, the crosstalk penalty is 1.75 dB as shown in Fig. 2.8(b). That crosstalk penalty value is reduced as the number of modules increases.

2.6 SDN control plane for future converged metro-access network

The SDN-based architecture proposed is depicted in Fig. 2.9. The figure depicts an overall design, which is valid for every type of optical nodes described in the previous sections. The architecture shows a full north-south integration, including the optical node to be controlled, the agent of the optical node that enables the SDN-based configuration of the node, the SDN controller itself, and the REST APIs that communicate the controller with the upper layers (i.e. applications, orchestration, etc.). The modelling of each node becomes crucial to define the requirements for the agent running on top of it. In this case, each particular agent contains a set of modules that allow the communication between the optical node and the SDN controller. As shown in Fig. 2.9, the hardware communication module establishes a connection towards the optical node, providing control and retrieval of optical features. The information model module sets up a local database, where the node state information is stored in XML format. Finally, the OpenFlow protocol module establishes an OpenFlow (OF) protocol-based connection [136] with the controller, exposing the particular node features and capabilities. For this purpose, an extended version of the OF protocol can be used, which allows handling the features of the optical nodes.

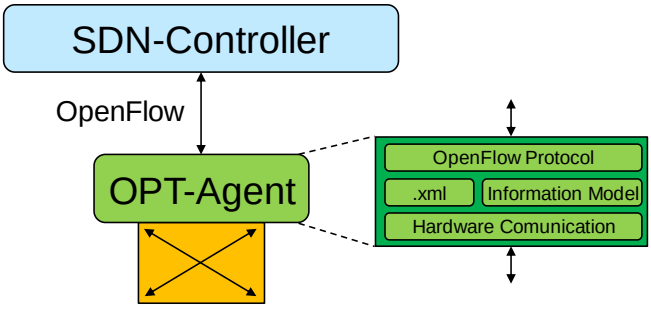

Fig. 2.9. SDN-based optical node.

The SDN controller defines the centralized logic component of this architecture, where the information received from the optical node, through OF protocol messages, is analysed and exposed to upper layers (e.g., applications, orchestration) by means of well-

implemented northbound REST APIs [137]. These types of APIs provide access to optical related data managed by the controller.

2.7 Conclusions

In this chapter, a model for each of the presented node is proposed: OMCN, OAN, ROADM, OXC, ONU. Each model includes the basic functionality of each network node and its most representative attributes. In particular, a set of transmitters and receivers proposed in the literature have been considered for the OMCN, OAN and ONU implementation supporting u-DWDM feature. Moreover, a cost-effective DWDM ROADM and OXC, whose implementation maximum cost value is at least 1 order of magnitude (or even 2 orders of magnitude, depending on the configuration) lower than a WSS-based ROADM and OXC, have been proposed in order to satisfy the future metro-access networks convergence requirements. Also, the investigated cost-effective DWDM ROADM and OXC requires a factor 5 less energy to operate than a WSS-based ROADM and OXC. A spectrum characterization of single module of the cost-effective DWDM ROADM and OXC has been also performed. From this characterization, a general insertion losses model for the cost-effective ROADM and OXC with N modules has been proposed. Finally, the north to south architecture of the network control plane is proposed as well. In this, the optical resources can be managed directly from the application level.

Chapter 3. Cost-effective DWDM ROADM Design to Maximize the Capacity of Ring-Based u-DWDM Coherent Metro-Access Networks

3.1 Introduction

ROADMs are considered as the key element for future converged metro-access networks because they reduce the instances of O-E-O conversions by setting all-optical links between metro and access nodes (see Fig. 3.1). Benefits of this solution include terabits per second bandwidth with low bit error rates, lower network's power consumption, data transparency, and freedom from interference leading to a secure communication system.

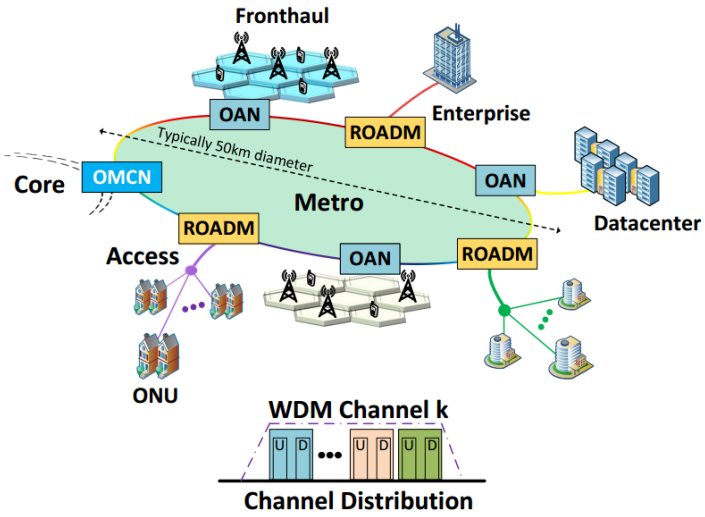

Fig. 3.1. Flexible 5G ring-based metro-access network scenario. (Inset) Considered flexible ultra-dense WDM frequency slot division.

The ROADM design is basically driven by new network-level requirements, such as full flexibility, adaptability, scalability, resilience and increased energy-efficiency [1], [45], [46], [47], [48], [49], [50]. In order to reach those features, two alternative colorless directionless ROADM architectures, which can be used in ring-based u-DWDM metro-access network scenarios as shown in Fig. 3.1, have been proposed in chapter 2. The first ROADM solution, being fully flexible and compacted but far more expensive, is based on wavelength selective switches (WSSs) that can work with frequency slot (FS) granularity. Using this WSS-based ROADM, the add/drop (A/D) and pass-through (PT) functions can be run over each FS individually (see Fig. 3.2). The second ROADM solution, more cost-

effective and modular, works with DWDM channel granularity. In particular, a module consists of two DWDM fixed filters and two switches that manage one DWDM channel (Fig. 3.2). Then, the A/D and PT functions can be applied on a group of FSs at the DWDM channels of the DWDM ROADM (D-ROADM), see Fig. 3.2. For a group of FSs whose DWDM channel is not supported by the D-ROADM, it is transparent for them, achieving vendors' requirements. Taking into account that the D-ROADM switches a group of FSs, the main target of the chapter is to demonstrate if networks based on cost-effective D-ROADM with a low number of modules (N) could achieve a similar performance as networks using colorless WSS-based ROADMs for both online and offline scenarios.

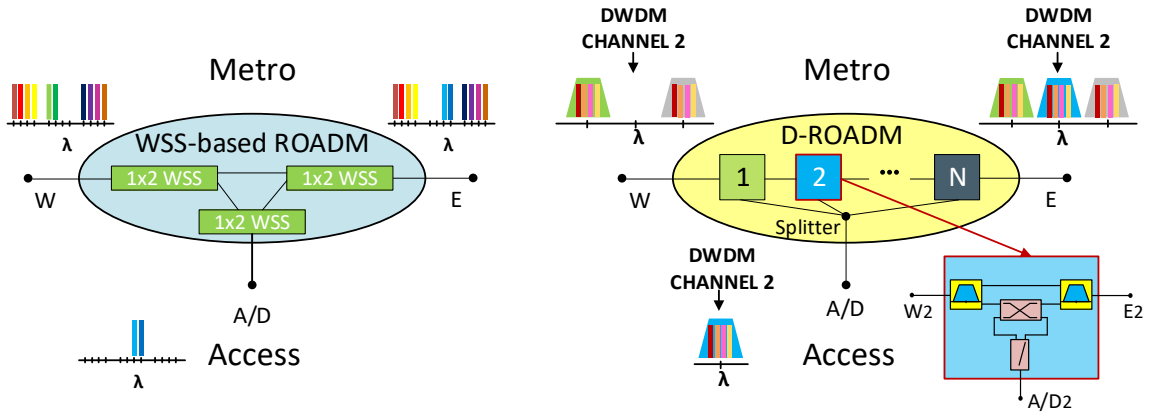

Fig. 3.2. WSS-based ROADM vs. DWDM ROADM (D-ROADM) functionalities.

The remainder of this chapter is structured as follows. Section 3.2 shows main concepts about resource allocation in FlexGrid networks, defining both offline and online scenarios. Section 3.3 studies the design of ring-based metro-access networks with D-ROADMs to prove the cost-effective D-ROADM capabilities in an offline scenario. Specifically, sub-section 3.3.1 presents the offline problem statement, sub-section 3.3.2 shows a heuristic based on an iterative process for the design of each D-ROADM of a network to obtain the achievable network throughput, sub-section 3.3.3 presents the details and assumptions of the evaluated u-DWDM metro-access network scenario and, sub-section 3.3.4 shows the obtained numerical results of evaluating the proposed heuristic with regarding to the throughput of a network against to the same network using WSS-based ROADMs. Section 3.4 studies the ring-based metro-access network design with D-ROADMs for an online scenario. Sub-section 3.4.1 shows the online problem statement for the design of ring-based metro-access networks with D-ROADMs, sub-section 3.4.2 presents two different heuristics for the design of the D-ROADMs of a network, sub-section 3.4.3 shows the details and assumptions of the evaluated networks, sub-section 3.4.4 gathers the obtained

numerical results of evaluating both heuristics with regarding to the traffic load capacity of a network compared to the same networks using WSS-based ROADMs. Finally, section 3.5 completes the chapter with the main conclusions.

3.2 Resource allocation in FlexGrid networks

Resource allocation (RA) is one of the important problems in optical networks for service provisioning since an efficient strategy increases the quality-of-service (QoS) and, hence, the incomes of network's operators. In this section, it is presented different aspects to be considered during RA process for both offline and online scenarios.

The RA problem consists of fulfilling connection demands given some input parameters such as network topology, frequency grid granularity, network equipment, traffic demand, etc. The RA is commonly oriented towards the minimization of the network cost, power consumption or maximization of QoS. In order to evaluate the efficiency of RA process, several network metrics can be used such as throughput, blocking probability, blocking bandwidth probability, spectral utilization, spectral occupation, spectrum fragmentation, connection provisioning time, etc.

At the data plane (or physical layer), connection demands are established through lightpaths. Essentially, a lightpath is a physical path (route) plus the spectrum range over which optical signals are transmitted. Initially, the spectrum range was denoted as wavelength in traditional WDM networks arising the well-known route and wavelength assignment (RWA) problem [138], [139], [140], [141]. This problem can be jointly solved or can be divided into sub-problems [142].

For solving the route assignment sub-problem, there are three basic approaches, namely, fixed, fixed-alternate and adaptive routing [138]. The fixed approach is the simplest and consists of assigning always the same path, for example, the Dijkstra shortest path (SP). Fixed-alternate maintains a kind of pre-computed routing table with an ordered set of K-SPs computed, for example, by means of Yen's algorithm [143]. Finally, adaptive routing approach is the most flexible allowing assigning dynamically different routes depending on the network state, e.g., the spectrum occupation, physical layer impairments, etc.

Regarding wavelength assignment, in WDM networks, channels of fixed spectral width (for example, 50 GHz) are assigned to connections. Later on, when the concept of FlexGrid networks appeared, the term wavelength was generalized to as FS (with spectral width of

12.5 GHz), thus giving rise to the route and spectrum assignment (RSA) problem [142], [144].

Finally, there are two important constraints to be considered for spectrum assignment. The first one is the spectrum continuity that imposes to assign the same spectrum range along the path for transparent routing. Since FlexGrid allows assigning a set of FSs, the second constraint, namely, spectrum contiguity states that these FSs have to be contiguous in all links of the selected path. Different allocation policies for spectrum assignment sub-problem can be used, e.g., first-fit, last-fit, best-fit, random-fit, etc.

3.2.1 Offline scenario

This scenario assumes that all traffic demands are known in advance and the target is to accommodate such traffic demands in the most efficient way. Essentially, RA problem for this scenario can be solved by using two approaches, namely, integer linear programming (ILP)-based and heuristic-based algorithms [145].

On the one hand, ILP-based algorithms are mathematical formulations of the problem expressed in the form of an objective function plus some constraints, which are linear. They provide optimal solutions pursuing a maximization or minimization objective. The main drawback of this type of solutions is that time complexity can significantly grow with the problem size. In fact, several works in the literature have demonstrated that RWA and RSA problems are non-deterministic polynomial (NP)-hard (i.e., the problem cannot be optimally solved in a deterministic time by means of an algorithm) [146], [147]. On the other hand, heuristics are practical methods of finding sub-optimal solutions.

3.2.2 Online scenario

Unlike offline scenarios, in an online scenario, traffic demands arrive/departure to/from the network randomly. Two parameters define the traffic demands profile in online scenarios. The first one is the inter-arrival time (IAT) which is defined as the time between each traffic demand arrival and the next. The second one is the holding time (HT) that corresponds to the time in which a traffic demand occupies some network resources [148]. In general, traffic demands are one-by-one allocated in a network as they arrive to the network. Since connections with different spectrum requirements are set-up and turn-down, the spectrum fragmentation is an “intrinsic issue” of dynamic FlexGrid networks [149], [150], affecting the overall network performance. Solving this issue requires of defragmentation techniques [151].

3.3 Metro ring network design based on cost-effective DWDM ROADM: offline scenario

In this section it is studied the performance of the proposed cost-effective D-ROADM as an all-optical metro-access converging element in an offline scenario. The assessment is, therefore, performed in terms of the maximum throughput that the network can achieve taken into account that each DWDM channel is divided into FS and the proposed cost-effective ROADM switches all frequency slots of a DWDM channel in the same direction, as described previously. It shall be also proved that to reach that maximum throughput value it is not necessary that all D-ROADMs of the network present the colorless feature. That also means a reduction of the implementation cost and the insertion loss of some of the D-ROADMs of the network. For that purpose, a network simulator has been implemented in MATLAB™.

3.3.1 Offline problem statement

In our study, two important aspects must be considered. The first one is that the proposed D-ROADM switches all frequency slots of a DWDM channel in the same direction through the configuration of the switches of each module. The second one is that the cost-effective ROADM provides higher switching flexibility and therefore higher network throughput when a higher number of modules is used. Nevertheless, the D-ROADM insertion loss increases with the number of modules. Hence, a problem to solve here is to find out the minimum number of modules of each D-ROADM of the network and their switches configuration so as to reach the network throughput maximum value, while keeping the cost-effective ROADM insertion losses as low as possible. In this way, the optimal design solution for a cost-effective D-ROADM may lose the colorless feature, therefore its implementation cost is thus reduced.

3.3.2 Cost-effective DWDM ROADM design with a heuristical approach

A greedy way to determine the best configuration of each D-ROADM to support the maximum throughput would be to consider firstly that each cost-effective D-ROADM is able to commute all the DWDM channels. In this way, the problem is simplified to search for the best configuration of the D-ROADM module's switches. Then, the useless modules or the modules which are configured to work as pass-through mode have to be removed. However, this technique may dramatically increase the computational complexity with the number of ROADMs (N_{ROADMs}) and DWDM channels (N_{DWDM-C}) of the network.

Specifically, knowing that each module of the D-ROADM has three possible operation modes, a set of $3^{N_{DWDM-C} \cdot N_{ROADMs}}$ different network configurations have to be analysed to learn the network configuration that best suits to the traffic demands set. This means that the offline RSA problem has to be solved for each possible network configuration. Thus, for example, for a simple network with N_{ROADMs}=2 and N_{DWDM-C}=3, the number of times that the offline RSA must be solved is 729 times, while for the same network working in the whole C band, i.e. $N_{channels}$=20 using modules with 125 GHz of effective bandwidth (bandwidth value measured in the chapter 2), is ~$1.2 \cdot 10^{19}$. Therefore, this technique is unviable. Alternatively, the following heuristic can be used:

1. A first step involves finding the best configuration of the switches per D-ROADM in a network to achieve a throughput maximum value when a different DWDM channel is assigned to each D-ROADM of a network. To find that throughput value out, the offline RSA problem must be solved $2^{N_{ROADMs}}$ times, covering all possible network configurations when E-A/D and W-A/D configurations are only considered for a D-ROADM's module. In this initial step, the D-ROADM pass-through configuration is not considered since it causes disconnection between the ring part of the network and the PONs. In case different configurations generate the same network throughput maximum value, the configuration of the D-ROADMs which presents a smaller value of the worst-case path attenuation of the network ($\alpha_{P_{WC}}$) is selected. The worst-case path of a network (P_{WC}) is defined as the path between a pair of source-destination nodes which presents the highest total attenuation of the network. Such P_{WC} value must always be lower than the considered power budget per connection; otherwise more sophisticated transmission technologies, providing a higher power budget, would be required.
2. For each D-ROADM, we calculate the utilization factor (UF). This factor is defined as the sum of the number of occupied FS between each pair of I/O ports, that is E-W, E-A/D, and W-A/D.
3. In this step, it is decided which D-ROADM is going to be upgraded to explore potential increase of the network's throughput. The considered upgrading rule is adding extra modules to the D-ROADM which presents the minimum UF value. If the D-ROADM with minimum UF is the same as the D-ROADM of the previous iteration, we select the D-ROADM with the next higher UF minimum value to the current D-ROADM. If different D-ROADMs have the same UF, we select one of them randomly.

4. After the selection of the D-ROADM to be upgraded, ROADM$_x$, it is determined the number of modules, N_x, for upgrading ROADM$_x$. For that purpose, the next equation can be used:

$$N_x = min\left\{ \frac{\frac{N_C \cdot BW_{DWDM-C}}{BW_{FS}} - UF_x}{\left(\frac{BW_{DWDM-C}}{BW_{FS}}\right)}, \frac{\left(\frac{AR}{100} - \frac{NDS_{PON_x}}{\frac{N_C \cdot BW_{DWDM-C}}{BW_{FS}}}\right) \cdot ND_{PON_x}}{\left(\frac{BW_{DWDM-C}}{BW_{FS}}\right)} \right\} \quad (3.1)$$

where:

- N_C is the number of the DWDM channels of the network, $N_C = N_{DWDM-C}$.
- BW_{DWDM-C} is the bandwidth of the DWDM channel. It coincides with the effective BW (BW_{eff}) of each ROADM module.
- BW_{FS} is the bandwidth of each frequency slot (FS).
- UF_x is the previous defined utilization factor of the ROADM$_x$.
- AR is a percentage that determines the amount of resources which can be assignment to each PON.
- ND_{PON_x} is the total number of demanded frequency slots that present origin or destination in a node belonging to the PON connected to ROADM$_x$.
- NDS_{PON_x} is the number of frequency slots of ND_{PON_x} that have been allocated until the current iteration.

The first term of Eq. (3.1) represents the potential maximum modules number taking into account the number of FSs that are available. The second one allows determining the modules number as a function of the resources assigned to each PON. It opens the possibility to assign different priorities to the different PONs connected to the metro network. The minimum of both terms has to be selected because there might not be enough allowed FSs to establish the priority required. This situation takes place when throughput of the network is close to the achievable maximum. If N_x value is a non-integer, it is rounded to the nearest integer.

5. For determining which DWDM channels can be allocated to ROADM$_x$, we select those DWDM channels whose FSs are not associated with any demand for the different pair of the D-ROADM I/O ports.
6. For the added modules, it is searched the best switches configuration in order to reach a new maximum throughput value, keeping the switches configuration of previous

D-ROADM modules unchanged. In this step, the RSA problem must be solved $2 \cdot N_x$ times.

7. This process is iterated from step two until all D-ROADMs have been treated.

Taking into account the proposed heuristic, the total number of times that the RSA problem must be solved is $(2^{N_{ROADMs}} + 2 \cdot N_x) \cdot N_{ROADMs} \ll 3^{N_{DWDM-C} \cdot N_{ROADMs}}$, since $N_x \leq N_{DWDM-C}$. Thus, for example, considering N_{ROADMs}=2, N_{DWDM-C}=20 and N_x=N_{DWDM-C} (the worst case), the number of times that the RSA problem must be solved using the proposed heuristic is 88 times, while using the greedy way is ~$1.2 \cdot 10^{19}$ times.

3.3.3 Scenario details and assumptions

The metro-access network shown in Fig. 3.3 is considered as a reference scenario. In fact, Fig. 3.3 presents a typical scenario for an urban/suburban use case, where a ring metro network, featuring a total maximum length of 60 km, serves different passive optical networks (PONs), each covering distances ranging from 2.3 km up to 2.6 km. Specifically, the proposed scenario consists of one OMCN, five OANs, four ROADMs and a PON connected to each ROADM. The ONUs numbers connected to the different PONs are 4, 8, 16 and 32, just to test different scenarios.

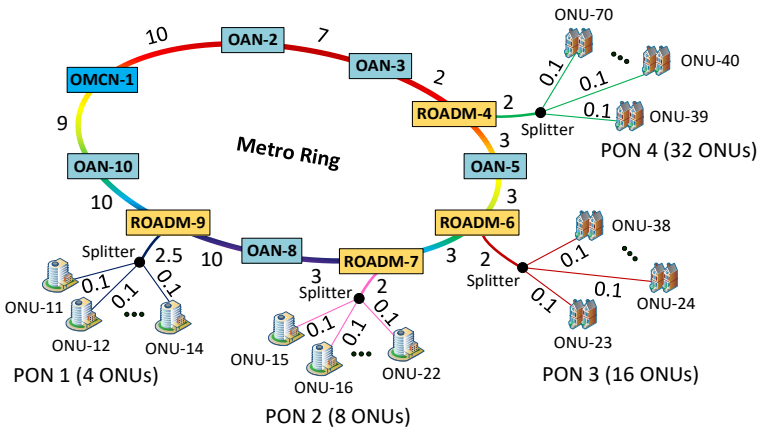

Fig. 3.3. Network topology considered. Link distances are shown in km.

For the sake of simplicity, it is considered that the OMCN, OAN and ONU nodes are able to add/remove specific channels to/from the network to which they are connected. In chapter 2, it has been proposed a set of different cost-effective solutions for transmitters and receivers and their main attributes for those opto-electrical nodes implementation. In addition, it has been indicated that all those transmitters and receivers can be adapted to implement different u-DWDM transmission techniques in which the uplink and downlink of each user can be established in each FS by frequency or polarization division

multiplexing. It is selected the pair of transmitter and receiver which provides the highest power budget for all opto-electrical nodes implementation. Following such premise, it is considered that the OMCN and OAN, which are usually more expensive equipment, are implemented by Mach-Zehnder transmitters able to provide modulation formats, as Nyquist-DPSK, featuring high spectral efficiency. On the other hand, ONU transmitters, much more cost sensitive, could be based on either distributed feedback (DFB) lasers or much lower cost vertical cavity surface emitting lasers (VCSEL). For the latter, it has been recently demonstrated the support of DPSK modulation [43] and potentially providing similar spectrum reduced Nyquist-DPSK modulation. The chosen receivers are based on a coherent receiver in which the detected signal is mixed with a local oscillator. As a reference, a DFB local oscillator has been considered, providing a sensitivity of -52 dBm [38], [44]. Therefore, the power budget per connection is 52 dB for transmitters providing 0 dBm output.

The power budget is considered to be only consumed by the fiber attenuation (0.25 dB/km is assumed), the ROADM insertion loss and the power splitter at PONs. Correspondingly, the OMCN, OAN and ONU insertion losses are null due to their O-E-O conversion. Chromatic Dispersion (CD) effects due to the optical fiber are not considered as the maximum transmission distance at the network is below the theoretical maximum distance of the link, before considering CD effects (e.g. 61 km for standard ITU G.652 fibres [152]). Nevertheless, if CD effects should be considered, extended coherent receivers providing CD compensation could also be considered.

A work band of 500 GHz has been considered as the network resource to share between all users. That work band is considered in order to reduce the computational cost. However, results would scale linearly for higher work bands. Three DWDM channel widths have been considered: 62.5 GHz, 125 GHz and 250 GHz. Being 125 GHz, the effective bandwidth obtained for a cost-effective D-ROADM with a single module characterized in chapter 2 and, 62.5 GHz and 250GHz are the half and double of that characterized effective bandwidth, respectively. Each DWDM channel has been divided into FSs, with width of 12.5 GHz, although other FS widths could be used, such as 6.25 GHz or 5 GHz.

The aforementioned network scenario is loaded with traffic demands distributed uniformly between all pairs of source-destination nodes. All demands are of 10 Gb/s so each accepted demand requires one FS. In particular, the two physically shortest paths have been pre-computed for every pair of source-destination of the network, and the spectrum resources, FSs, are allocated following the first-fit policy. That heuristical approach

delivers sub-optimal solutions for large-moderate size problems [153].

3.3.4 Simulation results and discussion

First, it will be evaluated the considered network scenario (Fig. 3.3) in which the work band of 500 GHz is divided into four DWDM channels of 125 GHz . For this situation, two cases will be discussed. The first one is when a different channel is assigned to each cost-effective D-ROADM. The second one consists of searching for the best configuration of each D-ROADM to reach the maximum throughput following the iterative process detailed previously. Both of them will be compared to the reference case in which the ROADMs are based on WSS and they can switch each frequency slot individually. Finally, it will also be discussed the throughput maximum value behaviour when the network DWDM channel width is changed. Fig. 3.4 shows a scheme of the methodology used to compare the network design using cost-effective D-ROADMs and WSS-based ROADMs. For a fair comparison, in both cases, 2 shortest paths (2-SPs) and first-fit policy have been considered to solve the RSA problem. Therefore, the proposed heuristic is focused on which DWDM channel or channels must be assigned to each D-ROADM of the network to reach the achievable throughput of the network.

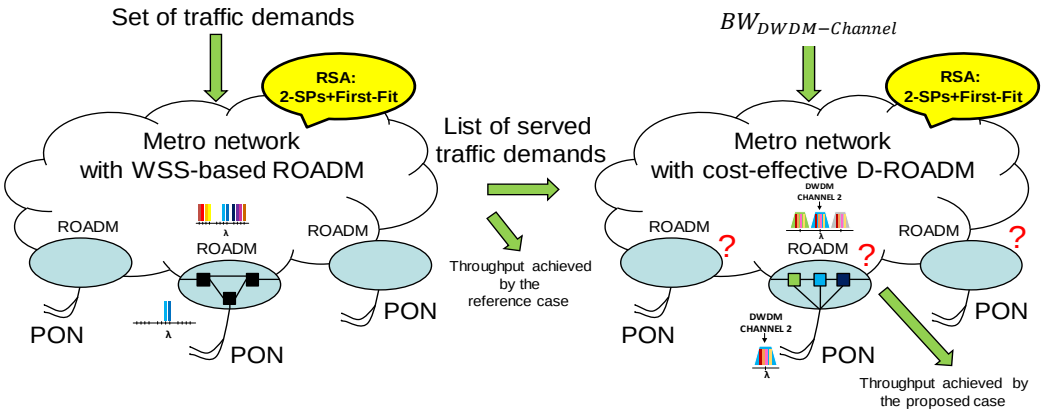

Fig. 3.4. Scheme of the methodology used to compare the network design with cost-effective D-ROADMs and WSS-based ROADMs.

An important aspect to study in the management of the network resources is how they are assigned. A way to allocate those DWDM channels is to assign one to each PON without repetition. In this way, all users of the same PON share the same DWDM channel. This strategy coincides with the first step of the iterative process proposed previously and it is the simplest solution in the design of a ring-based metro-access network with D-ROADMs. Starting with that solution and using the iterative process presented in section 3.3.2, a better solution can be achieved. In this situation, different PONs can share the same

DWDM channels.

Table 3.1 shows the maximum value of the throughput of the proposed network in three different cases: *i)* the Reference Case in which the ROADMs are based on WSS and they can switch each frequency slot individually without any constraint; *ii)* Case A that corresponds to the situation wherein the D-ROADMs commute all the FS of a DWDM channel in the same direction and a different DWDM channel is assigned to each D-ROADM, and, *iii)* Case B that is the result of using the iterative process to reach the throughput maximum value when cost-effective D-ROADMs are applied. For each case, the worst-case path attenuation of the network, $\alpha_{P_{WC}}$, and the percentage of allocated traffic demand, Δ, are also reported. That allocated traffic demand percentage is measured against the maximum throughput value of the Reference Case. From Table 3.1, it can be deduced that reusing DWDM channel for different PONs the allocated traffic demand can be increased up to 79% of the Reference Case whilst in Case A the allocated traffic demand is 53.6%. In addition, the worst-case path of Case B is 43.1 dB, well under the considered power budget of 52 dB.

Table 3.1. The worst-case path attenuation of the network ($\alpha_{P_{WC}}$), throughput and allocated traffic demand for the Reference Case, Case A and Case B.

Parameter	Reference Case	Case A	Case B
$\alpha_{P_{WC}}$ (dB)	32.3	35.8	43.1
Throughput (Gb/s)	1380	740	1090
Δ (%)	100	53.6	79

Table 3.2 shows the DWDM channel assigned to each ROADM in the Case B. That assignment is the result of using the iterative process for some assigned AR values, see Eq. (3.1). AR is the traffic priority assigned to a PON of the network. In particular, 100%, 50%, 25% and 25% are the considered AR values for the PONs connected to ROADM$_4$, ROADM$_6$, ROADM$_7$ and ROADM$_9$, respectively.

Table 3.2. ROADMs configuration for Case B. Grey colour is an assigned channel to the ROADM$_x$.

ROADM$_x$	*AR* (%)	Modules Number	Channel			
			1	2	3	4
4	100	4				
6	50	2				
7	25	1				
9	25	1				

Finally, Table 3.3 shows the throughput maximum value of the proposed network as a

function of the DWDM channel bandwidth (BW_{DWDM-C}), specifically for bandwidth of 62.5 GHz (Case C), 125 GHz (Case B, previously studied), and 250 GHz (Case D). For the same AR of each PON as in case B, the $\alpha_{P_{WC}}$ and Δ are also specified. For the cases C and D, the iterative process, described in sub-section 3.3.2, has been applied in order to determine the network's throughput maximum value. Hence, the modules number of each cost-effective D-ROADM shown in Fig. 3.3 and their assigned channels do not correspond to Case B. From Table 3.3, it is appreciated that the DWDM channel bandwidth is reduced and the allocated traffic demand is higher. It is due to the fact that the number of wasted FSs per DWDM channel to satisfy the assigned *AR* for each PON is smaller. However, the ROADMs' number of modules is higher, increasing thus the worst-case path attenuation $\alpha_{P_{WC}}$. So, a trade-off solution is when the cost-effective ROADM's DWDM channel width is of 125 GHz (Case B).

Table 3.3. The worst-case path attenuation of the network ($\alpha_{P_{WC}}$), throughput and allocated traffic demand as a function of the DWDM channel bandwidth (BW_{DWDM-C}).

Parameter	Case B	Case C	Case D
BW_{DWDM-C} (GHz)	125	62.5	250
$\alpha_{P_{WC}}$ (dB)	43.1	47	36
Throughput (Gb/s)	1090	1190	960
Δ (%)	79	86.2	69.7

3.4 Metro ring network design based on cost-effective DWDM ROADM: online scenario

In this section it is studied the performance of the proposed cost-effective D-ROADM as a metro-access ring network element in an online scenario knowing that each module of the D-ROADM switches a group of FSs and the D-ROADM optical insertion losses increase with the number of modules (N). Keeping that in mind, two different heuristics have been proposed to find out the best D-ROADMs design of a network that optimize the traffic load capacity of the network.

3.4.1 Online problem statement

In our study, three important aspects must be considered:

1. The first one is that the D-ROADM that does not support the contentionless feature. It can cause that the resulting logical graph from the union of each DWDM channel's equivalent graph of the network is disconnected if the D-ROADM design is not properly managed. In this way, a bad design of the network D-ROADMs can prevent

the establishment of connections between every possible pair of source-destination nodes of the network since may not be feasible to find a path for any DWDM channel of the network, leading to a high number of blocked traffic demands. Fig. 3.5 presents an example of the design of the D-ROADMs for a three-DWDM-channel network that permits to highlight the mentioned problem. For each DWDM channel of the network shown in the example (see Fig. 3.5), all possible logical paths are schematically depicted, as well as the channels assigned to each D-ROADM. The design strategy chosen for this example consists of assigning all DWDM channels to each D-ROADM and configuring the switches of each ROADM module to work in add/drop mode over its different ring ports (W port or E port). That is, a module settled allowing paths between A/D port and W port, and the others two modules for A/D port and E port. That strategy can in principle seem appropriate as the traffic demands of both PONs can be routed by two different physical paths. Nevertheless, making a deep inspection of the network, we can realize that the resulting network's logical graph is disconnected. In this way, for example, there is no a logical path between nodes with IDs 1 and 4, and between nodes with IDs 2 and 4. In order to solve that problem two different heuristics will be presented in sub-section 3.3.2.

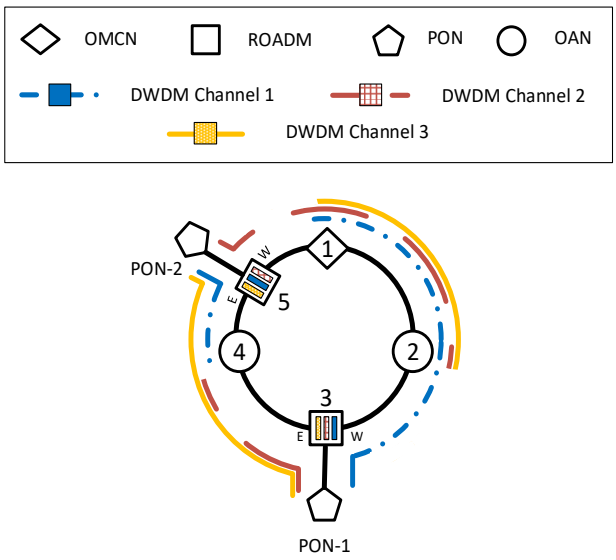

Fig. 3.5. An example of design of the D-ROADMs of a simple ring-based network whose resulting logical graphs from the union of the equivalent graph for each DWDM channel of the network is disconnected.

2. The second aspect to consider is that the D-ROADM provides higher switching flexibility when a higher number of modules is used. However, the D-ROADM insertion loss increases with the number of modules (N) due to the use of a power splitter (see Fig. 3.2) to combine the DWDM channels supported by the D-ROADM.

3. Finally, the third aspect is that it is considered an online scenario in which demands arrive at and depart from the network in a random manner. Moreover, it is also considered that traffic demands are distributed between all pair of source-destination nodes of the network randomly. Then, the D-ROADM design should be adapted to the dynamic traffic profile so as to reduce the total traffic demands blocked.

Table 3.4. Notations used in the description of the D-ROADM designs heuristics.

Symbol	Definition
$\mathcal{G} = (\mathcal{N}, \mathcal{E})$	Graph representing the optical network, where $\mathcal{N}$ is the set of nodes (OMCN, OAN, ROADM and ONU) and $\mathcal{E}$ is the set of optical links of the analysed network.
BW_N	Total network bandwidth (GHz).
BW_{DWDM-C}	DWDM channel bandwidth (GHz).
PB_o	Power budget available per connection (dB).
$\alpha_{P_{WC}}$	Worst-case path attenuation of the network (dB). P_{WC} is defined as the path between a pair of source-destination nodes which presents the highest total attenuation of the network.
$\mathcal{D}$	Dynamic traffic demands profile loaded to the network, characterized by: *i)* how the traffic is distributed between the nodes (e.g. uniformly), *ii)* what traffic arrival process follows and what type of distribution presents the durations (e.g. Poisson and negative exponential, respectively) and *iii)*, the average requested bit rate per demand, $\bar{C}$, arrived at the network. Each demand, $d \in D$, is determined by (s_d, t_d, n_d), where s_d and t_d are source and destination nodes, and $n_d \in \mathbb{Z}^+$ is the number of FSs requested by the demand.
ρ	Traffic load (in erlang units).
TLC	Traffic load capacity, defined as $\rho \cdot \bar{C}$ (b/s).
BBP	Blocking bandwidth probability, defined as the volume of rejected traffic divided by the volume of all traffic demanded to the network.
BD_{ring}	Number of blocked demands which have their origin and destination in a node of the ring part of the network.
BD_{PON-i}	Number of blocked demands which have their origin or destination in a node belonging to PON-i.
$RSA(\mathcal{G}, \mathcal{D}, BBP)$	Sub-routine that solves the dynamic routing and spectrum assignment of all traffic demands arrived at the network in the simulations. The input parameters are the network model ($\mathcal{G}$), the traffic demands profile loaded to the network ($\mathcal{D}$) and the considered blocking bandwidth probability (BBP). The output parameters are the *TLC* of $\mathcal{G}$ for the considered BBP value and the number of blocked demands of the different network's parts (BD_{ring} and BD_{PON-i}). Pre-computation of the two-lowest loss path between all pair of source-destination of the network and the first-fit policy for allocating FSs are considered to solve the dynamic RSA.

Taking into account the three aspects previously discussed, the problem to solve here is to find out the minimum number of modules of each D-ROADM of the network and their switches configuration that best suit to the traffic profile loaded to the network, while

keeping the D-ROADM insertion losses as low as possible. In next sub-section, two heuristics are proposed for solving mentioned problem. To ease the comprehension of the proposed heuristics, Table 3.4 details the notations used in their description.

3.4.2 Cost-effective DWDM ROADM design with heuristical approaches

3.4.2.1 Heuristic I

A strategy that allows solving the mentioned problem of the logical disconnection of the network is shown in Fig. 3.6. This strategy is based on assigning a different channel or channels between the D-ROADMs of the network and settling the switches of each module associate with each channel to work in add/drop mode over any ring port of the D-ROADM (E port or W port) as it is shown in Fig. 3.6.

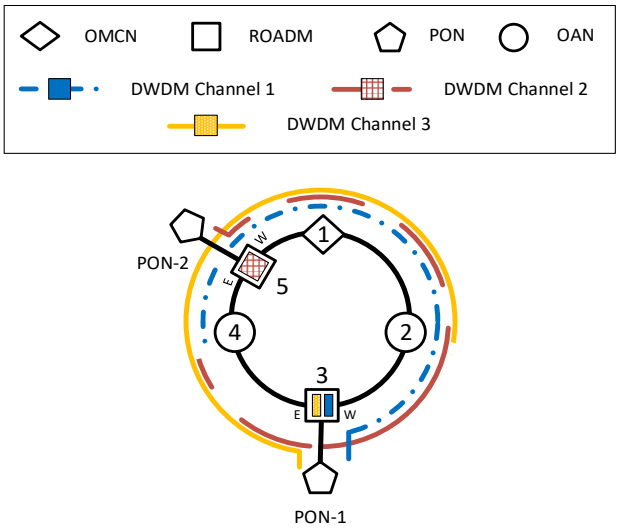

Fig. 3.6. An example of design of the D-ROADMs of a simple ring-based network whose resulting logical graphs from the union of the equivalent graph for each DWDM channel of the network is not disconnected by using heuristic I.

As it can be seen in Fig. 3.6, the connection between all possible nodes of the network can be established using the available resources. In this strategy, it is considered that for allocating traffic demands between nodes belonging to the ring part of the network and between nodes of the ring and nodes of a PON, it must be used the same available resources. Thus, for example, for allocating traffic demands between node with ID 4 and nodes of the PON, the DWDM Channel 2 can be used for such purpose (Fig. 3.6). On the contrary, if a traffic demand presents the origin and destination in a node belonging to the ring part of the network, the available frequency slots of any possible channel can be used. For example, for establishing a connection between nodes with IDs 1 and 4 shown in Fig. 3.6, the available set of FSs of the three DWDM channels of the considered network can be

utilized. At the same time, distributing the available DWDM channels between all the D-ROADMs of the network reduces the number of modules (N) per D-ROADM and consequently the D-ROADM insertion losses.

Fig. 3.7 shows a pseudo-code for the proposed heuristic. The input parameters are the model of the network ($\mathcal{G}$), the network bandwidth (BW_N) that is shared by all users, the considered DWDM channel bandwidth (BW_{DWDM-C}) which coincides with the bandwidth of each D-ROADM module, the considered power budget value per connection (PB_o), depending on the chosen modulation format technology, to the received signal can rightly be detected, the traffic nature loaded to the network, defined by $\mathcal{D}$, and the objective BBP value. The output is the network design that maximizes the TLC of the network using the strategy introduced in Fig. 3.6.

1: **Input:** $\mathcal{G}$, BW_N, BW_{DWDM-C}, PB_o, $\mathcal{D}$, BBP

2: **Output:** $NetworkSolutionDesign$

3: **Begin:**

4: $N_{ROADMs} \leftarrow$ Determining the number of ROADMs of $\mathcal{G}$

5: $MNC_N \leftarrow \mathrm{BW_N}/\mathrm{BW_{DWDM-C}}$

7: **if** $N_{ROADMs} \leq MNC_N$ **then**

8: $MNC_{N_0} \leftarrow N_{ROADMs}$

9: $NetworkSolutionDesign_0 \leftarrow$initial design of the network using MNC_{N_0} channels

10: $[TLC_0,\ BD_{ring}, BD_{PON-i}] \leftarrow RSA(NetworkSolutionDesign, \mathcal{D}, BBP)$

11: **while** $\alpha_{P_{WC}}$ of $NetworkSolutionDesign \leq PB_o$ **&&** there are available channels **do**

12: $NetworkSolutionDesign1 \leftarrow$ Adding a new different channel to the D-ROADM connected to the PON-i with the highest BD_{PON-i} of the $NetworkSolutionDesign$ so as to reduce BD_{ring} and BD_{PON-i}. If different PONs have the same number of blocked demands, one of them could be chosen randomly. The added new module's switches are configured to work in add/drop mode over E port.

13: $NetworkSolutionDesign2 \leftarrow$ The added new module's switches of the chosen D-ROADM are configured to work in add/drop mode over W port.

14: $[TLC_1,\ BD_{ring}, BD_{PON-i}] \leftarrow RSA(NetworkSolutionDesign1, \mathcal{D}, BBP)$

15: $[TLC_2,\ BD_{ring}, BD_{PON-i}] \leftarrow RSA(NetworkSolutionDesign2, \mathcal{D}, BBP)$

16: $NetworkSolutionDesign \leftarrow$ Select the module's switches configuration that better suits to the traffic profile according to the TLC of the network's design. If the different switches configurations result in the same TLC, one of them could be chosen randomly.

17: **end while**

18: **else**

19: More network bandwidth is required

20: **end if**

21: **return** $NetworkSolutionDesign$

Fig. 3.7. Pseudo-code of the proposed heuristic I.

As it can be deduced from Fig. 3.7, to make a good management of the network, its number of DWDM channels ($MNC_N = BW_N/BW_{DWDM-C}$) must be greater than or equal to the number of D-ROADMs (N_{ROADMs}) of the network. On the other hand, new modules can be added to the D-ROADMs as required according to $\mathcal{D}$ so as to improve the network TLC for a given BBP as long as the $\alpha_{P_{WC}}$ is lower than the considered PB_o. Then, once an initial network design is obtained ($NetworkSolutionDesign_0$), the dynamic RSA problem is solved to analyse the origin and destination of blocked demands. Extra DWDM channels are, thus, added to the D-ROADMs to allocate those demands. This is recursively done till exhausting the free DWDMs channels of the network. Therefore, this heuristic implements an efficient distribution of the available DWDM channels among the D-ROADMs of the network. From Fig. 3.7, the number of times that the dynamic RSA problem has to be solved is $2 \cdot \left(MNC_N - MNC_{N_0}\right) + 1$, where MNC_N is the number of DWDM channels of the network, previously defined, and MNC_{N_0} is the required number of DWDM channels for the first network design.

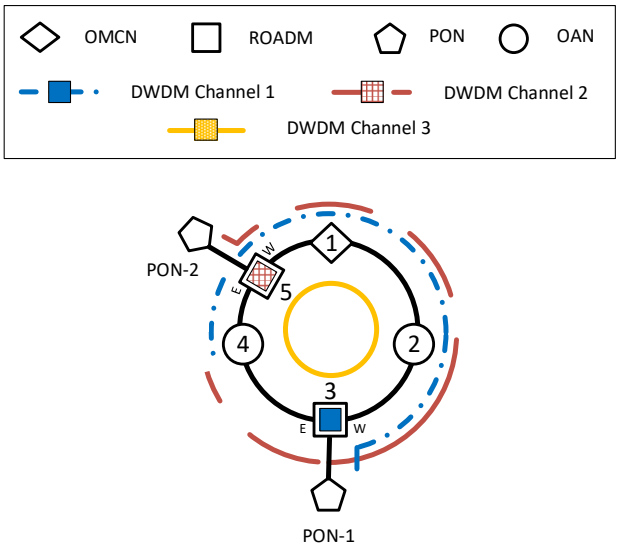

Fig. 3.8. An example of design of the D-ROADMs of a simple ring-based network whose resulting logical graphs from the union of the equivalent graph for each DWDM channel of the network is not disconnected by using heuristic II.

3.4.2.2 Heuristic II

Another strategy that also provides a full logical connection among all the network nodes is introduced Fig. 3.8. That strategy consists of booking one of the available channels for the connections between nodes pertaining to the ring part of the network and using the others two channels for the traffic of the PONs. That is, the DWDM channel 3 can just be used for allocating traffic demands between nodes 1, 2 and 4, and the channels 1 and 2 for

traffic demands of the PONs. This strategy is more efficient that the heuristic previously presented since it allows reusing the WDM channel between different PONs more easily as it shall be proved. Nevertheless, it requires a smarter allocation of the DWDM channels as the network size increases.

Fig. 3.9 shows a pseudo-code of the proposed heuristic II. The input parameters are the same than the heuristic I explained in sub-section 3.4.2.1. The output is the best network design that maximize the TLC of the network. To illustrate the proposed heuristic II, the metro-access network example shown in Fig. 3.10 is used. This example, which will be one of the studied network examples in the sub-section 3.4.4, considers that the network bandwidth (BW_N) is of 750 GHz and the DWDM channel bandwidth (BW_{DWDM-C}) is 125 GHz. The proposed heuristic can be divided into three smaller sub-problems.

1: **Input:** $\mathcal{G}$, $\mathrm{BW_N}$, $\mathrm{BW_{DWDM-C}}$, PB_o, $\mathcal{D}$, BBP

2: **Output:** $NetworkSolutionDesign$

3: **Begin:**

4: *//Sub-problem I*

5: $N_{sectors}$ ← Total number of OMCN and OANs of $\mathcal{G}$

6: MNC_{N_0} ←**MinNumChannelNetwork**($\mathcal{G}$, $N_{sectors}$)+1

8: $BW_{N_0} \leftarrow MNC_{N_0} \cdot BW_{DWDM-C}$

9: **if** $BW_{N_0} \leq \mathrm{BW_N}$ **then**

10: $\mathcal{G}_0$ ← Initial network design of $\mathcal{G}$

11: **if** $\mathrm{P_{WC}}$ of $\mathcal{G}_0 \leq PB_o$ **then**

12: // *Sub-problem II*

13: $\mathcal{G}_1$ ← reuse channel assigned to a mismatched ROADM of a sector of $\mathcal{G}_0$ between mismatched ROADMs of $\mathcal{G}_0$

14: // *Sub-problem III*

15: $NetworkSolutionDesign \leftarrow \mathcal{G}_1$

16: $[TLC_0,\ BD_{ring}, BD_{PON-i}] \leftarrow RSA(NetworkSolutionDesign, \mathcal{D}, BBP)$

17: **while** $\mathrm{P_{WC}}$ of $NetworkSolutionDesign \leq PB_o$ **&&** there are available channels **do**

18: $NetworkSolutionDesign1$ ← Adding a new different channel to the part of the network (ring or PONs) with the highest number of blocked demands according to BD_{ring} and BD_{PON-i}. If different PONs have the same number of blocked demands, one of them could be chosen randomly. The added new module's switches are configured to work in add/drop mode over E port.

19: $NetworkSolutionDesign2$ ← The added new module's switches of the chosen D-ROADM are configured to work in add/drop mode over W port.

20: $[TLC_1,\ BD_{ring}, BD_{PON-i}] \leftarrow RSA(NetworkSolutionDesign1, \mathcal{D}, BBP)$

21: $[TLC_2,\ BD_{ring}, BD_{PON-i}] \leftarrow RSA(NetworkSolutionDesign2, \mathcal{D}, BBP)$

22: $NetworkSolutionDesign$ ←Select the module's switches configuration that better suits to the traffic profile according to the *TLC* of the network's design. If the different switches configurations result in the same *TLC*, one of them could be chosen randomly.

23: **end while**

24: **Else**

25: More sophisticated transmission technologies providing more power budged is required
26: **end if**
27: **Else**
28: More network bandwidth is required
29: **end if**
30: **return** $NetworkSolutionDesign$

Fig. 3.9. Pseudo-code of the proposed heuristic II.

The first sub-problem involves finding out the minimum number of DWDM channels (MNC_{N_0}) that are required in order to make possible to establish the connection between every pair of source-destination nodes. In other words, it must be determined the minimum number of DWDM channels which are required to avoid that the resulting graph of the network is disconnected, following the strategy shown in Fig. 3.8. In that strategy, traffic demands among nodes of the ring part of the network and between ring nodes and nodes of a PON use different DWDM channels. Fig. 3.11 shows the proposed heuristic that can be used in order to reach that goal (MinNumChannelNetwork, in line 6 of the pseudo-code shown in Fig. 3.9).

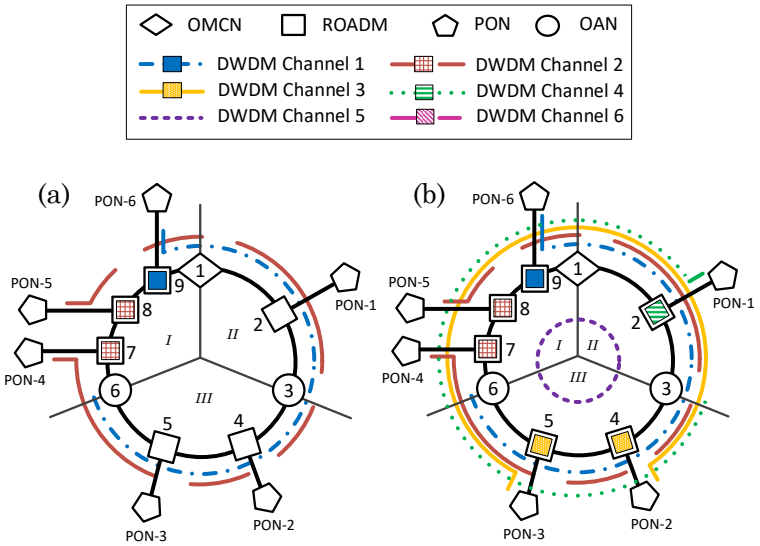

Fig. 3.10. (a) An example of sectioning of a network and (b) its initial design.

1: **Input:** $\mathcal{G}$, $N_{sectors}$
2: **Output:** MNC_{N_0}
3: **Begin:**
4: $MNC_{N_0} \leftarrow 0$
5: Sectorize network ($\mathcal{G}$) into $N_{sectors}$
6: **for** each sector of the network ($\mathcal{G}$) **do**
7: $N_{ROADMs} \leftarrow$ Determining the number of ROADMs
8: **if** N_{ROADMs} != 0 **then**

```
        if N_ROADMs is even then
            MNC_N0 ← MNC_N0 + N_ROADMs /2
        else
            MNC_N0 ← MNC_N0 + (N_ROADMs + 1) /2
        end if
    end if
end for
return MNC_N0
```

Fig. 3.11. Proposed pseudo-code of a heuristic that permits to determine the minimal number of channels required in a metro-access network design in order to ensure that every connection between all possible pair of source-destination nodes can be established.

The heuristic basically consists on dividing the ring part of the network in a certain number of sectors ($N_{sectors}$) and determining the minimum number of DWDM channels that are required in each sector to ensure that every possible connection between nodes of the PON connected to a D-ROADM of the sector and a node of the ring part of the network can be established. In particular, a sector is defined as a pair of two consecutives nodes with opto-electrical conversion functionalities (OMCN or OANs) among which there can or cannot be D-ROADMs. Fig. 3.10(a) shows the way of how the considered network example can be divided into different sectors. Specifically, the network is divided into three sectors (sector I, II and III) because the network has one OMCN and two OANs (see Fig. 3.10(a)). For determining the number of different channels that are required for the D-ROADMs in each sector, the following rule considered in the pseudo-code shown in Fig. 3.11 can be used:

- If the number of ROADMs of the sector (N_{ROADMs}) is even, the number of required channels is $N_{ROADMs}/2$. It is due to the fact that a DWDM channel can be assigned to two different ROADMs of the same sector but with opposite switches' configuration as it can be noticed in see Fig. 3.10(a), sector I, in which the DWDM channel 2 has been assigned to ROADMs with IDs 7 and 8.
- If N_{ROADMs} is odd, an extra channel is required for the ROADM that is mismatched. For example, the DWDM channel 1 has been committed to the ROADM with ID 9 of the sector I which is exhibited in Fig. 3.10(a).

Once determined the number of channels for the D-ROADMs of each sector of the network, and according to the strategy shown in Fig. 3.8, a new channel must be added for allocating the traffic demands among nodes of the ring part of the network. So, the minimal number of required DWDM channels (MNC_{N_0}) in the considered network example (Fig.

3.10) is five of the available six channels. Therefore, the required minimal network bandwidth (BW_{N_o}) to ensure that there are logical paths to establish any possible connection in the network can be calculated as $BW_{N_0} = MNC_{N_0} \cdot BW_{DWDM-C}$. In this way, for a predefined value of the BW_{DWDM-C}, if BW_{N_o} is higher than BW_N, more network bandwidth is required or smaller BW_{DWDM-C}, finer DWDM channel granularity, has to be considered. In other cases, an initial design of the network and its D-ROADMs configuration can be obtained. For the example shown in Fig. 3.10(a), the initial design of the network is shown in Fig. 3.10(b). It is the simplest solution in the design of a metro-access network based on D-ROADMs. This initial solution can be a proper solution as long as its $\alpha_{P_{WC}}$ value is lower than the considered power budget (PB_o); otherwise more sophisticated transmission technologies, providing a higher power budget, would be required.

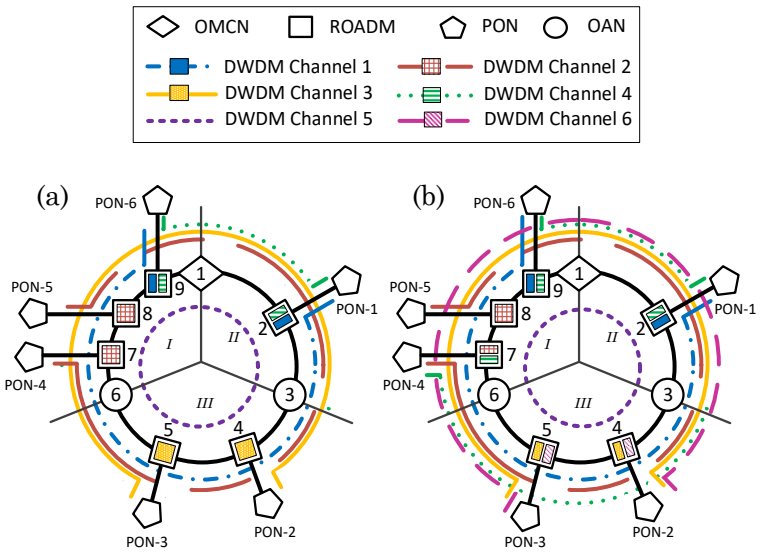

Fig. 3.12. (a) An example of how assigned channel to mismatched ROADMs of the network can be shared and (b) the final design of the considered network using the proposed heuristic II.

Starting from the configuration of the D-ROADMs obtained in the previous problem, a second sub-problem involves obtaining a better configuration for the mismatched D-ROADMs of the network (e.g. D-ROADMs with IDs 2 and 9 shown in Fig. 3.10). A way to reach that purpose can be the sharing of the channel assigned to a mismatched ROADM of a sector with another mismatched ROADM of the other sector. That is, referring to the network example shown in Fig. 3.10(b), the DWDM channel 1 can be assigned to the ROADM with ID 2 and the DWDM channel 4 to the ROADM with ID 9, realizing a new design for those ROADMs as it can be seen in Fig. 3.12(a). To ensure that any connection between a node of PON-1 or PON-6 and a node of the ring can be established, the switches of ROADM modules should have opposite configurations as it is

shown in Fig. 3.12(a). This strategy increases the flexibility of ROADMs with ID 2 and 9 but the DWDM channel 4 is underused because it is only considered for allocating traffic demands between node 1 and nodes pertaining to PON-1 and PON-6 (see Fig. 3.12(a)). To cope with that problem, it must be decided if the unused channel is assigned for allocating traffic demands between nodes of the ring part of the network or for allocating traffic demand from/to PONs. As it is indicated in Fig. 3.12(b), it was decided to re-assign the underused channel 4 to PON-4, adding a new module to ROADM with ID 7.

Once determined the best initial configuration of the network to ensure full connection between every pair of source-destination of the network and checking there are not underused channels, the third sub-problem involve assigning still available DWDM channels for increasing the TLC network so long the $\alpha_{P_{WC}}$ of the current network design is lower than the considered PB_o. To decide in which part of the network the resources could be assigned, the RSA problem over the previous network design has to be solved in order to discover the most congested network's parts to add a new available DWDM channel. This is recursively done still exhausting the free DWDMs channels. Following with the proposed example, just one channel is available in this step, DWDM channel 6 (Fig. 3.12(a)), so it is decided to assign it to ROADMs 4 and 5, as it can see in Fig. 3.12(b). According to Fig. 3.9, the number of times that the dynamic RSA problem has to be solved to obtain the best network's design is $2 \cdot \left(MNC_N - MNC_{N_0}\right) + 1$. That is the same number of times as the heuristic I.

3.4.3 Scenario details and assumptions

Fig. 3.13 shows two examples of ring-based metro-access networks to analyse. The first one envisions a dense urban scenario, consisting of one OMCN, two OANs and six ROADMs. The second one is based on one OMCN, five OANs and four ROADMs; covering an urban/suburban scenario. In both cases, a passive optical network (PON) with eight ONUs is considered to be connected to each ROADM.

It is considered that the transmitters of the OMCN and OAN use Mach-Zehnder modulators, while the ONU transmitter is based on a directly modulated DFB laser. In all cases, the receivers are based on a coherent receiver in which the detected signal is mixed with a DFB as local oscillator, providing a sensitivity of -52 dBm, as indicated in chapter 2. Therefore, the power budget per connection (PB_o) is 52 dB for transmitters providing 0 dBm output. The power budget is considered to be consumed by the fiber attenuation (0.25 dB/km is assumed), the power splitter settled in each PON and the ROADMs'

insertion loss. Chromatic dispersion (CD) effects due to the optical fiber are not considered in the study because it can be compensated using digital signal processing (DSP) at the receiver [154]. A work band of 750 GHz has been considered as the networks resource to share between all users. Two DWDM channel widths have been considered: 62.5 GHz and 125 GHz. Each DWDM channel has been divided into frequency slots, being all of them of 12.5 GHz.

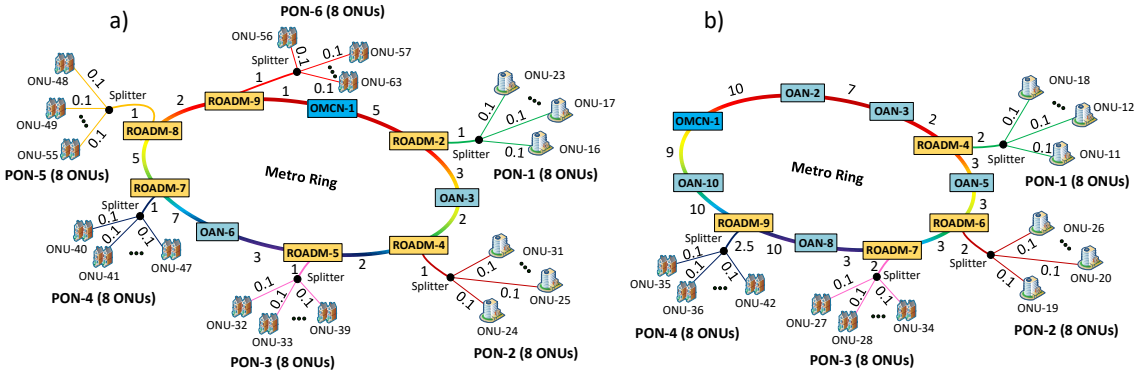

Fig. 3.13. Network examples considered: (a) Network I and (b) Network II. Link distances are shown in km.

The aforementioned networks can be loaded with dynamic traffic demands distributed uniformly between every pair of source-destination of the networks. Nevertheless, in that considered scenario, more than 90% of the traffic demands loaded in the network examples have their origin or destination in a node belonging to a PON, being that case unrealistic for a metro-access network scenario as it is posed in Fig. 3.1. This is due to considering any OAN, OMCN and any ONU having same priority, let us say probability for a demand. This is unrealistic as OANs and the OMCN, aggregating much more traffic and services, will realistically have a higher probability for a demand than an ONU. Therefore, the most suitable traffic demands distributions between every pair of networks nodes are considering that the probability for a demand presenting the origin or the destination in an ONU of a PON is 2.67 times lower than a demand that has origin and destination in the ring part of the network, for the first network example (see Fig. 3.13(a)) and 3.33 times, for the second network example (see Fig. 3.13(b)), respectively. These values are chosen in order to model the traffic generated by all ONUs of a PON as if they are a single node, reducing in this way the number of traffic demands which have the origin or the destination in a PON. In both considered network examples, the traffic demands arrival is a Poisson process with a given mean inter-arrival time (IAT) fixed to the unit and the durations—holding times, $HT = AIT \cdot \rho$, where ρ is the traffic load in erlang units—follow a negative exponential

distribution. Two cases for the requested bit rate have been considered. In the first one all demands are of 10 Gb/s so each accepted demand takes up one FS, and the second one where the requested bit rate is distributed among {10, 20, 40} Gb/s, taking {1, 2, 4} FSs, with probabilities {0.5, 0.25, 0.25}. In all studied cases, the dynamic RSA problem has been solved using a heuristic approach. In particular, the two physical shortest paths have been pre-computed for every pair of source-destination of the network, and the spectrum resources, FSs, are allocated to the incoming demand following the first-fit policy.

3.4.4 Simulation results and discussion

First, we will evaluate the considered network scenarios, see Fig. 3.13, taking into account that the network bandwidth of 750 GHz is divided into six DWDM channels of 125 GHz and the bit rate of every traffic demand is of 10 Gb/s. For this analysis, two cases will be discussed. A first one where the DWDM channels are assigned to the D-ROADMs of the network following the Heuristic I proposed in sub-section 3.4.2.1, in which a same channel can be used for allocating traffic demands between nodes of the ring part of the network and between nodes belonging to a PON and a node of the ring. The second one consists on finding out the best configuration of each D-ROADM of the network in order to improve the TLC of the network following the proposed Heuristic II, introduced in sub-section 3.4.2.2. That is characterised by using different channels for allocating traffic demands between nodes of the ring and nodes of a PON, and for allocating in a different channel, traffic demands between nodes of the ring. Both cases shall be compared to the reference, top performance and cost case, in which all the ROADMs are based on WSSs and they can switch each frequency slot individually.

Secondly, it shall be discussed the blocking bandwidth probability (*BBP*) behaviour vs. TLC of the considered networks when the bandwidth of the DWDM channels is halved (from 125 GHz to 62.5 GHz). Finally, the best configuration of the considered networks obtained after employing Heuristics I and II have been tested for a potential network evolution where bit rate of the demands can be {10, 20, 40} Gb/s with probabilities {0.5, 0.25, 0.25}, respectively. All results of this section have been obtained using a network simulator implemented in MATLAB^{TM} taking into account the insertion loss model of a D-ROADM proposed in chapter 2 as well as considering 10^5 offered traffic demands to the networks.

Fig. 3.14(a) and Fig. 3.14(b) show the BBP as a function of the traffic that is loaded to the network when D-ROADM and WSS-based ROADMs are used; the bit rate of all traffic

demands is 10 Gb/s and the bandwidth of the DWDM channels is 125 GHz. For the network based on D-ROADMs, the BBP is depicted for the proposed Heuristics I and II. From Fig. 3.14(a) and Fig. 3.14(b), it can be noticed that the proposed Heuristic II improves the TLC for the same BBP compared with the design derived from Heuristic I using the same spectral resources. For instance, the TLC obtained for Network I using Heuristic II when BBP=5% is 53% higher than the TLC obtained when Heuristic I is used. Similar BBP curve behaviour can be observed for Network II, in which the TLC when Heuristic II is used for a BBP=5% is 63% higher than the TLC of the network configuration when Heuristic I is used. From Fig. 3.14(a) and Fig. 3.14(b), it can also be noticed that the performance penalty of the networks based on D-ROADM against the same networks using WSS-based ROADMs when the Heuristic II is used for 125 GHz WDM channels is around 52%, while for the Heuristic I the performance penalty is around 64%.

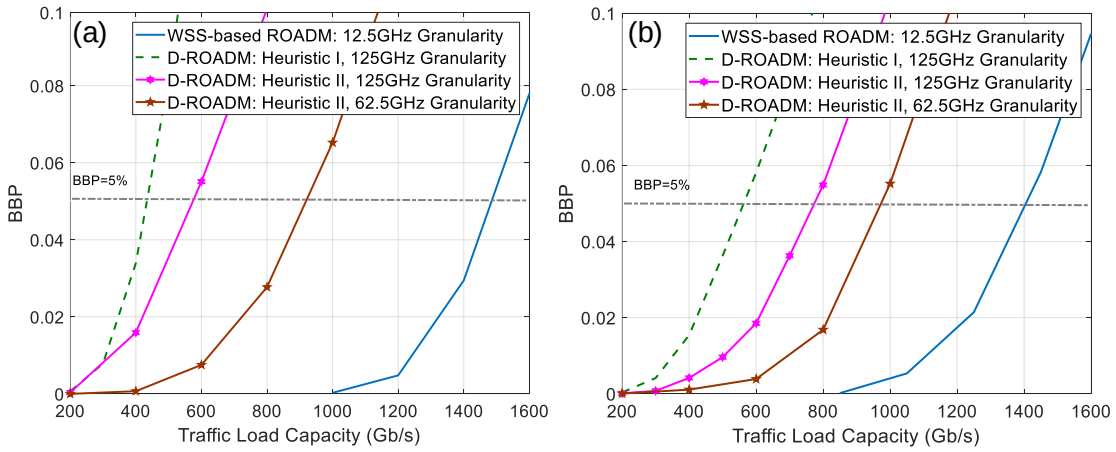

Fig. 3.14. Blocking bandwidth probability (BBP) vs. traffic load capacity when bit rate of every traffic demand is of 10 Gb/s for considered metro-access network I (a) and II (b).

Table 3.5. The worst-case path attenuation ($\alpha_{P_{WC}}$) of the considered networks when WSS-based ROADMs and D-ROADMs are used for different granularities.

Network	I					II				
ROADM	WSS-based	DWDM				WSS-based	DWDM			
Granularity (GHz)	12.5	62.5		125		12.5	62.5		125	
Heuristic		I	II	I	II		I	II	I	II
$\alpha_{P_{WC}}$ (dB)	47	28	35	21	26	24	40	39	31	35

Fig. 3.14(a) and Fig. 3.14(b) also show the BBP curve when the considered DWDM channel bandwidth is of 62.5 GHz and the process of design of the D-ROADMs is based on Heuristic II. In this case, the performance penalty in the TLC of the considered networks is close to 35% (in average) regarding to the same networks using WSS-based ROADMs

for a BBP value of 5%, providing a significant improvement. This enhancement is due to a higher granularity and therefore the distribution of channels for each part of the network fits better to their bandwidth requirement.

Table 3.5 shows the worst-case path attenuation ($\alpha_{P_{WC}}$) of the considered networks (see Fig. 3.13) when they are constituted by WSS-based and D-ROADMs and designed by the two proposed heuristics, showing that is always well under the considered power budget per connection of 52 dB.

Fig. 3.15 shows the BBP curves vs. TLC of the networks based on D-ROADMs after using both proposed heuristics as well as of the same networks using WSS-based ROADMs for the case in which the bit rate of the traffic demands can be {10, 20, 40} Gb/s with probabilities {0.5, 0.25, 0.25}, respectively. As we can notice from Fig. 3.15(a) and Fig. 3.15(b), using Heuristic II for the design of the D-ROADMs, the TLC is, in average, 1.43 times higher than Heuristic I for DWDM channel of 125 GHz; and 2.04 higher for DWDM channels of 62.5 GHz. The average penalty in the TLC of the D-ROADM-based networks using Heuristic II compared to the same networks using WSS-based ROADMs is of 72.2% and 59.2% for 125 GHz and 62.5 GHz, respectively, as it can be deduced from Fig. 3.15. That performance loss is due to the fact that the D-ROADMs do not have the colourless feature.

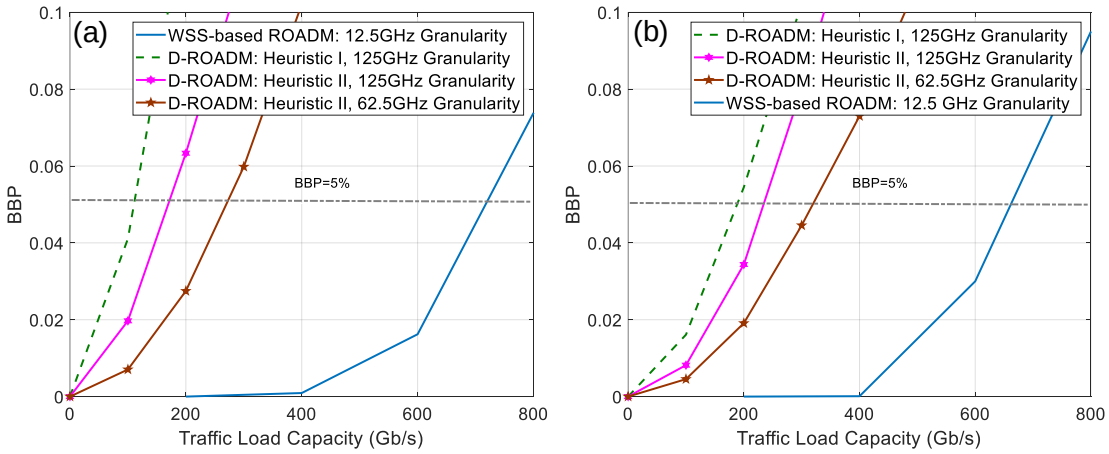

Fig. 3.15. Blocking bandwidth probability (BBP) vs. traffic load capacity when bit rate of traffic demands can be {10, 20, 40} Gb/s for considered metro-access network I (a) and II (b).

3.5 Conclusions

In this chapter, it has been assessed the performance of the proposed cost-effective DWDM ROADM as a metro-access ring network element for offline and online scenarios. For the offline scenario, an iterative process to determine the optimal design of the cost-effective

DWDM ROADMs of the network to maximize the throughput has been presented. Using that process, the allocated traffic is of 80% to the total traffic that a network using WSS-based ROADMs with frequency slot granularity of 12.5 GHz. It has also been demonstrated that the trade-off solution for different DWDM channel widths is of 125 GHz which corresponds to the effective band of the single module cost-effective ROADM/OXC characterized in chapter 2.

For the online scenario, it has been demonstrated that a proper heuristic design can provide a significant improvement, doubling the performance using same network resources and just a 35% performance penalty for a D-ROADM with DWDM channels of 62.5 GHz compared with a fully capable, 12.5 GHz granularity WSS-based ROADM design. In particular, network's traffic load capacity for a blocking bandwidth probability=5%, has been used as reference. In order to verify the validity of these heuristics, two different metro-access networks have been analysed. In both cases, allocating traffic demands between nodes of the ring part of the network and nodes of a PON, and for allocating in a different channel, traffic demands between nodes of the ring significantly improves the traffic load capacity.

Chapter 4. Cost-effective DWDM OXC and ROADM Design to Maximize the Capacity of Mesh-Based u-DWDM Metro-Access Networks

4.1 Introduction

Optical metro networks are migrating from ring to mesh topology as shown Fig. 4.1. This is basically due to the low scalability of rings and the excessive resource redundancy required in ring-based failure management schemes. Moreover, metro networks are converging with access networks and evolving towards all-optical solutions, where u-DWDM technique is considered as an excellent alternative solution to increase the network spectral efficiency. In this context, the cost-effective DWDM OXC (D-OXC) and ROADM (D-ROADM) node shown in Fig. 4.2(a) have been proposed in chapter 2 to enable mesh-based converged metro-access networks using u-DWDM technology. Both proposed nodes are characterized for being modular and working with DWDM channel granularity. In this way, a module of the proposed nodes is designed to manage one DWDM channel. Then, for u-DWDM network scenarios, as the one considered in Fig. 4.1, in which each DWDM is divided into FSs, the nodes functions are applied on a group of FSs at the DWDM channel of the node. For a group of FSs whose DWDM channel is not supported by the node, it is transparent for them.

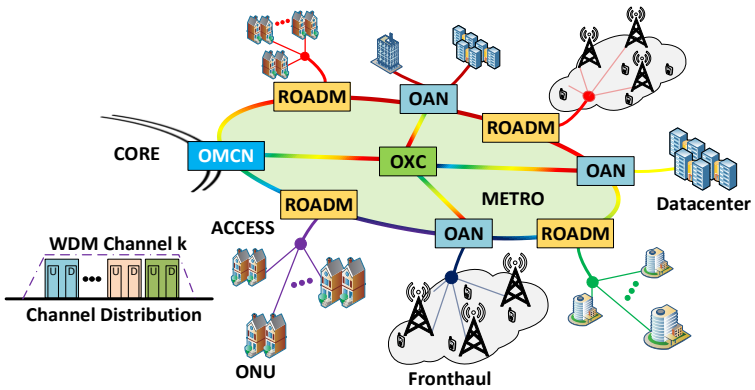

Fig. 4.1. Flexible 5G mesh-based metro-access network scenario. (Inset) Considered flexible ultra-dense WDM frequency slot division.

Bearing in mind the idea, one module of the D-OXC/D-ROADM switches a group of FSs and new modules can be added when they are required; the main target of this chapter

is to demonstrate if a network using D-OXC and D-ROADM nodes with a low number of modules would achieve a similar throughput as networks using colorless WSS-based OXCs and ROADMs working with FS granularity (Fig. 4.2(b)) in an offline scenario. To solve that problem, it is proposed a heuristic approach that permits to reach an efficient design of the D-OXCs and D-ROADMs of a network.

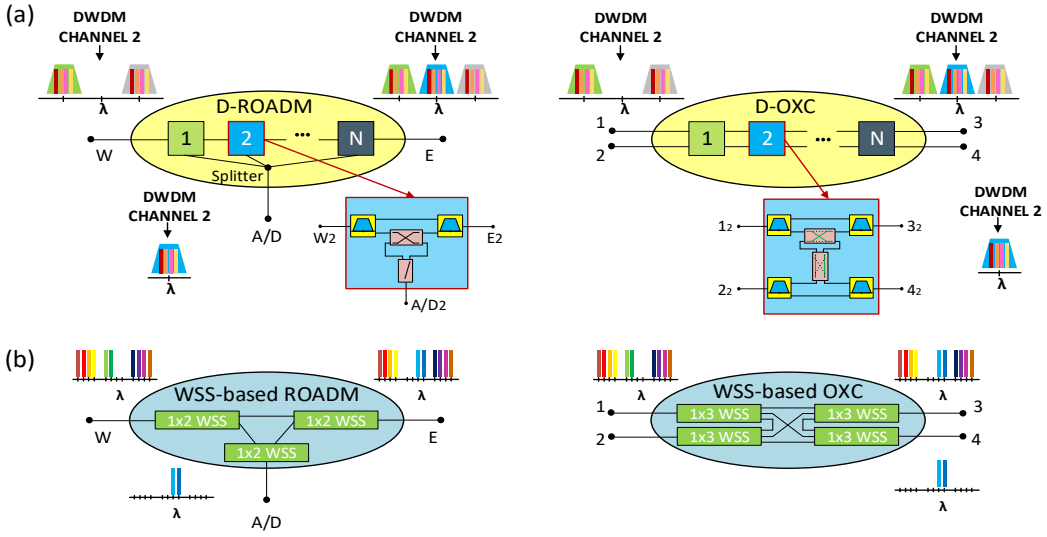

Fig. 4.2. ROADM/OXC node architecture using: (a) cost-effective DWDM and (b) WSS technology.

The remainder of this chapter is structured as follows. Section 4.2 presents the problem statement. Section 4.3 shows the proposed heuristic based on an iterative process for the design of the D-OXCs and D-ROADMs. Section 4.4 presents the details and assumptions of the evaluated u-DWDM metro-access network scenario with mesh topology. Section 4.5 shows the obtained numerical results of evaluating the proposed heuristic. Finally, section 4.6 completes the chapter with the main conclusions.

4.2 Problem statement

The objective of the problem is to find out the best suitable design of the D-OXCs and D-ROADMs of a network (minimum number of modules and their switches configuration) to allocate an already known set of FSs demands, with the objective of maximizing the network's throughput while keeping the D-OXC and D-ROADM's insertion losses as low as possible. Restricted to:

1) The logical graph of the network, defined as the resulting logical graph from the union of each DWDM channel's equivalent graph of the network, must not be disconnected. That ensures that there is, at least, a logical path to the establishment of connections between every possible pair of source-destination nodes.

2) The total attenuation for any path between every pair of source-destination nodes must be lower than the power budget available per connection (PB_o).
3) A demand which has its source or destination in a node belonging to a PON cannot be blocked, for protecting low bandwidth end-user demands as any other service could be prioritized.

To ease the comprehension of the proposed heuristic, Table 4.1 details the notations used in its description.

Table 4.1. Notations used in the description of the D-OXC and D-ROADM design heuristic.

Symbol	Definition
$\mathcal{G} = (\mathcal{N}, \mathcal{E})$	Graph representing the optical network, where $\mathcal{N}$ is the set of nodes (OMCN, OAN, OXC, ROADM and ONU) and $\mathcal{E}$ is the set of optical links of the analysed network.
BW_N	Total network bandwidth (GHz).
BW_{DWDM-C}	DWDM channel bandwidth (GHz).
NFS_{DWDM-C}	Number of FSs per DWDM channel, $BW_{DWDM-C} = BW_{DWDM-C}/BW_{FS}$, where BW_{FS} is the FS bandwidth.
PB_o	Power budget available per connection (dB).
P_{WC}	Worst-case path, defined as the path between a pair of source-destination nodes which presents the highest total attenuation of the network (dB).
α	The total attenuation of the worst-case path of the network P_{wc} (dB).
$\mathcal{D}$	Set of demands, where each demand corresponds to a connection request. Each demand $d \in D$ is determined by (s_d, t_d, n_d), where s_d and t_d are source and destination nodes, and $n_d \in \mathbb{Z}^+$ is the number of FSs requested by the demand.
T	Network's throghput (Gb/s).
ΔT	Minimal throughput gain between iterations (Gb/s).
$\Delta\alpha$	Maximal increment in the total attenuation of the worst-case path of the network P_{wc} (dB).
φ	Parameter determines if all demands $d \in D$ with source or destination in a node belonging to a PON of the network have been addressed.
ND_{PON-x}	Total number of requested FSs by PON-x.
Γ	Set with the different logical graphs of the network resulting from changing the configuration of the module associated with the assigned channel to each D-OXC of the network.
$\mathrm{SortSet}(D)$	Sub-routine sorts a set of the demands D following a certain rule to determine which demands will be allocated first. The considered rule is to allocate first, the traffic demands that belong to the network's PONs. Then, the remaining demands are allocated form the highest to the lowest number of requested FSs.
$RSA(\mathcal{G}, \mathcal{D})$	Sub-routine that solves the offline routing and spectrum assignment problem for all $d \in \mathcal{D}$. The input parameters are the network model ($\mathcal{G}$) and the set of demands $\mathcal{D}$ to be loaded to the network. The output parameters are the network throughput (T) and the total attenuation of the worst-case path of the network (α). Pre-computation of the three shortest paths between all pair of source-destination of the network and the first-fit policy for allocating FSs are considered to solve the RSA.

4.3 Heuristic

Fig. 4.3 shows a pseudo-code of the proposed heuristic that permits to solve the problem presented before. The input parameters are the model of the network ($\mathcal{G}$), the network bandwidth (BW_N), the considered DWDM channel bandwidth (BW_{DWDM-C}), which coincides with the bandwidth of each D-ROADM/D-OXC module, the considered power budget value per connection (PB_o), depending on the chosen transmission technology, and the set of demands to be loaded to the network (D). The output is the best network design that maximizes the network's throughput ($NetworkSolutionDesign$).

1: **Input:** $\mathcal{G}$, BW_N, BW_{DWDM-C}, PB_o, D
2: **Output:** $NetworkSolutionDesign$
3: **Begin:**
4: $\Delta T \leftarrow 50$ *//[Gb/s]*
5: $\Delta\alpha \leftarrow 1$ *//[dB]*
6: $\Omega \leftarrow BW_N / BW_{DWDM-C}$
7: $D_1 \leftarrow$ **SortSet(**D**)** *//Sort set of traffic demands*
8: *//Sub-problem I*
9: $\mathcal{G}_0 \leftarrow$ **NetworkRoadmsDesign(**$\mathcal{G}, D_1$**)**
10: *//Sub-problem II*
11: **for** $i = 1$ **to** Ω **do**
12: Add the module that can manage the DWDM channel i to each OXC of $\mathcal{G}_0$
13: **if** $i > 1$ **then**
14: Remove the modules associated with DWDM channel $i-1$ of those OXCs of $\mathcal{G}_0$ with are settled with Conf. 1.
15: **end if**
16: $\Gamma \leftarrow$ Generate a set with all possible configurations of the OXCs of $\mathcal{G}_0$ when the module associated with the DWDM channel i is changed
17: **for** $j = 1$ **to** $|\Gamma|$ **do**
18: $[T_j, \alpha_j] \leftarrow$ **RSA(**$\mathcal{G}(\Gamma_j), D_1$**)**
19: **if** $\alpha_j > PB_o$ **then**
20: $T_j \leftarrow 0$
21: $\alpha_j \leftarrow +\infty$
22: **end if**
23: **end for**
24: $\alpha_0 \leftarrow \min\{\alpha_j\}, with\ j = 1\ to\ |\Gamma|$
25: **if** $(\alpha_0 + \Delta\alpha) < PB_o$ **then**
26: $\alpha_0 \leftarrow \alpha_0 + \Delta\alpha$
27: **end if**
28: $S \leftarrow \{\gamma_j \in \Gamma \mid \alpha_j\ of\ \gamma_j \leq \alpha_0\}$ *//possible sub-set of OXC configuration solutions*
29: $SOL \leftarrow \{s_j \in S \mid T_j\ of\ s_j\ is\ a\ maximum\}$ *//select the solution(s) that has the highest throughput*
30: **if** $|SOL| > 1$ **then**

31: $sol \leftarrow$ Select a $sol_j \in SOL$ with the highest number of OXC whose module associate with the DWDM channel i is settled with Conf. 1. If there is no solution with the module associate with DWDM channel i, select a $sol_j \in SOL$ randomly.
32: **else**
33: $sol \leftarrow$ SOL
34: **end if**
35: **end for**
36: $NetworkSolutionDesign \leftarrow sol$

Fig. 4.3. Pseudo-code of the proposed heuristic.

To illustrate the proposed heuristic, it shall be applied over the metro-access network example shown in Fig. 4.4. This example, which will be one of the studied network examples in the next section, considers that the bandwidth of the network (BW_N) is of 750 GHz, BW_{DWDM-C} is 125 GHz, BW_{FS} is 12.5 GHz and the number of requested FSs per PON-x (ND_{PON-x}) is 10. The proposed heuristic can be divided into two smaller sub-problems. The first sub-problem corresponds to the design of the D-ROADMs of the network to ensure that there is, at least, a logical path from/to any node of a PON to/from any node of the metro part of the network (Restriction 1). To reach that goal, the sub-routine NetworkRoadmsDesign has been defined in line 9 of the proposed pseudo-code shown in Fig. 4.3. This sub-routine solves two issues: *i)* determining the number of DWDM channels required by each D-ROADM of the network ($N_{D-ROADM_x}$) to address all demands with origin or destination in the PON connected to the D-ROADM$_x$, and *ii)* deciding what DWDM channel or channels shall be assigned to each D-ROADM$_x$ of the network. While $N_{D-ROADM_x}$ can be deduced from D as $ceil(\sum ND_{PONx}/NFS_{DWDM-C})$, where NFS_{DWDM-C} is the number of FSs per DWDM channel; the DWDM channel assignation rule must be designed. A strategy could be to assign different DWDM channels to the D-ROADMs of the network as it was proposed in chapter 3. Nevertheless, although this strategy ensures Restriction 1, it is less efficient since a DWDM channel is restricted to a single PON, as demonstrated in chapter 3. Fig. 4.4(a) shows a more efficient strategy for the channel assignation that also ensure Restriction 1 and it has been introduced in chapter 3 for online ring-based metro-access scenarios. This strategy is based on dividing the metro part of the network into different sectors. This sectorization, shown in Fig. 4.4(a), involves only the ring part of the considered metro network. That is, it can be considered that there are no OXCs in the network. Then, a sector is defined as a pair of two consecutives nodes of the ring part with opto-electrical conversion functionalities (OMCN or OANs) among which there can or cannot be ROADMs as shown in Fig. 4.4(a). The idea of the network

sectorization is to assign the same DWDM channel or channels to a pair of D-ROADMs of the same sector. If the pairing of two D-ROADMs for sharing the same DWDM channel between two different PONs of the same sector is not possible, as occurs with DWDM channel 1 in Fig. 4.4(a), it remains mismatched and the A/D function can be established randomly over E or W port of the D-ROADM. Finally, note that when two D-ROADMs share the same DWDM channel, the A/D function over the E or W port of those D-ROADMs has to be opposite as shown Fig. 4.4(a) for the ROADMs with ID 9 and 10. Fig. 4.4(b) shows the resulting design of each D-ROADM of the considered network example following the proposed strategy based on sectorizing the network and assigning the same DWDM channel to two D-ROADMs of the same sector.

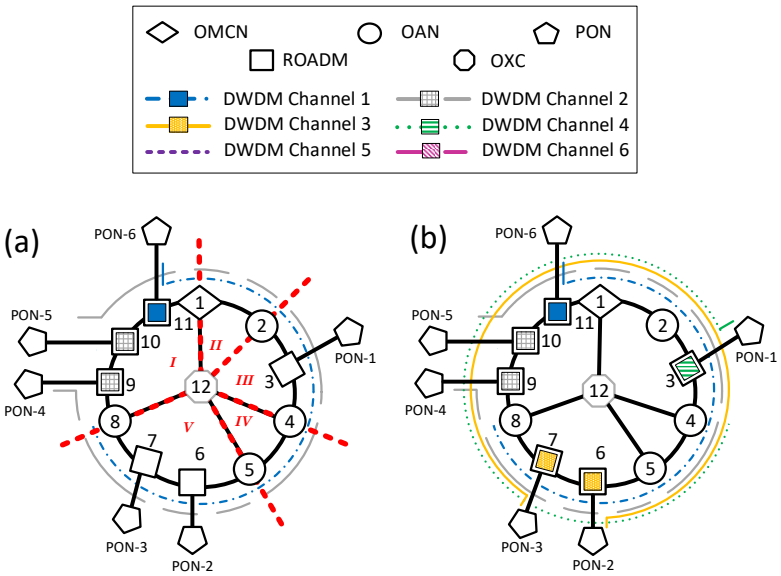

Fig. 4.4. (a) Example of sectorization of a network. (b) Final D-ROADMs design.

Once the configuration of the D-ROADMs has been fixed in the previous sub-problem, the second sub-problem is the D-OXCs design. To achieve that goal, an iterative process is presented in the pseudo-code shown in Fig. 4.3. Fig. 4.5 graphically exhibits that iterative process over the considered network example shown in Fig. 4.4. Basically, an iteration can be divided into 2 stages. The first one, is to add the same DWDM channel to all D-OXCs of the network and generate a set, Γ, with the different logical graphs of the network resulting from changing the configuration of the module associate with the assigned channel to each D-OXC of the network. Thus, for instance, in the considered network example shown in Fig. 4.5 with just one D-OXC, the total number of logical graphs of the network when the DWDM channel 1 is assigned to the D-OXC, $|\Gamma|$, is three since a

D-OXC's module has three possible configurations. In general, $|\Gamma| = 3^{N_{OXCs}}$, where N_{OXCs} is the number of OXCs of the network.

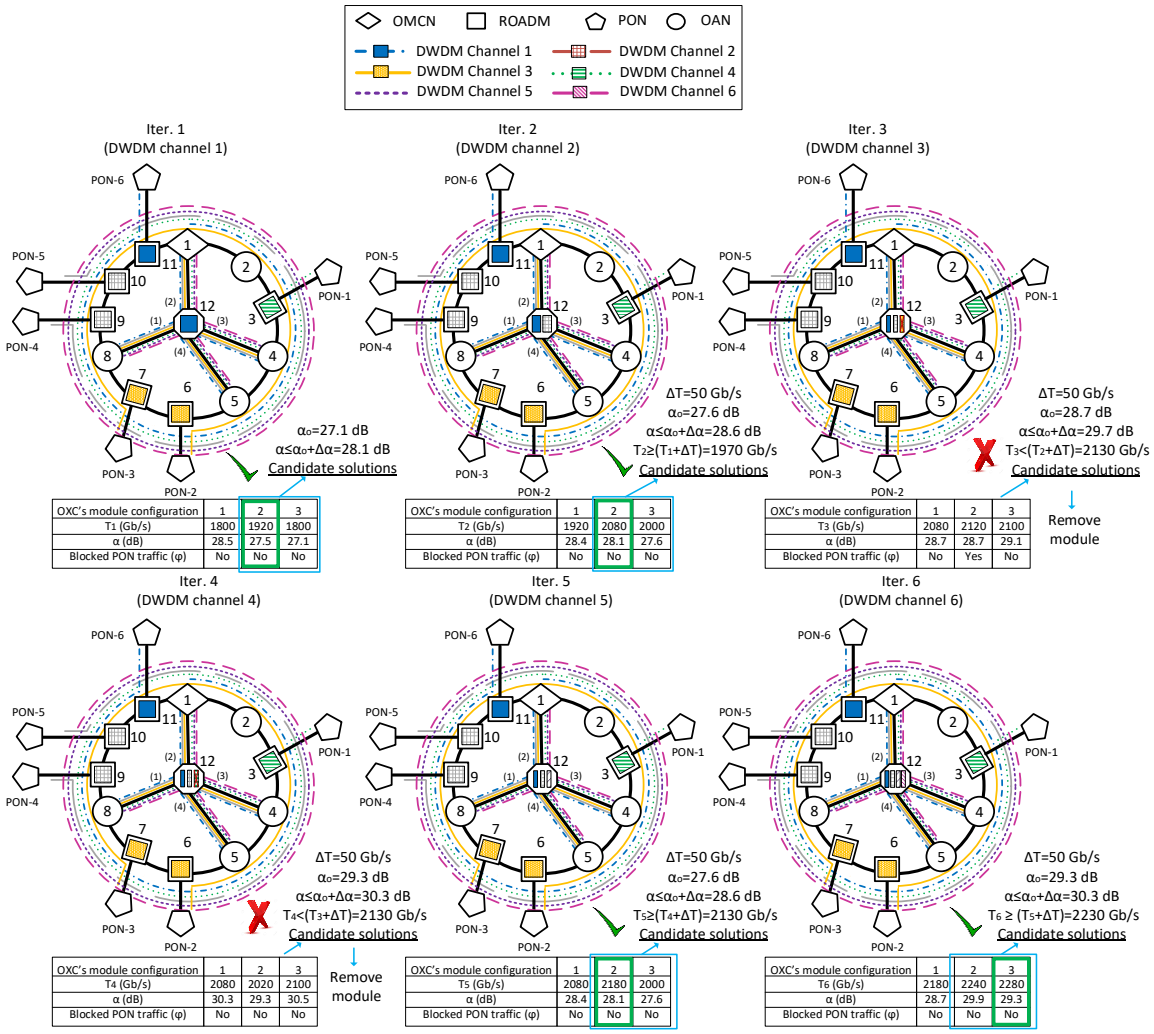

OXC's module configuration	1	2	3
T1 (Gb/s)	1800	1920	1800
α (dB)	28.5	27.5	27.1
Blocked PON traffic (φ)	No	No	No

OXC's module configuration	1	2	3
T2 (Gb/s)	1920	2080	2000
α (dB)	28.4	28.1	27.6
Blocked PON traffic (φ)	No	No	No

OXC's module configuration	1	2	3
T3 (Gb/s)	2080	2120	2100
α (dB)	28.7	28.7	29.1
Blocked PON traffic (φ)	No	Yes	No

OXC's module configuration	1	2	3
T4 (Gb/s)	2080	2020	2100
α (dB)	30.3	29.3	30.5
Blocked PON traffic (φ)	No	No	No

OXC's module configuration	1	2	3
T5 (Gb/s)	2080	2180	2000
α (dB)	28.4	28.1	27.6
Blocked PON traffic (φ)	No	No	No

OXC's module configuration	1	2	3
T6 (Gb/s)	2180	2240	2280
α (dB)	28.7	29.9	29.3
Blocked PON traffic (φ)	No	No	No

Fig. 4.5. Detailed OXC's design of considered network example following the proposed heuristic for six DWDM channels. Coloured lines represent the logical path of each DWDM channel of the network.

The second stage is to determine which network configuration resulting from changing the configuration of the module associate with the considered DWDM channel assigned to the D-OXC (or D-OXCs), defined by the logical graph $\gamma \in \Gamma$, is the best one. To make that decision, the routing and spectrum assignment (RSA) problem has to be solved for each $\gamma \in \Gamma$. In the proposed heuristic, pre-computation of the three-shortest paths between all pair of source-destination nodes of the network and the first-fit policy for allocating FSs are considered. Form this stage, three important parameters to decide the best configuration can be obtained. The first one is the total attenuation α of the worst-case path P_{wc} of $\gamma \in \Gamma$. P_{wc} is defined as the path between a pair of source-destination nodes which presents the highest total attenuation of $\gamma \in \Gamma$. The second one, is the network throughput, T, offered

by $\gamma \in \Gamma$. Finally, the third parameter, φ, determines if all demands $d \in D$ with source or destination in a node belonging to a PON of the network have been addressed. According to Restriction 3, a demand with source or destination in a node belonging to a PON cannot be blocked. Thus, if all demands with origin or termination in a PON of the network have been satisfied, a criterion to select the best solution shall be that one that minimizes α at the same time that the T is maximized. Nevertheless, that situation rarely occurs as shown in Fig. 4.5. Therefore, it is necessary to relax that criterion. The criterion is then to choose the solution $\gamma \in \Gamma$ which maximizes the network throughput within a range of α. That is, the heuristic selects the network configuration that presents the highest T value of a sub-set of Γ that addresses $\alpha \leq \alpha_0 + \Delta\alpha$, where α_0 is the minimum value of α among all $\gamma \in \Gamma$ and, $\Delta\alpha$ is a predefined value that allows selecting the group of solutions to be considered. Form the point of view of minimizing α of the final network design, $\Delta\alpha$ should be a low value. In the proposed heuristic, $\Delta\alpha$ is fixed to 1 dB. Moreover, for each iteration, it must be satisfied that α and $\alpha_0 + \Delta\alpha$ are lower than the maximum power budget available per connection, PB_o. Thus, for the first iteration of the considered example shown in Fig. 4.5, corresponding to assign the DWDM channel 1 to the D-OXC, the second and third configuration of the D-OXC's module associated with that channel are selected. This is because both modules configuration fulfil the condition $\alpha \leq \alpha_0 + \Delta\alpha$. Then, it is chosen the second configuration of the module since the resulting network throughput T is maximum with this configuration (see Fig. 4.5). The following iterations will seek to improve that network throughput through the addition of other DWDM channels to the D-OXC.

In the second iteration, the module corresponding to the DWDM channel 2 is assigned to the D-OXC, as shown in Fig. 4.5. Now, the next stage is to determine if the module assigned to the D-OXC in the previous iteration can be removed. It is possible when the chosen module configuration is Conf. 1. Note that, for that module configuration, the D-OXC functionality over the associated DWDM channel is the same as if the module is not supported by the D-OXC, as explained in chapter 2. In the case in which the module associated with the DWDM channel 1 cannot be removed, the module configuration remains always unchanged. Once removed the module assigned to the D-OXC in the previous iteration, if possible or not, the next stage is to generate a new set Γ with the new logical graphs of the network resulting from changing the configuration of the module associate with DWDM channel 2. Then, the RSA must be solved again for each $\gamma \in \Gamma$ to

find out the best network configuration following the same criterion explained for the first iteration. Nevertheless, if we only consider that criterion, it may happen that the new maximum throghput value is just slightly higher than the maximum one obtained in the previous iteration. To solve this problem, we choose the network configuration that also fulfil $T_i \geq T_{i-1} + \Delta T$, where T_i, T_{i-1} and ΔT are the maximum throughput obtained in the current iteration, in the previous iteration and, a given minimal throughput gain between iteration, respectively. In the proposed heuristic, Fig. 4.3, ΔT has been fixed to 50 Gb/s. Then, the chosen module configuration obtained in the second iteration, related with the DWDM channel 2, is the second one. Finally, this iterative process ends when all DWDM channels of the network have been treated as shown in Fig. 4.5.

4.4 Scenario details and assumptions

In order to generalize our results as much as possible, the two examples of mesh-based metro-access networks shown in Fig. 4.6 are analysed. The first one consists of one OMCN, two OANs, six ROADMs, and one OXC. The second one is based on one OMCN, five OANs, four ROADMs and two OXCs. In both cases, a PON with eight ONUs is considered to be connected to each ROADM.

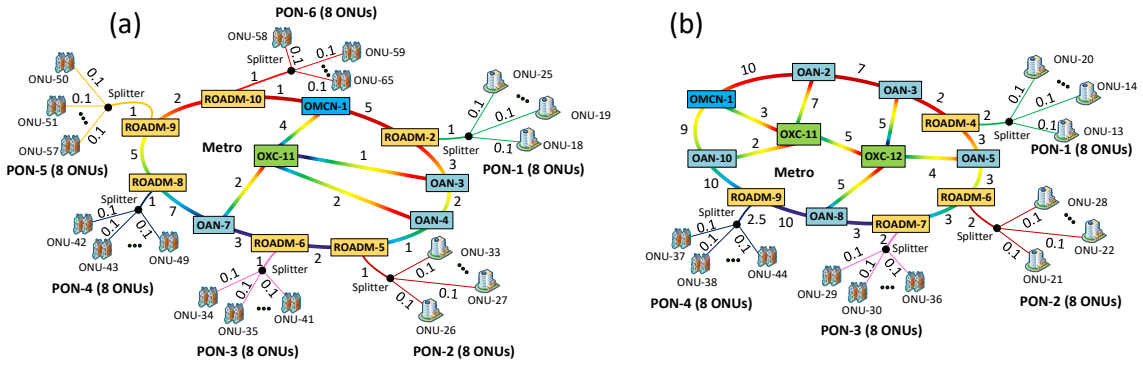

Fig. 4.6. Network examples considered: (a) Network I and (b) Network II. Links distances are shown in km.

It is assumed that the OMCN and OAN are implemented by Mach-Zehnder transmitters, using Nyquist-DPSK. The ONUs' transmitter is based on distributed feedback lasers (DFB). Receivers are based on a coherent receiver in which the detected signal is mixed with a DFB local oscillator, providing a sensitivity of -52 dBm, as indicated in chapter 2. The power budget available per connection, PB_o, is therefore 52 dB for transmitters providing 0 dBm output. PB_o is considered to be consumed by the fiber attenuation (0.25 dB/km), the power splitter settled at each PON and the ROADMs/OXCs insertion loss. It is also assumed that the OMCN, OAN and ONU insertion loss are null owing to

their O-E-O conversion. Chromatic dispersion (CD) effects due to the optical fiber are compensated using digital signal processing (DSP) at the receiver side [154]. A network bandwidth of 750 GHz, divided into six DWDM channel of width of 125 GHz, has been considered. Each DWDM channel is divided into FSs, being all of them of 12.5 GHz.

The aforementioned networks are loaded with a set of demands configured to provide a total aggregated capacity of 100 Gb/s per PON. In a PON, the demands are distributed uniformly among all ONUs and the requested bit rate per demand is of 10 Gb/s, taking up one FS. In case in which the demands have their source and destination in nodes belonging to the metro part of the network, the requested bit rate is {10, 20, 40} Gb/s, corresponding to {1, 2, 4} FSs, with the same probability of 1/3.

4.5 Simulation results and discussion

Table 4.2 summarizes the performance of evaluated network examples shown in Fig. 4.6 in terms of the network's throughput (T), the total attenuation of the worst-case path of the network ($\alpha_{P_{WC}}$) and the execution time (ET) required to allocated a set of demands in the network when WSS-based OXCs/ROADMs and D-OXCs/D-ROADMs are used. In the case of the networks based on D-OXCs and D-ROADMs, the average number of modules per D-OXC/D-ROADM node ($\bar{N}$) and the percentage of blocked bit rate (BB) after using the proposed heuristic is also reported. The BB is measured against the maximum throughput value of the same network using WSS-based OXCs/ROADMs working at FS granularity. For a fair comparison, the same set of demands were used for both WSS-based and DWDM-based cases. Moreover, the RSA problem in both cases was solved considering the pre-computation of the three shortest paths between all pair of source-destination of the network and the first-fit policy for the FSs allocation. Therefore, the proposed heuristic is focused on how DWDM channels are assigned to each D-OXC and D-ROADM of the network and how they are configured.

Table 4.2. Summary of the network performances in terms of the throughput (T), the total attenuation of the worst-case path ($\alpha_{P_{WC}}$) and the execution time (ET). For networks using DWDM-based nodes, the average number of modules per D-OXC/D-ROADM node ($\bar{N}$) and the percentage of blocked bit rate (BB) is also summarized.

OXC/ROADM	WSS-based			DWDM				
Network	T (Gb/s)	$\alpha_{P_{WC}}$ (dB)	ET (s)	T (Gb/s)	$\alpha_{P_{WC}}$ (dB)	$\bar{N}$	BB (%)	ET (s)
I	2622.0	49.2	1.5	2366.5	30.63	1.2	9.7	31.5
II	4080.0	48.1	1.7	3829.5	44.4	1.2	10.8	749.7

From Table 4.2, it can be observed that the proposed heuristic for the design of the

D-OXCs and D-ROADMs of a network leads to BB close to 10% with an average number of modules per D-OXC/D-ROADM node, $\overline{N}$, of 1.2. In terms of the attenuation of the worst-case path of the network, $\alpha_{P_{WC}}$, the networks based on D-OXCs and D-ROADMs show lower $\alpha_{P_{WC}}$ values than the networks using WSS-based OXCs and ROADMs. This is due to the fact that the average number of modules $\overline{N}$ obtained per D-OXC and D-ROADM node is of 1. In this case, the maximum insertion loss of the D-OXC and D-ROADM are of 2 dB and 3 dB, respectively, while the insertion loss of the OXC and ROADM based on WSSs is of 10 dB, as it was indicated in chapter 2. Finally, regarding the execution time ET required to allocated a set of demands in the network, networks based on D-OXCs and D-ROADMs shows worse results. Moreover, ET increases with the number of OXC of the network. This is because the number of times that the RSA problem has to be solved following the proposed heuristic depends on the number of D-OXCs of the network. In particular, the number of times that de RSA has to be solve in the case of network based on D-OXCs and D-ROADMs using the proposed heuristic shown in Fig. 4.3 is $(3 \cdot N_{DWDM-C})^{N_{OXCs}}$, where N_{DWDM-C} is the number of DWDM channels of the network and N_{OXCs} is the number of OXCs of the network. Thus, while for networks with WSS-based OXCs and ROADMs, the RSA problem just has to be solve one time, using the proposed heuristic, the RSA problem is solve 21 times and 441 for the Network I (1 OXC, see Fig. 4.6(a)) and Network II (2 OXCs, see Fig. 4.6(b)), respectively. Note that, if a greedy heuristic, where all possible network configuration is evaluated, were used, the number of times that the RSA has to be solved is $3^{(N_{OXCs} + N_{ROADMs}) \cdot N_{DWDM-C}}$, where N_{ROADMs} is the number of ROADMs of the network. In this case, the number of time that the RSA has to be solved is ~$2.4 \cdot 10^{23}$ and ~$1.1 \cdot 10^{20}$ for the Network I (1 OXC and 6 RADMs, see Fig. 4.6(a)) and Network II (2 OXCs and 4 ROADMs, see Fig. 4.6(b)), respectively. Therefore, proposed heuristic shown in Fig. 4.3 reduces drastically the number of times that the RSA problem has to be solved, leading to assumable execution times.

4.6 Conclusions

In this chapter, it has been assessed the performance of the proposed cost-effective D-OXC and D-ROADM as metro-access mesh network elements for offline scenarios. A heuristic based on an iterative process to determine an efficient design of the cost-effective D-OXC and D-ROADMs of a network to maximize the network's throughput has been presented.

Using that heuristic, the total blocked bit rate is just of 10% regarding the total bit rate supported by the same network using WSS-based OXCs and ROADMs with frequency slot granularity of 12.5 GHz. Finally, although the proposed heuristic increases the execution time, it is assumable for offline scenarios where less than 1 hour is a good heuristic.

Chapter 5. 5G Multicarrier Modulation Formats for High-Layer Split Fronthaul with u-DWDM-PON-based Technology

5.1 Introduction

The current constant growth in mobile networks' traffic demands caused by the popularisation of cloud and streaming services on personal devices, requires architectural changes so as to fulfil all new 5G mobile network requirements. C-RAN architecture in combination with the massive deployment of small cell antenna sites have recently been proposed as a promising solution but will be demanding for high capacity mobile fronthaul links. An efficient way for performing that connectivity is to make use of the DWDM-PON infrastructure. In this context, OFDM has been extensively explored as a potential candidate. Nevertheless, the main drawback of OFDM is its high out-of-band (OOB) radiation. In order to overcome that drawback, filter bank multicarrier (FBMC), universal filtered multicarrier (UFMC) and generalised frequency division multiplexing (GFDM) have recently been proposed for mobile access networks [86]. Several papers have already reported the benefits of these alternative 5G multicarrier modulations over wireless links, but just few works have focused on the transmission of these new modulations through the optical fronthaul segment of the network. In [155], authors study the performance of GFDM for upstream in PONs in terms of the tolerance to multiple access interference due to the OOB. In [156], authors reported a performance comparison between OFDM and GFDM in term of the sensitivity of an optical receiver based on an avalanche photodetector for fronthaul applications using RoF technology. In [157], authors have demonstrated a full-duplex asynchronous quasi-gapless optical transmission using FBMC, showing better spectral efficiency than OFDM. In [158], authors have proposed a UFMC modulation scheme based on RoF technology for the asynchronous transmission of multiple services. In this chapter, using RoF technique it is experimentally assessed and compared 10 Gb/s 32-QAM-OFDM/FBMC/UFMC/GFDM system performance for a high-layer split u-DWDM-PON-based fronthaul scenario, as shown in Fig. 5.1. The u-DWDM is accomplished by dividing each 100(200) GHz WDM channel into two sub-channels, one

for uplink and other for downlink, where different user demands can be allocated (Fig. 5.1). In this way, all antennas connected to the same PON share the same DWDM channel. Benefits of this network architecture solution include the coexistence of different traffic natures and policies, low congestion at the access nodes, compatibility with legacy systems and industrial temperature ranges, and it provides similar performances to standard dual fiber networks [159], [160]. The system performance has been done in terms of spectral efficiency, peak-to-average power ratio, spectral density and receiver sensitivity. In particular, intensity-modulation with direct detection (DD) and quasi-coherent detection (QCD) (to be introduced in section 5.3) have been considered. In order to improve the multicarrier system energy efficiency, the effect of using a hard-clipping technique over transmitted signals is studied as well. Moreover, it is evaluated the crosstalk interference between two adjacent channels of the same modulation scheme, as a function of their electrical frequency span for downlink applications. Finally, the maximum fronthaul network split layer is discussed.

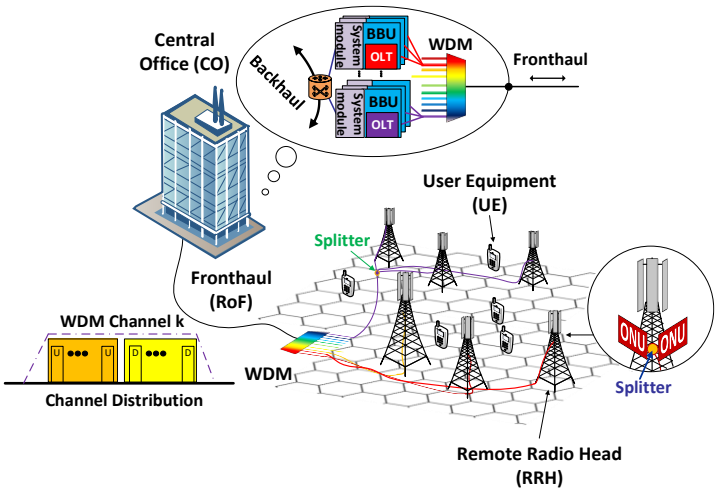

Fig. 5.1. High-layer split DWDM-PON-based fronthaul solution. (Inset) Proposed flexible full-duplex DWDM division.

The remainder of this chapter is organised as follows. Section 5.2 presents alternative 5G multicarrier modulation formats (FBMC, UFMC and GFDM) as well as OFDM, considered as the reference multicarrier modulation to compare. Section 5.3 describes the experimental setup used for the multicarrier modulation schemes evaluation. Sections 5.4, 5.5 and 5.6 show obtained results of comparing alternative 5G multicarrier modulations and OFDM. Section 5.7 discusses the maximum fronthaul network split layer. Finally, section 5.8 completes the chapter with the main conclusions.

5.2 Multicarrier modulation formats

These new multicarrier modulations (FBMC, UFMC and GFDM) can be classified into two categories depending on the orthogonal modulation technique used [86]. While FBMC and GFDM use a pulse shaping technique, UFMC is based on sub-band filtering to reduce the OOB noise. In this section, it is briefly introduced the alternative 5G multicarrier modulation formats as well as OFDM that will be assessed and compared in this chapter for fronthaul applications.

5.2.1 Orthogonal frequency division multiplexing (OFDM)

OFDM is a well-known multicarrier modulation format used in 4G wireless networks. In this modulation format, a block of complex symbols is mapped into a set of orthogonal subcarriers. The OFDM transceiver scheme is shown in Fig. 5.2. The most important feature of OFDM is that the frequency to time (time to frequency) transform can be performed with the inverse fast Fourier transform (fast Fourier transform) process of size N_{FFT}, allowing a transmitter (receiver) with low complexity. Moreover, in case of requiring an equalization process, it can be reduced to a one-tap-coefficient equalizer per subcarrier since the bandwidth is divided into N_{FFT} subcarriers. Finally, as the subcarrier orthogonality can be broken by the transmission channel, leading, e.g., to a strong inter-subcarrier interference, a cyclic prefix (CP) can be inserted to each OFDM symbol. This CP, usually the end of the OFDM symbol, is placed at the beginning of the same OFDM symbol. The CP guarantees circularity of the OFDM symbol, avoiding the inter-subcarrier interference, if the delay spread of the channel is lower than the CP length. It nevertheless leads to a loss spectral efficiency since the CP is used to transmit redundant data.

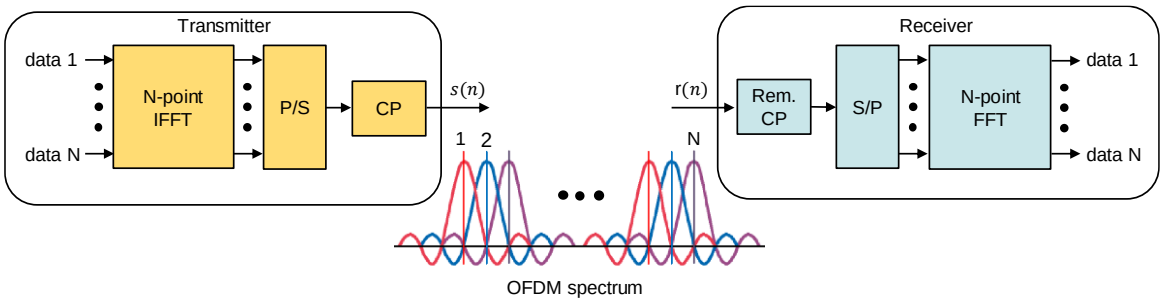

Fig. 5.2. OFDM transceiver with cyclic prefix (CP). (Inset) OFDM spectrum with N orthogonal subcarriers.

The most important drawback of OFDM is the high OOB noise that it presents. The sinc-shaped response that defines the spectrum of the different subcarriers, see Fig. 5.2, generates secondary lobes with high power. These lobes extend further than the frequency band used to transmit data, converging to a loss in the total spectral efficiency of the system.

Other drawbacks of OFDM are high peak-to-average power ratio (PAPR) and, the high sensitivity to phase and frequency noises.

5.2.2 Filter bank multicarrier (FBMC)

FBMC can be understood as a modification of the legacy OFDM in which each subcarrier is filtered to minimize its side-lobes, reducing interference among different subcarriers and the OOB noise level of the global allocated bandwidth. Thus, in FBMC, a set of parallel data that are transmitted through a bank of modulated filters. It is parametrized by the prototype filter that controls the time and frequency localization of each subcarrier. The choice of the filter can reduce the OOB noise, leading hence to a lower crosstalk between adjacent channels. Nevertheless, filtering the OOB noise introduces interference between consecutives subcarrier and between FBMC symbols. To solve this problem, offset-quadrature amplitude modulation (O-QAM) technique can be used [161], maximizing the spectral efficiency. This technique consists of splitting real and imaginary parts and set them alternatively in frequency domain, guaranteeing orthogonality.

The classical architecture for FBMC is based on synthesis and analysis polyphase filter banks in which the filtering is performed in time domain. Alternatively, the frequency spreading FBMC architecture shown in Fig. 5.3 has been proposed [162]. This alternative uses the frequency sampling technique. The typical prototype filter is the proposed in the PHYDYAS project [161]. This prototype filter is defined in frequency domain and it depends on the overlapping factor K, which defines $2 \cdot K - 1$ non-null points of the filter in the frequency domain.

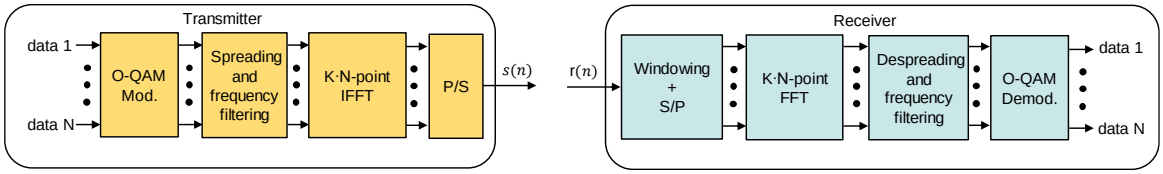

Fig. 5.3. FBMC transceiver based on frequency spreading.

Firstly, complex data are transformed into O-QAM data, then the O-QAM symbols are filtered in the frequency domain. The results then feed an IFFT of size $K \cdot N_{FFT}$. The final step is a parallel to serial converter, which performs an overlap and sum operation between O-QAM symbols. Each O-QAM symbol is transmitted every $N_{FFT}/2$ samples, and has a length of $K \cdot N_{FFT}$ samples. At the receiver side, the dual operation of the overlap-and-sum operation of the transmitter is a sliding window in the time domain that selects $K \cdot N_{FFT}$ points every $N_{FFT}/2$ samples. A FFT is then applied over every block of $K \cdot N_{FFT}$ selected

points. Equalization can be applied using a single tap equalizer and it is followed by filtering at the prototype matched filter. Because the size of the FFT is K times larger than the multicarrier symbol time period, the signal at the output of the FFT is oversampled by a factor of K with respect to the carrier spacing.

The greatest advantage of FBMC is the overlapping between subcarriers, only restricted to adjacent ones, making it robust against synchronism problems. Moreover, the CP is not required, allowing higher data rates, but making it difficult to support multiple-input multiple-output (MIMO) schemes. In contrast, the computational complexity is high [163].

5.2.3 Universal-filtered multicarrier (UFMC)

UFMC, introduced by Alcatel-Lucent [164], is a variation of OFDM where a group of subcarriers is filtered in the frequency domain. This filtering operation leads to a reduction of the OOB noise level compare to OFDM. The UFMC transmitter is depicted in Fig. 5.4. It is composed of N_{SB} sub-bands filtering operation that modulate the N_{SB} data blocks. The N_{SB} signals are then summed. Although the transmitted UFMC symbol does not use CP, a spectral efficiency loss occurs due to the transient state of the shaping filter (of length L) introduced by the convolution. In this case, the filter is defined by the stop-band attenuation. The receiver stage is composed of a $2 \cdot N_{FFT}$ point FFT. The initial received UFMC symbol length is of $NFFT + L - 1$ samples, so zero padding must be applied before the FFT. Next, the received signal is downsampled by a factor of 2 to recover the data [165]. Equalization process must be run over each sub-band, as shown in Fig. 5.4.

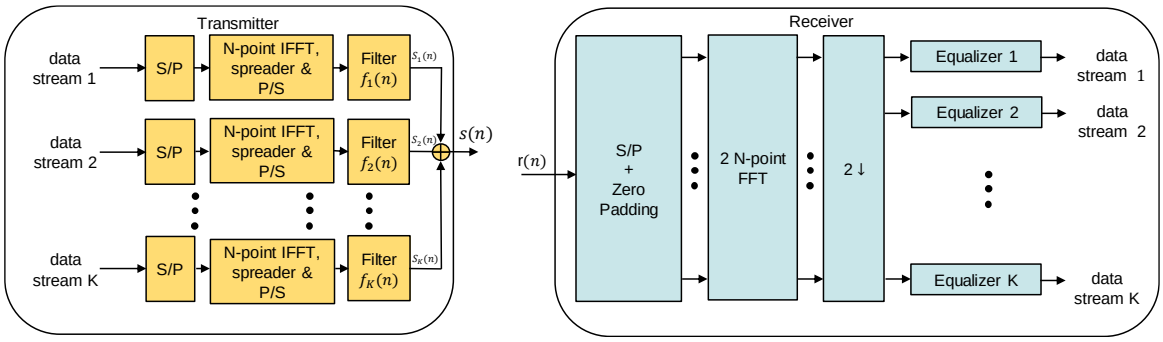

Fig. 5.4. UFMC transceiver.

5.2.4 Generalised frequency division multiplexing (GFDM)

GFDM, introduced by Vodafone Chair Mobile Communications Systems [166], is based on the time-frequency filtering of a data block, which leads to a flexible but non-orthogonal waveform. A data block is composed of K subcarriers and M time slots, and transmit $K \cdot M$ complex modulated data. Each data block is filtered by a filter that is translated into both

frequency and time domains. Thus, as the symbols overlap both in time and in frequency, interference between sub-symbols and between symbols occurs. To avoid inter-symbol interference, a CP can be added at the end of each symbol of size $K \cdot M$. The GFDM waveform is parametrized by its shaping filter. To further reduce the OOB noise level, a windowing process can be added in the transmission stage. It however increases the interference level, that can be mitigated at the receiver side using tail-biting approach [166]. Several receiver architectures can be used, but the most typical approach is using zero forcing (ZF) technique since no interference cancellation is required. The GFDM transceiver is described in Fig. 5.5. The main advantage of GFDM is its high degree of flexibility, giving the possibility to modify it according to each situation requirements. Moreover, since CP is used in GFDM, MIMO techniques are supported.

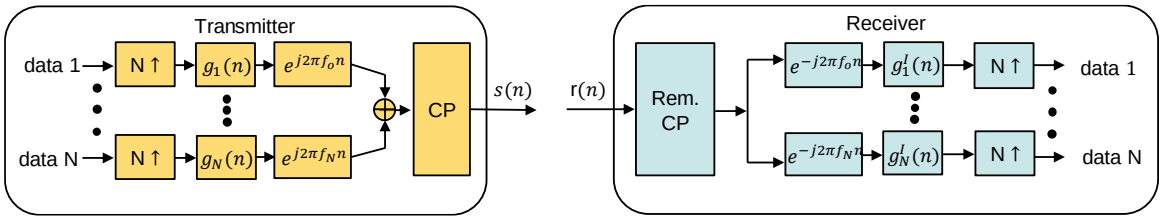

Fig. 5.5. GFDM transceiver.

5.3 Experimental setup description

The experimental setup is depicted in Fig. 5.6. The BBU's transmitter (BBU-TX) was based on an external cavity tuneable laser source (TLS), modulated by a Mach-Zehnder Modulator (MZM). The MZM was biased at its quadrature point. The BBU-TX used a digital transmitter (DTX) where bits were randomly generated and coded into 32-QAM format. The obtained complex symbols were digitally modulated according to OFDM, UFMC, FBMC and GFDM modulation schemes presented in section 5.2 with N_{FFT}=1024 of which 512 are data sub-carriers. To maximize the OOB noise of FBMC waveform as much as possible, a PHYDYAS filter with an overlapping symbol factor, K, of 4 was considered. For GFDM, a root raised cosine (RRC) filter with different roll off factors, α, was considered, defining M=15 for each GFDM block and 2 overlapped sub-carriers. Finally, in UFMC, each sub-band was filtered with a shifted version of the same prototype filter. Specifically, a Dolph-Chebyshev filter with a length of 73, a side-lobe attenuation of 40 dB and different sub-band size, were contemplated. A cyclic prefix length, N_{CP}, of 72 samples was added to OFDM and GFDM. In order to adapt the obtained complex signals to real ones that can be modulated and detected in amplitude, a juxtaposing technique in

time domain was used [167]. This technique consists of splitting the complex output into real and imaginary parts and sending one after the other. The obtained real signal, oversampled to avoid aliasing issues, was optionally hard clipped and filtered so as to reduce the OOB clipping noise. A low-pass, finite-impulse response (FIR) filter was considered.

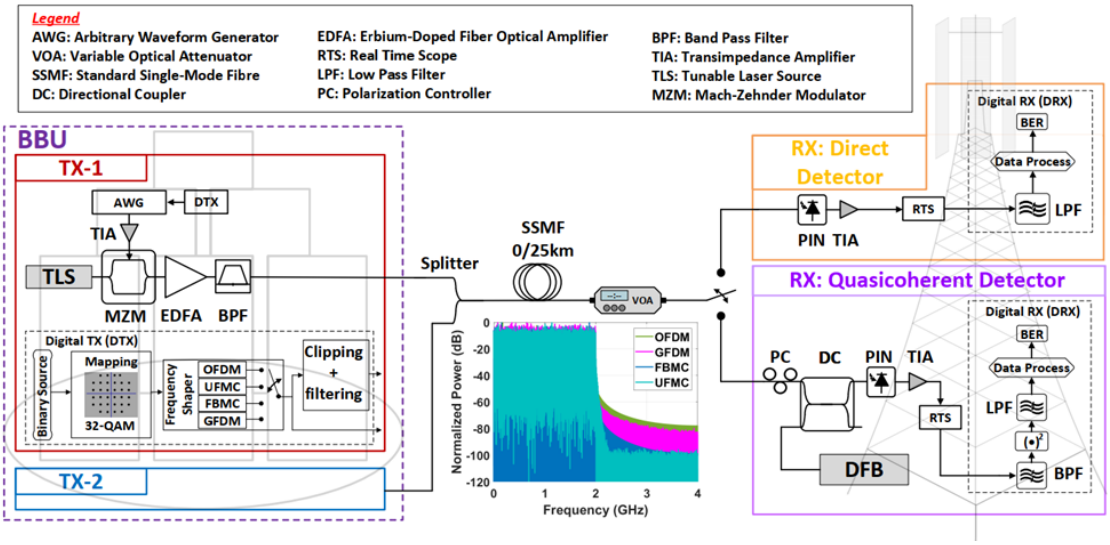

Fig. 5.6. Experimental setup. (Inset) Measured electrical base-band spectra at the transmitter of 10 Gb/s 32-QAM-OFDM/GFDM/FBMC/UFMC before its optical conversion.

The modulated signals were converted from digital-to-analogue using a 4 GHz 3 dB bandwidth arbitrary waveform generator (AWG) set at 8 GSa/s, obtaining the 2 GHz bandwidth signals shown in Fig. 5.6. To exhaust the MZM linear range, electrical amplification was used. The modulated optical signal was amplified to obtain 0 dBm at BBU-TX's output by an erbium-doped fiber optical amplifier (EDFA). The optical signal-to-noise ratio (OSNR) was then at 41 dB. So, to reduce the amplified spontaneous emission noise over the optical signal, it was filtered using a 100 GHz bandpass filter, i.e., emulating a WDM channel at 1545 nm. The optical signal was launched into 25 km of standard single-mode fiber (SSMF). A second transmitter, with features similar to the described one, was added to the setup, so as to evaluate the crosstalk penalty between two adjacent channels.

Two different cost-effective optical receivers were considered for the RRH implementation (see Fig. 5.6). The first one, a DD receiver, simply based on a PIN photodetector, combined with an electrical amplifier (EA), and the second one, a single ended QCD receiver based on the DD receiver. A detailed cost analysis comparing DD and QCD receivers can be found in [71]. For the QCD receiver, the local oscillator (LO) was a cost-effective distributed feedback laser (DFB). In the proposed setup, the LO and the

signal were coupled at the photodiode using an optical coupler and a polarisation controller (PC). This QCD receiver can be easily upgraded to a polarisation insensitive QCD receiver as indicated in [75], [135]. The bias current of the DFB was configured to provide +14.3 dBm. After the heterodyne detector, the received signal was optically down-converted to an intermediate frequency (IF) equal to 5 GHz. For both proposed receivers, the detected signal was digitized with a 25 GSa/s digital oscilloscope to be processed offline.

Both DD and QCD receivers had a digital receiver (DRX) in which the first step was the low-pass and band-pass filtering of the digitized signal with a FIR filter so as to reduce the noise, respectively. In the case of the QCD receiver, the band-pass filtered signal was multiplied with itself and low-pass filtered with a FIR filter as well. The filtered signals were digitally demodulated according to the received signal scheme shown in section 5.2. Finally, the bit-error rate (BER) was calculated, comparing the detected data stream to the original one.

5.4 Spectral efficiency, PAPR and power spectral density comparison

In the following, a broad set of experimental results that allows comparison of the spectral efficiency, the PAPR and the power spectral density (PSD) of considered multicarrier waveforms is shown. For the sake of simplicity, they were done using the DD receiver, which is simply based on the PIN photodiode, plus the electrical amplifier (see Fig. 5.6).

Fig. 5.7(a) shows the spectral efficiency (SE) of OFDM, UFMC, GFDM and FBMC, in bits/s/Hz, for a frame with a different number of symbols. From Fig. 5.7(a), it can be deduced that for OFDM, UFMC and GFDM, the SE does not depend on the burst duration, while for FBMC it does so. In particular, the SE loss of FBMC for a low number of symbols is due to the transient state of the shaping filter. For a high number of symbols, the SE of FBMC is similar to GFDM. For GFDM, the SE is higher than OFDM; this is because the GFDM symbol is M times longer than an OFDM symbol. Then, the SE relation between OFDM and GFDM is $\sim (1 + N_{CP})/N_{FFT}$ [163]. The UFMC SE is equal to OFDM since the length of the Dolph-Chebyshev filter used is chosen for a fair comparison [163]. Finally, different values of α and number of sub-bands (N_{SB}) were considered for GFDM and UFMC, respectively. No significant changes were obtained in the SE.

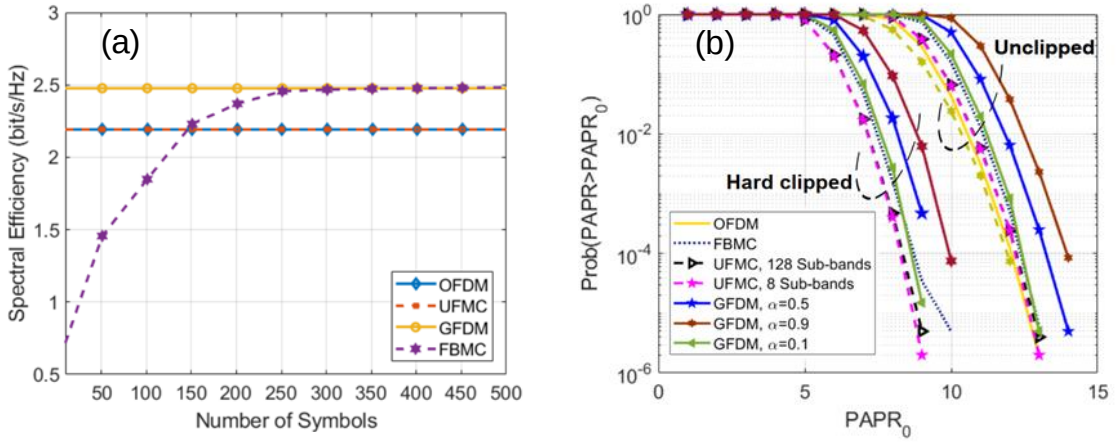

Fig. 5.7. (a) Measurement of spectral efficiency for different burst duration for OFDM, FBMC, UFMC and GFDM. (b) Measurement of complementary cumulative distribution function (CCDF) of PAPR for OFDM, FBMC, UFMC and GFDM through the optical system when the transmitted signals are unclipped and clipped.

PAPR, defined as $|x_{peak}|^2/{x_{rms}}^2$, where x represents the signal samples of a symbol, is a key performance parameter of a multicarrier communication system, since it has a direct bearing on the cost and energy efficiency of the hardware equipment expended. Moreover, any multicarrier signal with a high number of sub-carriers, as those under consideration here, N_{FFT}=1024, has high PAPR. Several alternative solutions to reduce the PAPR of transmitted signals have been proposed in the literature and most of them are overviewed in [168]. One of these approaches, and the simplest, is amplitude clipping of the multicarrier signal. Since high peaks take place in the transmission with very low probability, clipping could be an effective technique for PAPR reduction. Nevertheless, clipping is a non-linear process that causes significant in-band distortion, degrading BER performance and increasing OOB noise. Filtering after clipping shrinks the OOB noise but also leads to some peak regrowth. Here, we studied, through extensive experimental measurements, the effects of clipping and filtering on the PAPR and PSD of OFDM, UFMC, FBMC and GFDM, for considered optical system. By measuring the PAPR of the received signal and comparing the PAPR values of the generated signals before and after their transmission, it is possible to know if the complete system introduces important non-linear distortions over the transmitted signals. In all checked cases, no variation on the PAPR values was obtained, and, hence, the use of the clipping technique is justified to improve the energy efficiency of the communication system, as long as the BER degradation can be bearable, as it shall be studied in section 5.5.

Fig. 5.7(b) shows the complementary cumulative distribution function (CCDF), defined as the probability that PAPR exceeds a certain value of $PAPR_0$ vs. $PAPR_0$, of OFDM,

FBMC, UFMC and GFDM, measured at the receiver side, when the transmitted signal is unclipped and hard clipped to 50% of the peak. These results represent an average of 10^6 realisations of a transmitted sequence through the system, each having the length of 10 symbols. For GFDM and UFMC signal generation, α={0.1, 0.5, 0.9} and N_{SB}={8, 128} have been considered, respectively. From Fig. 5.7(b), it can be observed that OFDM exhibits the best performance within the chosen parameters. However, it should also be noted that, for example, for a probability (P) of 10^{-3}, the gap between OFDM and the alternative 5G multicarrier waveforms is small, around 0.5 dB when α=0.1 for GFDM. From Fig. 5.7(b), the additional degree of freedom of GFDM to control the PAPR by just changing the roll off factor of the raised cosine used as pulse shaper, can also be observed. Thus, varying α from 0.9 to 0.1, a PAPR reduction of 1.5 dB can be achieved for P=10^{-3}. For UFMC, different sub-band sizes do not change the CCDF of the PAPR curves. Fig. 5.7(b) also shows the CCDF of PAPR for OFDM, FBMC, UFMC and GFDM when signals are clipped to 50% of the peak of each transmitted symbol. As it can be observed, the OFDM PAPR is reduced from ~11.5 dB to ~7.5 dB for P=10^{-3}. That is a reduction of 4 dB. Similar PAPR reduction can be seen for FBMC, UFMC and GFDM.

In Fig. 5.8, the measured PSD of OFDM, FBMC, UFMC and GFDM signals when they are unclipped and hard clipped to 50% of the peak, is shown, in comparison with the electrical spectrum shown in Fig. 5.6, corresponding to an ideal wireless base-band signal, non-affected by optical modulator non-linearity. The effect of clipping over the OOB noise is clear. Thus, for example, for a frequency of 3 GHz, the OOB noise power of hard clipped OFDM, see Fig. 5.8(a), is -15 dB lower than the signal power, while for unclipped OFDM it is -40 dB. Similar OOB noise behaviour to OFDM can be observed for FBMC, UFMC and GFDM, when the signal is hard clipped, see Fig. 5.8(b)-(d). In these cases, the OOB noise level of FBMC, UFMC and GFDM are -20 dB, -25 dB and -18 dB lower than the signal power, respectively. For GFDM and UFMC, changing the α and N_{SB} values do not significantly impact on the OOB noise. All those results show that filtering is required to reduce the increase of the OOB noise level caused by clipping. Fig. 5.8(e) shows the PSD when OFDM, FBMC, UFMC and GFDM signals are hard clipped and filtered with a FIR filter. Now, for a considered frequency of 3 GHz, the difference between the power signal and OOB noise are around -28 dB, -30 dB, -37 dB and -37 dB for OFDM, GFDM, FBMC and UFMC, respectively. From Fig. 5.8(e), it can be noticed that UFMC offers the best spectral localisation followed by FBMC. GFDM has a little lower OOB noise level

compared to OFDM.

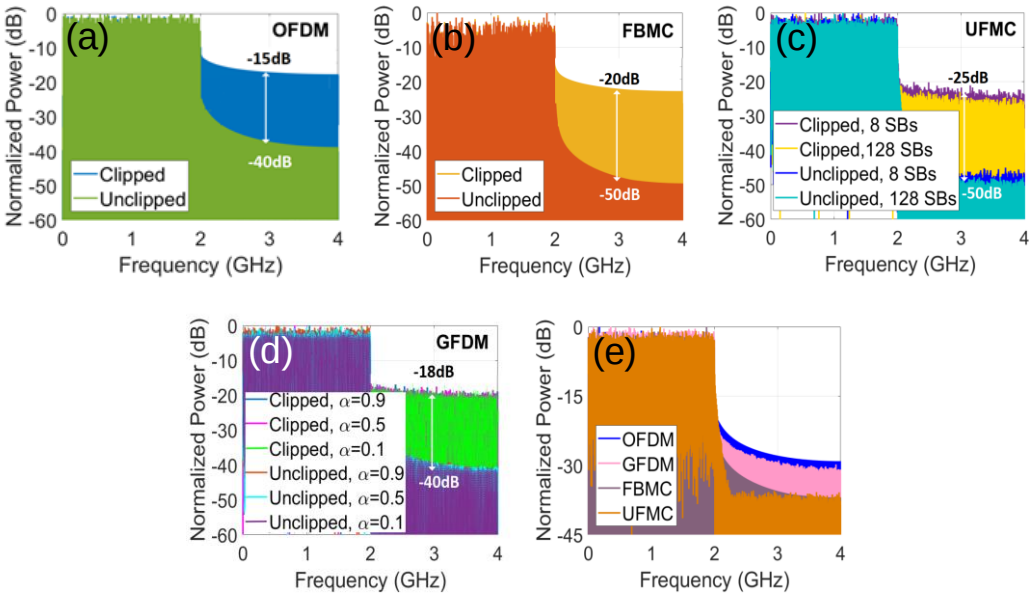

Fig. 5.8. Measurement of power spectral density of: (a) OFDM, (b) FBMC, (c) UFMC and (d) GFDM signals when they are unclipped and clipped to 50% of the peak. (e) Comparison of measured power spectral density of OFDM, FBMC, UFMC and GFDM when signals are clipped and filtered.

5.5 Sensitivity measurement

In this section, OFDM, FBMC, UFMC (N_{SB}=128) and GFDM (α=0.1) performances have been measured in terms of the sensitivity for the two different cost-effective receivers proposed in Fig. 5.6. The first one consists of a simple DD receiver, and the second one is the single ended QCD receiver, based on the previous one, and uses a DFB as LO, Fig. 5.6. In particular, the bit-error rate (BER) vs. received optical power (P_{RX}) has been evaluated for back-to-back (B2B) and 25 km of SSMF as shown in Fig. 5.9(a) and Fig. 5.9(b). The BER limit of $2.2 \cdot 10^{-3}$, corresponding to 7% OH for FEC has been considered [120]. The sensitivity is then defined as the minimum received power for reaching that BER limit.

Table 5.1 summarises the sensitivities depicted in Fig. 5.9(a) of unclipped and hard clipped-and-filtered OFDM, FBMC, UFMC and GFDM signals for the DD receiver. From Table 5.1, it can be observed that unclipped OFDM, FBMC and UFMC have similar sensitivities, around -14.3 dBm, while the GFDM sensitivity is ~0.6 dB worse. That sensitivity degradation is due to the loss of orthogonality between subcarriers, owing to the pulse shaping used at the transmitter. From Table 5.1, it can also be observed that the penalty in the sensitivity when the signals are hard clipped to 50% of the peak is around 2.4 dB. That penalty in the sensitivity is due to the in-band noise caused by the clipping.

Negligible transmission penalties are observed on the obtained sensitivities shown in Fig. 5.9(a) when the optical signal is launched into 25 km of SSMF.

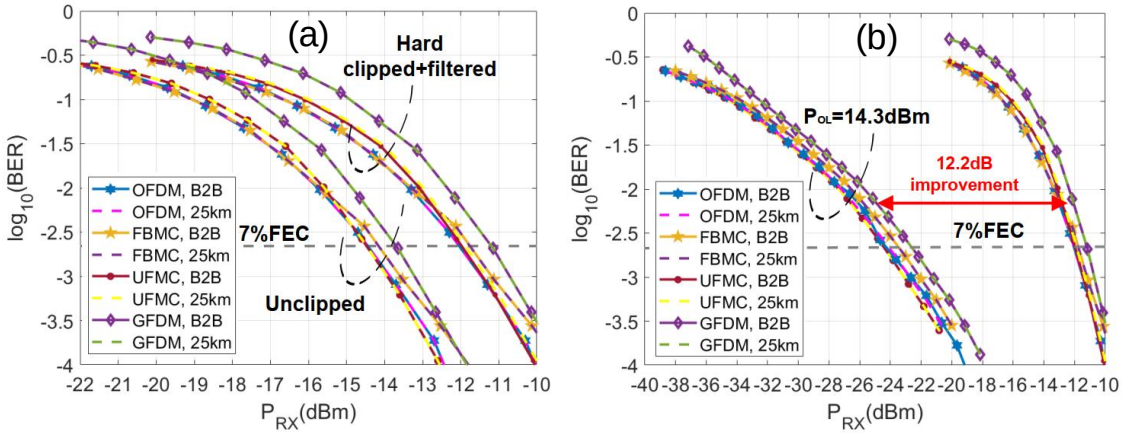

Fig. 5.9. (a) BER vs. received optical power (P_{RX}) of unclipped and clipped-and-filtered OFDM, UFMC, GFDM and FBMC signals for DD receiver. (b) BER vs. received optical power (P_{RX}) comparison of clipped-and-filtered OFDM, UFMC, GFDM and FBMC signals for the DD and QCD receivers.

Table 5.1. Summary of B2B sensitivities of unclipped and clipped-and-filtered OFDM, FBMC, UFMC and GFDM signals for DD receiver as well as the penalty (Δ) between them.

Mod. Scheme	Sensitivity (dBm)		Δ(dB)
	Unclipping	Hard Clipping+filtering	
OFDM	-14.4	-12.1	2.3
FBMC	-14.2	-11.8	2.4
UFMC	-14.4	-12.0	2.4
GFDM	-13.7	-11.1	2.6

Table 5.2. Summary of B2B sensitivities of unclipped and clipped-and-filtered OFDM, FBMC, UFMC and GFDM signals for QCD receiver.

Mod. Scheme	Sensitivity (dBm)	
	Unclipping	Hard Clipping+filtering
OFDM	-26.8	-24.5
FBMC	-25.9	-23.5
UFMC	-27.2	-24.8
GFDM	-25.4	-22.8

Fig. 5.9(b) shows ~12.2 dB enhancement in the sensitivity of the considered transmission system when the DD receiver is upgraded to a QCD receiver with a DFB, biased to provide +14.3 dBm of output power, as LO. That system enhancement has been measured when signals are clipped and filtered. Similar improvement in the sensitivity can be obtained for unclipped signals. New B2B sensitivities are outlined in Table 5.2. From Fig. 5.9(b), it can be observed that those sensitivities do not change when 25 km SSMF is used. Finally, it has also been experimentally checked that the evolution of the sensitivity

of the QCD versus the LO power follows a similar behaviour of the QCD receiver analysed in [75].

5.6 Crosstalk interference measurement

As can be observed in Fig. 5.8, different multicarrier waveforms present different OOB noise levels. For a fronthaul network scenario, as proposed in this chapter, see Fig. 5.1, in which each DWDM channel is divided into two sub-channels, one for upstream and the other for downstream, the OOB noise determines the minimal frequency grid required between different end-users' spectral demands. On the other hand, Fig. 5.8 also shows that the OOB noise depends on if the clipping+filtering technique is used or not to reduce the PAPR of transmitted signals. Thus, the OOB noise is maximum when clipping+filtering technique is used and, minimum when not. Therefore, the worst case to determine the required grid is established by the clipping+filtering technique.

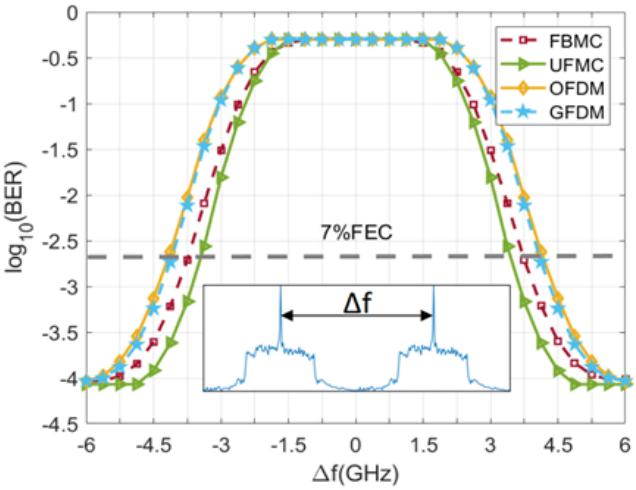

Fig. 5.10. BER vs. electrical frequency span (Δf) between two adjacent channels of the same type: OFDM, UFMC, GFDM and FBMC. (Inset) Electrical frequency span definition between two adjacent channels.

Fig. 5.10 shows the BER penalty for clipped-and-filtered OFDM/FBMC/UFMC/ GFDM, when the frequency difference (Δf) between two adjacent channels, with similar features, is modified. That BER penalty has been measured using the QCD receiver, defining Δf as the electrical frequency separation between the central carrier of the measured channel and the interfering channel. For this measurement, the second transmitter has been enabled in the setup proposed in Fig. 5.6, so as to generate the interfering channel, whose wavelength has been tuned in steps of 0.75 GHz for a maximum spectral span of ±6 GHz. Eventually, to reduce as much as possible the interference of the adjacent channel, a digital 128-coefficient band-pass FIR filter has been considered for the IF at the receiver

side (see Fig. 5.6). From Fig. 5.10, it can be observed that for an FEC limit of 7% OH, the required Δf for OFDM and GFDM are very similar, ~4.125 GHz. For that same FEC limit, the required Δf for FBMC and UFMC are ~3.750 GHz and ~3.375 GHz, respectively. These results confirm that UFMC, with 18.2% of the required frequency difference less than OFDM, provides the best spectral localization, followed by FBMC, with a reduction of 9.1%. In the case of GFDM, no improvement has been obtained with regard to OFDM due to the fact that GFDM's OOB noise level is slightly lower compared to OFDM, see Fig. 5.8(e). For the obtained required frequency difference, the penalty over the sensitivity of the considered receiver gets worse in just 1 dB for all measured multicarrier waveforms.

5.7 Discussion: optical splitting ratio

High energy efficiency, low power consumption, and high throughput performance are the main motivations behind mobile network architectures and technological evolution. In the context of incoming C-RANs, in which massive small cells have to be deployed, high-layer split fronthaul will play an important role. In general, the optical splitting ratio of the physical layer of a network depends on the available power budget (PB) according to the technology used. Thus, the sensitivity of the optical receiver used for the RRH implementation is an important parameter to determine the available PB. Based on previous analysis, beside the type of receiver used, a DD or QCD receiver, the sensitivity also depends on if a clipping technique is used to improve the energy efficiency or not, the presence of adjacent channels, and, to a lesser extent, the multicarrier modulation scheme. Table 5.3 shows the available PB for OFDM, FBMC, UFMC and GFDM for both DD and QCD receivers when signals are unclipped and, clipped and filtered. These values have been calculated bearing in mind that the optical power at the central office's output is 0 dBm. Different end-users' spectral demands are allocated into the same DWDM channel, with the minimal spectral separation calculated in section 5.6, for a penalty of 1 dB, 25 km of SSMF, and the sensitivity values shown in Table 5.1 and Table 5.2. Then, the available PB values, shown in Table 5.3, are supposed to be consumed by a DWDM multiplexer and a power splitter, see Fig. 5.1. The main idea of using a power splitter is to share the same DWDM channel between different antennas. Typically, the insertion loss of an arrayed waveguide grating based WDM multiplexer that works for all C-band (4THz of bandwidth) is of 5 dB for DWDM channel bandwidths of 100(200) GHz. Therefore, the total optical splitting ratio (TOSR) reachable when RRHs are based on DD receivers, is of 40(20), while

the TOSR value when QCD receivers are used is of 640(320). That means that, for QCD-receiver-based RRH, the TOSR is 16 times higher than DD-receiver-based RRH. As can be expected, these TNSR do not depend on either the modulation scheme used or if a clipping technique is applied over the transmitted signals.

Table 5.3. Summary of available power budget (PB) of unclipped and clipped-and-filtered OFDM, FBMC, UFMC and GFDM signals for direct-detection (DD) and quasi-coherent-detection (QCD) receiver.

Mod. Scheme	PB (dB)			
	DD Receiver		QCD Receiver	
	Unclipped	Clipped-and-filtered	Unclipped	Clipped-and-filtered
OFDM	8.4	6.1	21.8	19.5
FBMC	8.2	5.8	20.9	18.5
UFMC	8.4	6.0	22.2	19.8
GFDM	7.7	5.1	20.4	17.8

5.8 Conclusions

In this chapter, alternative 5G multicarrier modulation formats (FBMC, UFMC and GFDM) and OFDM have been experimentally assessed for high-layer split DWDM-PON-based fronthaul with RoF technology. In particular, spectral efficiency, peak-to-average power ratio, power spectral density and, the sensitivity for a direct-detection receiver and for a quasi-coherent-detection receiver have been studied. In order to increase the energy efficiency of the communication system, the effects of the use of a hard-clipping technique over transmitted signals has also been experimentally assessed. Additionally, for u-DWDM application, the frequency difference between two similar adjacent channels with a 1 dB penalty has been measured.

Two main conclusions can be extracted from this detailed experimental assessment. On the one hand, it has been demonstrated that good performance can be achieved with hard clipping in spectral conformed, considered modulation formats: OFDM and alternative 5G multicarrier waveforms (FBMC, UFMC and GFDM). In particular, results show that: *i)* GFDM and FBMC present a slightly higher spectral efficiency (16%) than OFDM and UFMC, *ii)* hard clipping (50% of the peak of the transmitted symbol) provides 4 dB PAPR reduction, at the cost of 2.3 dB (ODFM) to 2.6 dB (GFDM) sensitivity penalty, after the appropriated filtering of the transmitted signal, to reduce the out-of-band noise, and *iii)* the respectively direct-detection and quasi-coherent sensitivities are around -14 dBm and -24.2 dBm. On the other hand, UFMC and FBMC have been identified as the most appropriate modulation formats for u-DWDM-PON. The UFMC shows the best spectral

localisation followed by FBMC, which reduce by 18.2% and 9.1%, respectively, the required frequency differences between two adjacent channels regarding OFDM, while GFDM does not provide improvement. Finally, while alternative 5G multicarrier modulations (FBMC, UFMC and GFDM) provide similar sensitivities as the previous OFDM, and, for example, considering 100(200) GHz bandwidth DWDM channels, the total network splitting ratio is 640(320) for quasi-coherent-detection receivers, UFMC provides an increase of the network's capacity close to 20%, potentially delivering up to 29(59) 2 GHz channels with 290(590) Gb/s per DWDM channel, whereas CPRI would transmit 2(4) 100 MHz channels in that same optical bandwidth.

Chapter 6. NOMA-CAP Modulation for High-Capacity PON and DC Optical Interconnect Applications

6.1 Introduction

In order to reach all new 5G OCNs' requirements, several researches have pointed out the necessity of overcome the current bottlenecks that have been presented in the access networks and in the connections inside data centers (DCs). On the one hand, access systems rely on non-return to zero (NRZ) and lately 4-level pulse-amplitude modulation (PAM-4) to encode the binary streams in the link; however, scaling beyond 25 Gb/s in access systems where cost is a key parameter indicator is challenging. On the other hand, there is a reasonable concern on whether PAM-4 can scale beyond 100 Gb/s per lane in DC optical interconnects [169]. The electrical bandwidth requirement for 200 Gb/s PAM-4 would be near 80-100 GHz, and silicon photonics, indium phosphide or heterogeneous integration are promising technologies but not yet mature enough to have significant yield with this specification in volume production [170]. Alternatively, multi-band orthogonal frequency division multiplexing (MB-OFDM) has been extensively explored as a potential candidate due to its numerous benefits such as high spectral efficiency, high resilience to chromatic dispersion and efficient/flexible resource management [83], [84], [85]. Nevertheless, one of the main drawbacks of MB-OFDM is its high computational complexity [87]. To overcome this problem, multi-band carrierless amplitude phase (MB-CAP) modulation format has been proposed [171]. CAP technique essentially consists of a quadrature amplitude modulation (QAM) using a low frequency carrier where the modulated signal is generated by combining two PAM signals filtered through two specifically designed filters so that it is not necessary to modulate two orthogonal carriers (quadrature carriers) with the baseband signal using the inverse discrete Fourier transform (IDFT) [172].

Non-orthogonal multiple access (NOMA) technique has recently been proposed as an alternative solution to increase the spectral efficiency, enabled by multiplexing different users in the power/amplitude domain at the transmitter side [86], [89]. Successive interference cancellation (SIC) must be conducted at the receiver side for multi-user signal

separation [173], [174], which increases the receiver complexity for a high number of users. To mitigate this issue, redundancy can be added to the users signals through spectrum spreading or coding techniques since it facilitates the user's signal separation, but decreasing the spectral efficiency [175]. Alternatively, SIC can be implemented with moderate complexity, without the need for spreading/coding redundancy, by limiting the number of power-multiplexed users to two and the constellation alphabet to four symbols, as demonstrated in [176]. Moreover, SIC with moderate complexity can be implemented using available technology with a tolerable increase of the energy consumption [90].

NOMA and MB-CAP working together has been reported in [89] yielding a capacity of 30 Gb/s in an fronthaul scenario. In this chapter, a new record of 90 Gb/s per lane using NOMA-CAP is achieved. In particular, NOMA-CAP modulation, providing a total aggregated capacity from 50 Gb/s to 90 Gb/s, has been assessed for downstream applications in high-capacity PONs and DC optical interconnects with cost-effective intensity modulation and direct detection (IM-DD). For downstream applications in PONs, SOA-based amplification has been considered to increase available power budget, while for DC optical interconnects, multi-core fiber (MCF) has been deemed to increase link capacity.

The remainder of this chapter is organized as follows. Section 6.2 presents the NOMA-CAP digital signal processing (DSP) for signal generation and detection when two NOMA power levels and different number of CAP bands of 2.5 GHz are considered. Section 6.3 studies the optical power budget enhancement in 50-90 Gb/s IM-DD PONs using NOMA-CAP modulation and SOA-based amplification. This section is divided into five sub-sections. Sub-section 6.3.1 describes the experimental PON setup including SOAs, sub-section 6.3.2 shows the power spectral density of transmitted NOMA-CAP signal, spectral efficiency and channel characterization measurements, sub-section 6.3.3 describes the experimental NOMA power ratio optimization that maximizes the receiver sensitivity for the two considered power levels, sub-section 6.3.4 shows the system receiver sensitivities and, sub-section 6.3.5 discusses the system optical power budget available. Section 6.4 studies the transmission of 50-90 Gb/s NOMA-CAP through 7-core MCF for DC optical interconnects applications, providing a maximum total aggregated data traffic of 350-630 Gb/s. This section is divided into two sub-sections. Sub-section 6.4.1 describes the MCF-based optical interconnect experimental setup and sub-section 6.4.2 shows the receiver sensitivities for each core. Finally, section 6.5 concludes the chapter and draws the main conclusions.

6.2 NOMA-CAP signal generation and detection

The transmitter DSP architecture for NOMA-CAP transmission with two NOMA levels per band is shown in Fig. 6.1(a).

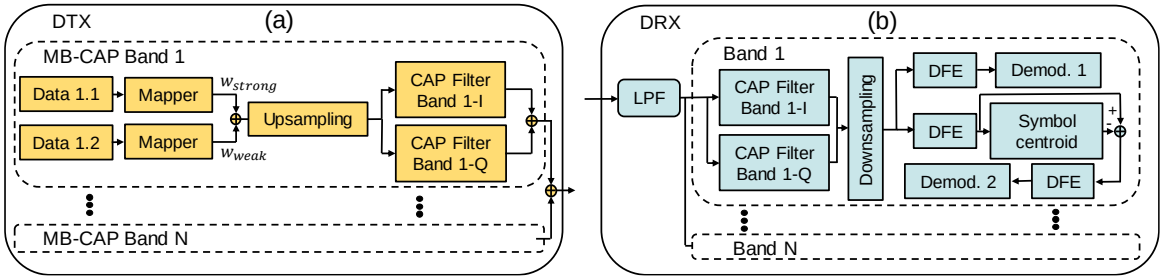

Fig. 6.1. NOMA-CAP DSP block diagram for: (a) the digital transmitter (DTX) and (b) digital receiver (DRX).

First, the data of both NOMA level were distributed among all the MB-CAP bands and mapped to quadrature phase shift keying (QPSK) symbols using Gray coding. The two NOMA levels, named "weak NOMA" and "strong NOMA", were power weighted according to the power ratio r_p, defined as the relation between the two NOMA levels, $r_p = 20log_{10}10(w_{strong}/w_{weak})$, and added for each MB-CAP band. The NOMA signal of each MB-CAP band was upsampled to the ratio between the sampling frequency and the symbol rate. The symbol rate was set at 2.5 GBd to provide a total bit rate of 10 Gb/s per band. After the upsampling process, the resulting complex NOMA signals were splitted into real and imaginary parts and filtered with a pair of band-specific MB-CAP orthogonal filters (h_{I_i} and h_{Q_i}) defined, in time domain, in Eq. (6.1) and Eq. (6.2), where $p(t)$ and f_{c_i} are the pulse shaper and the frequency carrier of the MB-CAP band i, respectively. In order to improve the spectral efficiency, a square-root raised cosine (SRRC) filter with a roll factor equal to 0.2 and a length of 20 symbols was employed as $p(t)$. Therefore, the filtering of each MB-CAP band with the matched filters at the reception side allows extracting the signal and simultaneously minimizing the inter-symbol interference (ISI). Finally, the MB-CAP bands were aggregated to form the full data transmitted signal. In this work, two NOMA levels with varying numbers of 2.5 GHz CAP bands, N_{bands}={5, 7, 9}, corresponding to bit rates R_b={50, 70, 90} Gb/s, were assessed. Both the SRRC filter roll off factor and the MB-CAP band bandwidth were empirically chosen to reduce the effect of the power fading dips of IM-DD transmission systems due to chromatic dispersion (CD) in the C band. Fig. 6.2 shows the temporal response of all considered MB-CAP band filters as well as an example of a NOMA-CAP signal to be transmitted in time domain.

$$h_{I_i} = p(t)\, cos\left(2\pi f_{c_i}\right) \tag{6.1}$$

$$h_{Q_i} = p(t)\, sin\left(2\pi f_{c_i}\right) \tag{6.2}$$

The receiver DSP block diagram is shown in Fig. 6.1(b). The first step was the low-pass filtering of the digitized signal with a finite impulse response (FIR) filter to reduce noise, and then each MB-CAP band was extracted using the inverted pair of orthogonal filters used at the transmitter side for the band of interest. For the weak NOMA level, it is necessary to implement SIC as shown in Fig. 6.1(b), consisting of a decision feedback equalizer (DFE) with 30 forward and 20 backward taps, calculation of the symbol centroid of the strong NOMA level and subtraction from the equalized signal. After SIC, the DFE was applied again to the resulting signal and finally the signal was de-mapped. For the strong NOMA level, only the DFE and the de-mapping were performed.

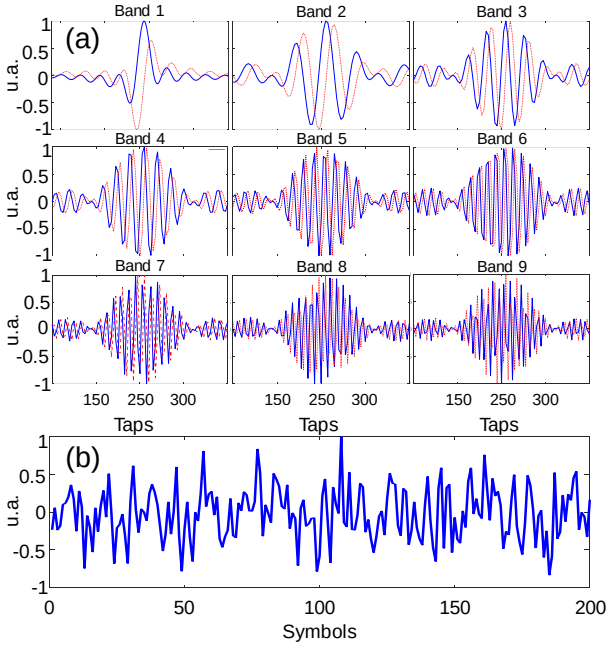

Fig. 6.2. (a) Temporal response of considered nine MB-CAP band filters (blue line is the I-component and red dotted line is the Q-component). (b) Example of transmitted NOMA-CAP signal in time domain.

6.3 Optical power budget enhancement in 50-90 Gb/s IM-DD PONs with NOMA-CAP modulation and SOA-based amplification

Going to 50 Gb/s IM-DD PONs and beyond, optical amplification, including semiconductor optical amplifiers (SOAs) or erbium doped fiber amplifiers (EDFAs), is required. Recently, SOA has attracted more attention due to its large optical bandwidth for

booster amplification and pre-amplification applications in 25G EPON [177], [178] , beside its small size and its ability to be integrated with other optical devices. Nevertheless, SOAs may have an impact on the data pattern quality due to its fast-dynamic gain, i.e., the patterning effect, and non-linearities [77]. Alternatively, avalanche photodiodes (APDs) can also be used to increase the optical power budget of the link. However, low-cost APDs bandwidth is still limited to 10 GHz. 18 GHz bandwidth APDs are becoming available in the market but their high cost makes them prohibitive for access networks [179].

50 Gb/s IM-DD PON with SOA-based amplification has recently been investigated for NRZ and PAM-4 in [180], [181], [182], [183]. In particular, 50 Gb/s PAM-4 PON based on 25G optics in the O band has been achieved in [180], providing an optical power budget compatible with the PR-30 (>29 dB) [21] thanks to the use of a SOA. In [181], a SOA+PIN photodetector (PD) receiver module has been demonstrated, providing a sensitivity at 40 Gb/s NRZ of -21 dBm using 10G optics. In [182], it has been accomplished the transmission of 50 Gb/s NRZ signal using a 40 GHz bandwidth externally modulated laser (EML) and an 18 GHz bandwidth APD at C band. Finally, in [183], 50 Gb/s PAM-4 transmission has been demonstrated over 20 km SSMF using 10G optics providing 21 dB power budget in C band.

Until now, 50-100 Gb/s IM-DD PON using other modulation formats different from NRZ and PAM-4 has not been investigated. In this section, NOMA-CAP modulation, providing a total aggregated capacity from 50 Gb/s to 90 Gb/s, has been assessed when a SOA is used for booster amplification and pre-amplification for downstream applications at the C band in a PON scenario with an optical span of 25 km. Specifically, it is characterized the SOA with NOMA-CAP signals with data rates ranging from 50 to 90 Gb/s in terms of the sensitivity of a PIN-based receiver. For comparison purposes, an EDFA for booster amplification applications has also been investigated.

6.3.1 Experimental setup description

The PON experimental setup is depicted in Fig. 6.3. The optical transmitter (TX) was based on an external cavity laser (ECL) tuned at 1548 nm and modulated with a Mach-Zehnder modulator (MZM) biased at its quadrature point. Although an ECL was used, a distributed feedback (DFB) laser can also be considered to reduce implementation costs since the increased phase noise of the DFB compared to the ECL does not affect the system performance. The MZM was driven with an arbitrary waveform generator (AWG) with 20 GHz 3 dB electrical bandwidth, generating the NOMA-CAP modulation. The

modulated optical signal was then amplified at the TX output by a SOA or an EDFA. The SOA bandwidth was 70.9 nm, centred around 1497.7 nm, the saturation output power was +16 dBm, the noise figure (NF) was 8.4 dB and the measured gain was 10 dB for an input power of 0 dBm. The EDFA bandwidth was 35 nm centred at 1548 nm, the saturation output power was +26 dBm, the NF was 4.5 dB and the gain was 18 dB at an input power of 0 dBm. The optical power at the transmitter output was +3.4 dBm for which the SOA is still operating in the linear regime, as shown in Fig. 6.3. The amplified signal was optionally filtered by a 100(200) GHz band pass filter (BPF) to study the effect of the amplified spontaneous emission (ASE) noise over the optical signal. The optical signal was then launched into a span of 25 km of standard single-mode fiber (SSMF). Two configurations were considered for the optical receiver (RX). The first one based on a PIN photodetector (PD) combined with an electrical amplifier (RX Config. I, refer to Fig. 6.3), and the second one, a pre-amplified receiver with the same PD (RX Config. II, in Fig. 6.3). A SOA with similar characteristics to the one used in the TX output was used in the pre-amplified receiver configuration. The detected signal was finally digitized with a 100 GSa/s real time oscilloscope with 33 GHz of electrical bandwidth and processed offline.

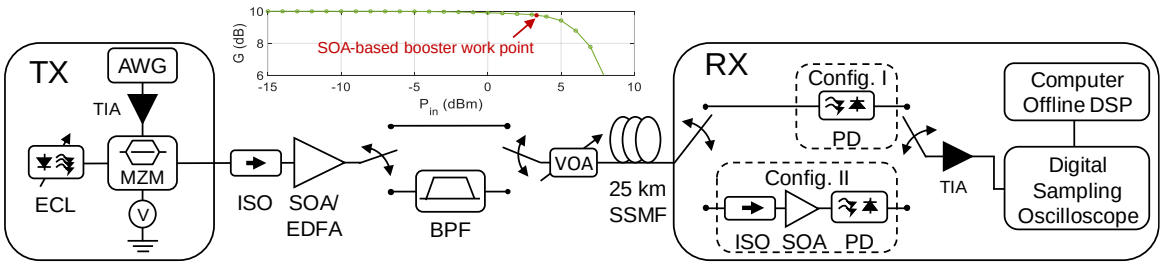

Fig. 6.3. PON experimental setup for the NOMA-CAP transmission. (Inset) Optical gain (G) vs. input power (P_{in}) characterization of used SOA.

6.3.2 Power spectral density, spectral efficiency and channel characterization measures

Fig. 6.4 depicts the received NOMA-CAP spectra after 25 km SSMF for N_{bands}=9, corresponding to R_b=90 Gb/s. There, it can be observed that the required electrical bandwidth for N_{bands}=9 is 27 GHz, while for N_{bands}={5, 7}, corresponding to R_b={50, 70} Gb/s, is 15 GHz and 21 GHz, respectively. The spectral efficiency, considering two NOMA levels per band, is close to 3.3 b/(s·Hz). This is an improvement of 3.3 and 1.6 times compared to OOK and PAM-4, respectively. Therefore, the electrical/optical bandwidth reduction provided by MB-CAP plus NOMA technique increases the total data rate and spectral efficiency in the optical link. Fig. 6.4 also depicts the frequency response of the 25 km SSMF channel for the IM-DD system proposed in Fig. 6.3. In Fig. 6.4, it can

be observed that the frequencies of the fading dips due to CD are between two different bands, overcoming therefore the bandwidth limitation of the transmission channel for IM-DD systems.

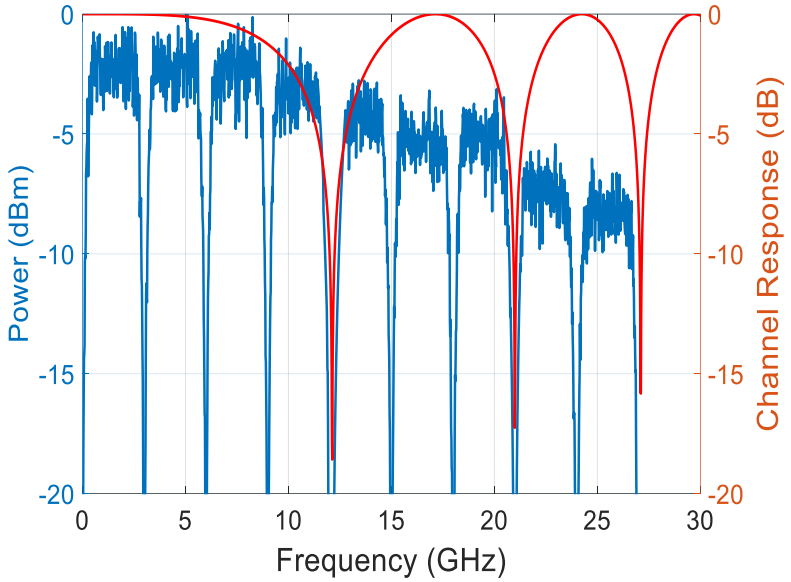

Fig. 6.4. Received NOMA-CAP spectra for 9 CAP bands, providing an aggregated bit rate of 90 Gb/s, as well as the IM-DD channel frequency response for 25 km SSMF.

6.3.3 Experimental NOMA power ratio optimization

Fig. 6.5 shows the measured NOMA-CAP system performance in terms of the bit-error rate (BER), averaged for all bands, vs. r_p vs. the received optical power (P_{RX}) for the strong and weak NOMA levels in back-to-back configuration when R_b=70 Gb/s (N_{bands}=7). For the strong NOMA level, the power multiplexing with the signal of the weak NOMA level can be considered as an increment of the received noise. In this way, reduced r_p values cause a BER degradation and it decreases the achievable receiver sensitivity, defined as the minimal P_{RX} required to reach the FEC limit of $2.2\text{x}10^{-3}$ which corresponds to 7% FEC OH limit [120], as shown in Fig. 6.5(a). Hence, the best scenario for the strong NOMA level corresponds to higher r_p values.

In the case of the weak NOMA level, SIC cancellation must be performed before demodulation to remove the contribution of the strong NOMA level signal. Any error in the calculation of the centroid of the strong NOMA level affect the decoding of weak NOMA level in the SIC stage, causing a higher BER, and hence a reduction of the P_{RX} for weak NOMA level increases the number of errors in the centroid calculation, causing a degradation of the BER of weak NOMA level signal, as can be observed in Fig. 6.5(b). The use of lower r_p values has a similar effect as reducing the P_{RX}, resulting in errors in the

calculation of the strong NOMA level centroid and consequently propagating the error to the decoding of the weak NOMA level. Finally, the BER of weak NOMA level also increases with higher r_p values as the signal is too weak after SIC, even if the SIC process perfectly calculates the strong NOMA level centroids. Consequently, the weak NOMA level is only successfully demodulated for intermediate r_p values and for high P_{RX} values, as observed in Fig. 6.5(b). Similar behaviour was obtained for the strong and weak NOMA levels in the case of N_{bands}={5, 9}. It is established a r_p=7 dB as a good trade-off that optimizes the reception of both NOMA levels for all considered aggregated bit rates.

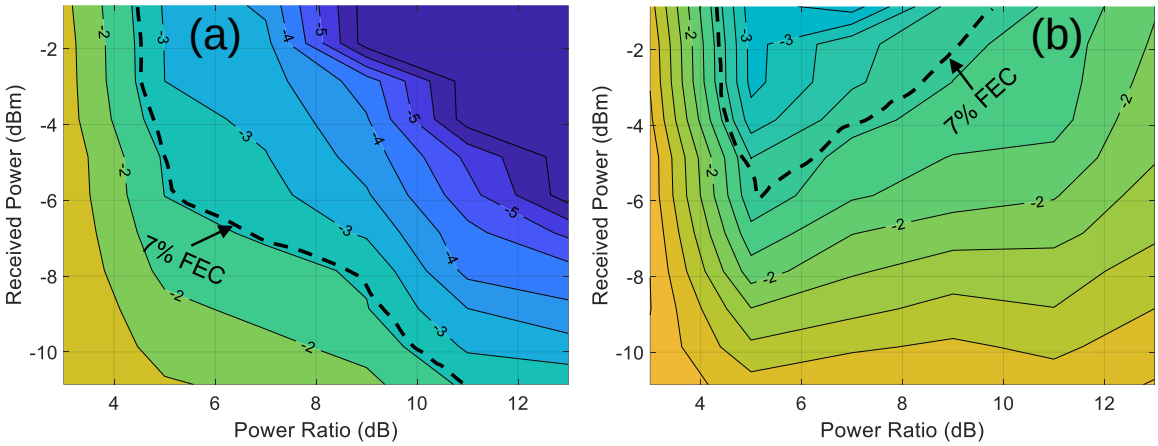

Fig. 6.5. Contour $\log_{10}$(BER) vs. received power vs. power ratio plots for (a) strong NOMA and (b) weak NOMA levels in back-to-back configuration when the number of MB-CAP bands is equal to 7, providing an aggregated bit rate of 70 Gb/s.

6.3.4 Sensitivity measurement

Fig. 6.6(a-c) shows the BER vs. P_{RX} curves for the strong and weak NOMA levels for R_b={50, 70, 90} Gb/s when r_p is fixed to the optimized value of 7 dB for the cases in which the NOMA-CAP signal has been optically boosted by the SOA/EDFA at the transmitter output and with no optical amplification. In these measurements, the optical receiver based simply on a PD (see Fig. 6.3, Config. I) has been considered. To determine the effect of the SOA ASE noise over the receiver sensitivities, Fig. 6.6 also shows the BER curves when the optical signal is filtered at the SOA output with an optical band pass filter with bandwidths of 100 and 200 GHz. When using the EDFA, no optical filtering is required since a high optical signal to noise ratio (OSNR) is obtained (>40 dB).

Table 6.1 summarizes the receiver sensitivities depicted in Fig. 6.6 for R_b={50, 70, 90} Gb/s. For both the strong and weak NOMA levels, the sensitivity penalty when the bit rate is increased from 50 Gb/s to 70 Gb/s is close to 2 dB, while increasing the bit rate from 50 Gb/s to 90 Gb/s, the penalty in the sensitivity is of 4 dB. From Table 6.1, the averaged

penalty $\bar{\Delta}$ (defined as the average receiver sensitivities among all bit rates) is of 0.8 dB and 1.8 dB for the strong and weak NOMA levels when the SOA is used without optical band pass filtering, respectively, while the penalties over the receiver sensitivity of the strong and the weak NOMA levels when the EDFA is used are just 0.1 dB and 0.4 dB, respectively. For the SOA plus filtering case, $\bar{\Delta}$ for the strong and weak NOMA levels are now reduced to 0.1(0.3) dB and 0.7(1.0) dB when the 100(200) GHz bandwidth band pass filter is used, respectively. The penalty reduction is due to the ASE noise reduction in the optical filter. Despite those small penalties, the SOA and EDFA provide output power gains of 10 dB and 18 dB, respectively. Finally, from Fig. 6.6, no penalty was observed in the receiver sensitivity after 25 km transmission when the optical signal is amplified by the SOA/EDFA due to the high resilience of MB-CAP to the CD [171], since the SRRC roll off factor and the MB-CAP band bandwidth have been chosen to overcome the penalty caused by the CD.

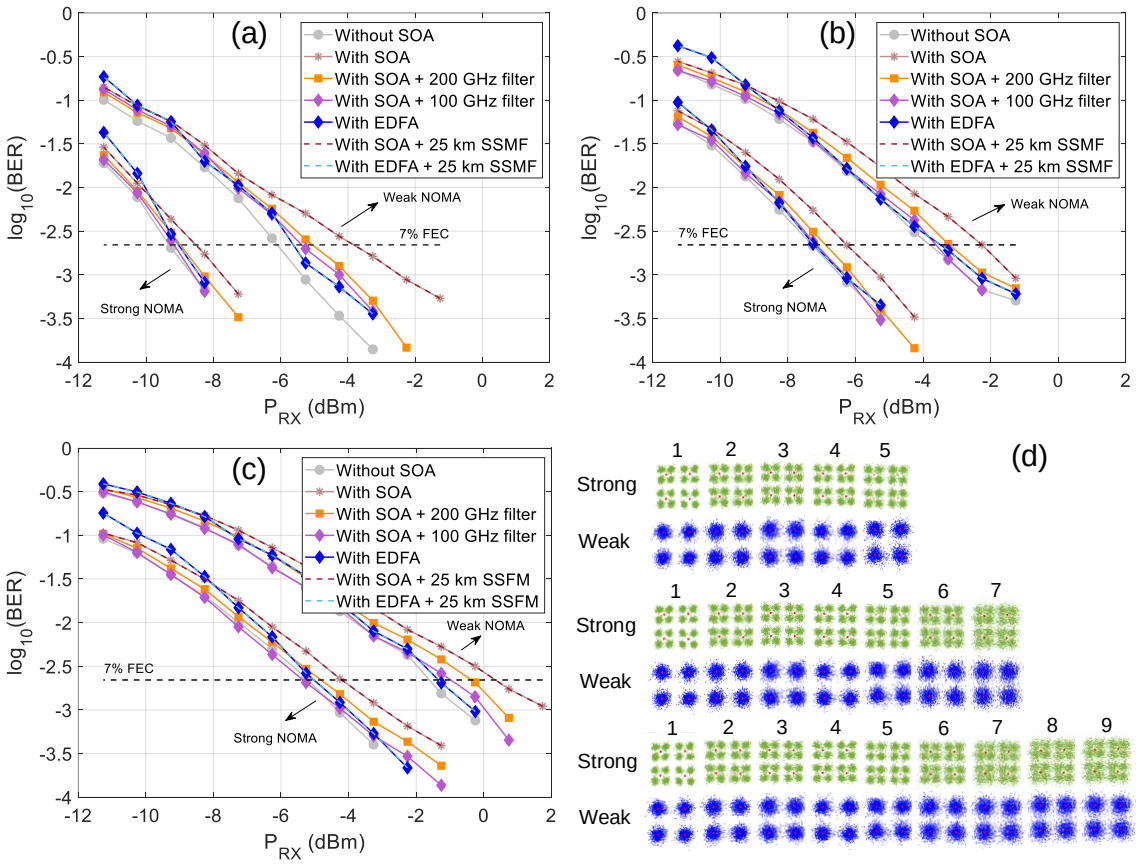

Fig. 6.6. BER vs. received power (P_{RX}) for the strong and weak NOMA levels when the optical signal is amplified by SOA/EDFA and optionally filtered with 0 km and 25 km of SSMF for: (a) 5 CAP bands, (b) 7 CAP bands and (c) 9 CAP bands providing an aggregated bit rate of 50 Gb/s, 70 Gb/s, and 90 Gb/s, respectively. (d) Received constellations at the considered FEC OH limit after the SOA and 25 km SSMF for both NOMA levels for N_{bands}={5, 7, 9}. Red circles are the constellation centroids.

Table 6.1. Summary of receiver sensitivities (Ss) of the weak and strong NOMA levels for R_b={50, 70, 90} Gb/s when the signal is amplified by SOA/EDFA, optically band pass filtered and the receiver is based on a PIN PD as well as their power penalty (Δ) compared to the case in which no optical amplification is used. $\bar{\Delta}$ is the averaged power penalty among all considered bit rates.

R_b (Gb/s)	NOMA level	Strong					Weak				
	Optical amplifier	No	SOA			EDFA	No	SOA			EDFA
	BW filter (GHz)	∞	100	200	∞	∞	∞	100	200	∞	∞
50	S (dBm)	-9.0	-8.9	-8.8	-8.5	-8.9	-6.0	-5.2	-5.1	-4.0	-5.6
	Δ (dB)		0.1	0.2	0.5	0.1		0.8	0.9	2.0	0.4
70	S (dBm)	-7.3	-7.2	-7.1	-6.3	-7.2	-3.8	-3.6	-3.3	-2.3	-3.5
	Δ (dB)		0.1	0.4	1.0	0.1		0.7	0.5	1.5	0.3
90	S (dBm)	-5.3	-5.1	-4.9	-4.3	-5.1	-1.8	-1.2	-0.3	0.2	-1.3
	Δ (dB)		0.2	0.4	1.0	0.2		0.6	1.5	2.0	0.5
$\bar{\Delta}$ (dB)			0.1	0.3	0.8	0.1		0.7	1.0	1.8	0.4

Fig. 6.6(d) shows the received constellations after the NOMA-CAP signal transmission through the SOA and 25 km SSMF on each CAP band and each NOMA level at the FEC limit of 7% OH for each considered R_b value. Table 6.2 summarizes the BER of each band and each NOMA level at the considered FEC limit. Form Table 6.2, it can be observed that the BER of each CAP band is lower than $7.8\text{x}10^{-4}$, BER value corresponding a maximum penalty of 1 dB over the receiver sensitivity of the proposed system, see Fig. 6.3.

Table 6.2. Summary of BER tributaries of the strong and weak NOMA levels for different aggregated bit rates (R_b) when the power ratio is fixed to 7 dB as well as the BER of each MB-CAP band at the considered FEC limit of 7% (2.2×10^{-3}). The received optical powers are {-9, -7.3, -5.3} dBm and {-6.0, -3.8, -1.8} dBm for the strong and weak NOMA levels at R_b={50, 70, 90} Gb/s, respectively.

NOMA level	R_b (Gb/s)	BER per each MB-CAP band ($\text{x}10^{-4}$)								
		1	2	3	4	5	6	7	8	9
Strong	50	4.0	4.1	4.3	4.7	4.9				
	70	1.2	1.3	1.7	1.8	2.0	6.5	7.5		
	90	0.9	1.1	1.3	1.4	1.6	2.9	3.5	3.9	5.4
Weak	50	3.7	4.1	4.2	4.8	5.2				
	70	1.1	1.2	1.8	2.3	2.6	5.9	7.1		
	90	1.2	1.3	1.3	1.6	1.9	2.5	2.8	3.5	5.9

Fig. 6.7 shows the measured sensitivity enhancement in the receiver when the proposed PD-based receiver is upgraded with a SOA in a pre-amplifier configuration, as shown in Fig. 6.3 (Config. II) and no amplification is performed at the transmitter output for R_b={50, 70, 90} Gb/s and a 25 km of SSMF. Now, the BER is measured in terms of the input power to the SOA at the receiver. This leads to an OSNR variation which is different from the previously studied cases, resulting therefore in different BER curves. The new receiver sensitivities are, for the strong NOMA level, -15.3 dBm, -13.3 dBm and -10.8 dBm for 50 Gb/s, 70 Gb/s and 90 Gb/s, respectively, while, for the weak NOMA level are -11.7 dBm, -9.3 dBm and -7.0 dBm for 50 Gb/s, 70 Gb/s and 90 Gb/s, respectively.

Therefore, for the strong NOMA level, the receiver sensitivity enhancement is close to 6.0 dB, while, for the weak NOMA level, the enhancement is close to 5.5 dB. Higher enhancements cannot be achieved since the ASE noise of the SOA degrades the output OSNR. In these measurements, optical filtering to reduce the impact of the ASE noise has not been performed to reduce costs at the receiver. Therefore, future SOA-PD photonic integrated circuits (PICs) could be a very suitable solution.

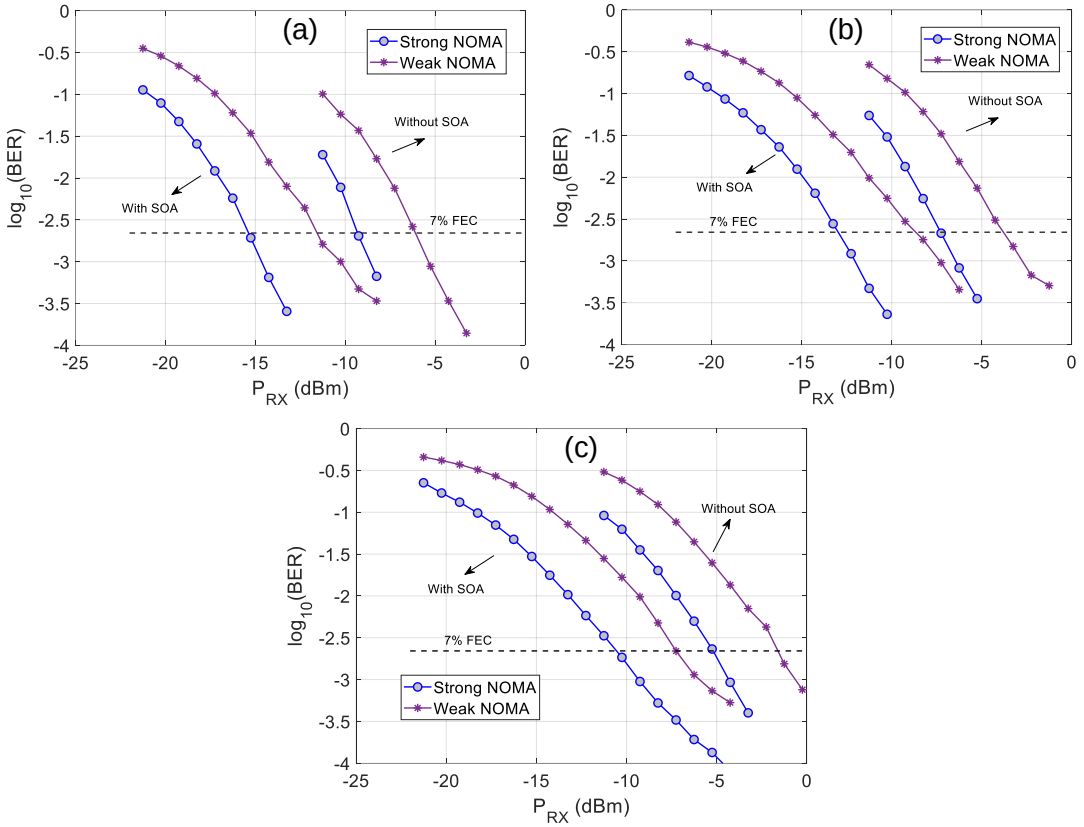

Fig. 6.7. BER vs. received power (P_{RX}) comparison when the NOMA-CAP signal is pre-amplified by a SOA at the receiver and not for: (a) 5 CAP bands, (b) 7 CAP bands and (c) 9 CAP bands providing an aggregated bit rate of 50 Gb/s, 70 Gb/s, and 90 Gb/s, respectively.

6.3.5 Discussion: optical power budged available

Given all the measured sensitives and considering that the transmitter output power is +3.4 dBm, Table 6.3 shows the available optical power budgets (PB) for the strong and weak NOMA levels when no optical amplification is used, and when SOA-based amplification is performed at the transmitter side (booster), at the receiver side (pre-amplifier) and at both sides for R_b={50,70,90} Gb/s. If optical filtering is performed at the booster SOA, e.g., emulating a WDM-based PON, the power budget of the strong NOMA level decreases in 5 dB (typical insertion loss of an arrayed waveguide grating based multiplexer) while for the weak NOMA level it is reduced by 4 dB due to the gain of an approximately 1 dB

obtained when the ASE noise is filtered. From Table 6.3, it can be observed a PB reduction of 3.5 dB when the pre-amplification configuration is used regarding the booster configuration. An enhancement of 15.6 dB and 14.2 dB in the PB can also be observed in Table 6.3 for the strong and weak NOMA levels, respectively, when both booster and pre-amplifier are used compared no optical amplification case.

Table 6.3. Summary of available power budget (PB) of the weak and strong NOMA levels for R_b={50, 70, 90} Gb/s when no optical amplification is performed and when SOA-based amplification is used at the transmitter side (booster), at the receiver side (pre-amplifier), and at both sides.

NOMA level	Strong PB (dB)			Weak PB (dB)		
R_b (Gb/s)	50	70	90	50	70	90
Without optical amplification	12.4	10.7	8.7	9.4	7.2	5.2
With booster	22.4	20.2	18.2	17.9	16.2	13.7
With pre-amplifier	18.7	16.7	14.2	15.1	12.7	10.4
With both booster and pre-amplifier	28.7	26.2	23.7	23.6	21.7	18.9

6.4 Split-enabled 350-630 Gb/s optical interconnect with direct detection NOMA-CAP and 7-core multi-core fiber

Current DC optical interconnects, relying on legacy IM-DD systems with PAM-4, are about to reach their limits in terms of capacity and flexibility. There is therefore a need to exploit and investigate alternative dimensions and/or modulation formats to increase the capacity and flexibility of optical interconnects while keeping the end-to-end link latency as low as possible. Currently, there is momentum for coherent technologies to penetrate the short-range segment in data centers, although costs remain a huge challenge given the complexity of the optical layer, the power consumption, the DSP complexity and the increased latency. Alternatively, exploiting spatial diversity through MCFs enables the parallel multiplexing of several spatial channels, while facilitating the assembly process between fiber and the photonic integrated circuits (PICs), most likely through constellations of vertical gratings tapping light in and out of the PIC [184], with a reasonable cost impact. Furthermore, link splitters are becoming more relevant when designing the topology of the network in data centre environments as shown in Fig. 6.8. Spit-cables or H-cables allow a system unit with a connector on one side and two or more separate connectors on the other side, such as a top of rack (ToR) switch and two or more servers, thereby allowing network topologies relevant for hyperscalers [185]. This feature is particularly interesting in large configurations of high-performance clusters (HPC) within data centers, as the number of layers of switches is reduced and frees up switching ports. In this section, it is proposed NOMA-CAP as a flexible and efficient modulation format combined with MCFs to

increase DC interconnects capacity and flexibility. Specifically, it is experimentally demonstrated the transmission of NOMA-CAP through 2 km 7-core MCF using DD for different total aggregated traffics ranging from 350 Gb/s to 630 Gb/s.

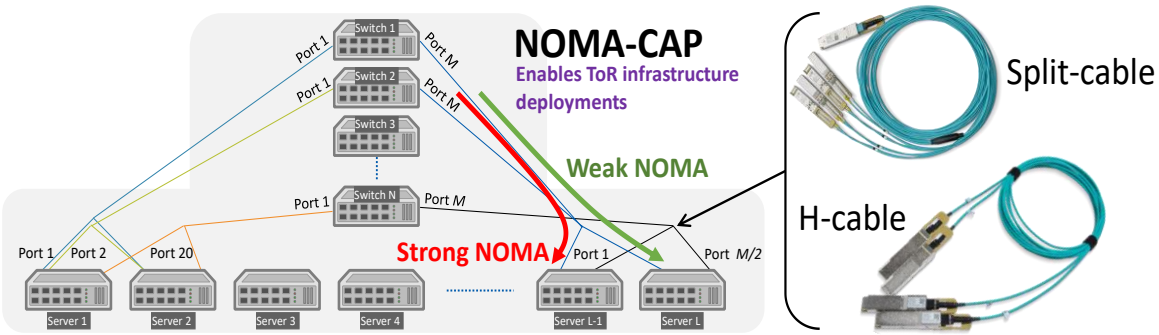

Fig. 6.8. Architecture of a highly scalable top of rack (ToR) data centre architecture enhanced by split-cables or H-cables.

6.4.1 Experimental setup description

The MCF-based optical interconnect experimental setup is shown in Fig. 6.9. The transmitter used a distributed feedback laser (DFB) as a light source which was feed to a Mach-Zehnder modulator (MZM) using a manual polarization controller (PC). This simple transmitter can be integrated through heterogeneous integration, in high-performing indium phosphide, or most likely, through a silicon photonic PIC containing the modulators and arrays of flip-chip DFB lasers [186], [187]. The bias of the MZM was provided by a voltage source. The MZM was driven with an arbitrary waveform generator (AWG) with 25 GHz 3 dB electrical bandwidth, which generated the NOMA-CAP modulation, and amplified with a linear electrical driver. After the MZM, an erbium-doped fiber amplifier (EDFA) was used to amplify the signal and compensate for the losses of the 1x8 splitter, used to simulate traffic coming from 7 different transmitters each containing two independent data-streams. As the patch-cord length of each path was different, the channels were effectively decorrelated. The seven information-bearing signals were connected to a fan-in device, used to multiplex the signals into a 7-core 2 km MCF span. After transmission, the signals were demultiplexed using a fan-out device. The receiver consisted of a standard PIN photodiode with an optical bandwidth of 33 GHz followed by a digital sampling oscilloscope (DSO), which was connected manually to each core of the MCF under measurement. The signal was digitized at 100 GS/s.

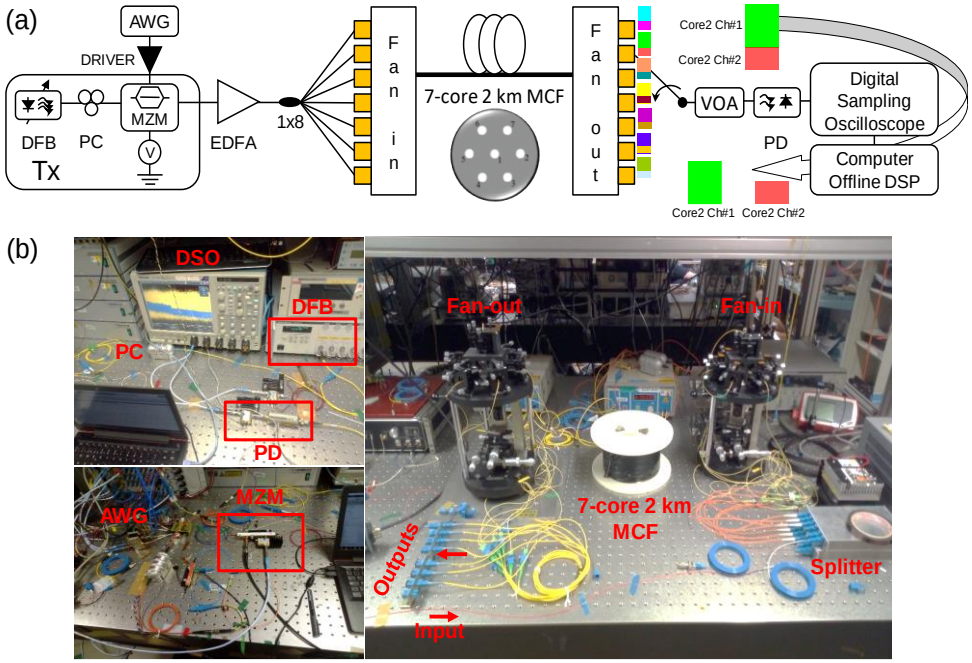

Fig. 6.9. (a) Schematic of the experimental setup for the NOMA-CAP transmission. (Inset) Microphotography of the 7-core 2 km MCF fiber used in this demonstration. (b) Laboratory setup.

6.4.2 Sensitivity measurement

Fig. 6.10 shows BER vs. P_{RX} when the NOMA-CAP signal is simultaneously transmitted through the cores of the 7-core 2 km MCF, providing a total transmission aggregated bit rate T_{R_b}={350, 490, 630} Gb/s for R_b={50, 70, 90} Gb/s per spatial channel, respectively. The BER curves for each core have been measured as the averaged among all bands of the transmitted NOMA-CAP signal when the power ratio between the two NOMA levels has been fixed to 7 dB. From Fig. 6.10 it can be observed that the receiver sensitivity of the strong NOMA level in back-to-back configuration are -9.7 dBm, -7.1 dBm, -3.9 dBm for 50 Gb/s , 70 Gb/s and 90 Gb/s, respectively, while for the weak NOMA level are -6.9 dBm, -4.7 dBm and -0.1 dBm for 50 Gb/s, 70 Gb/s and 90 Gb/s, respectively. Finally, negligible penalty is measured in the receiver sensitivity over 2 km fiber transmission compared to the back-to-back case due to the high resilience of NOMA-CAP to the CD [171].

6.5 Conclusions

In this chapter, NOMA-CAP has been experimentally assessed for high capacity PON and DC optical interconnect applications. On the one hand, 50-90 Gb/s NOMA-CAP with two power levels has been experimentally measured in an IM-DD system with a PIN-based receiver and 25 km of SSMF. To increase the low available optical power budget of the system, SOA-based amplification at the transmitter and receiver sides has been considered.

Two main conclusions can be extracted from this experimental assessment for PON applications. First, the SOA shows better performance in terms of power budget as booster since the system enhancement is of 3.5 dB compared to the pre-amplifier case. Second, obtaining high power budgets require both boosters and pre-amplifiers. In this case, SOA-based amplification for NOMA-CAP modulation provides optical power budgets of 28.7(23.7) dB and 23.6(18.9) dB at 50(90) Gb/s for the strong and weak NOMA levels, respectively, while the budgets for the strong and weak NOMA levels are 12.4(8.7) dB and 9.4(5.2) dB at 50(90) Gb/s when no optical amplification is used. Finally, it is considered that NOMA-CAP with SOA-based amplification, e.g., offering a maximum optical splitting ratio of 64(32) at 50(90) Gb/s for an optical reach between 25(24.8) km and 10.4(5.6) km, could be a good modulation format candidate for next generation PONs. Particularly, it is believed the power budget levels achieved are aligned with current standards employed in the field, such as 10G-EPON [21], which requires power budgets in the order of 20-24 dB for the PR10 and PR20 options (for 10 km and 20 km reach, respectively). If high power budgets are required, low-density parity-check (LDPC) codes could be considered, allowing to comply with the PR-30 requirements for 50 Gb/s.

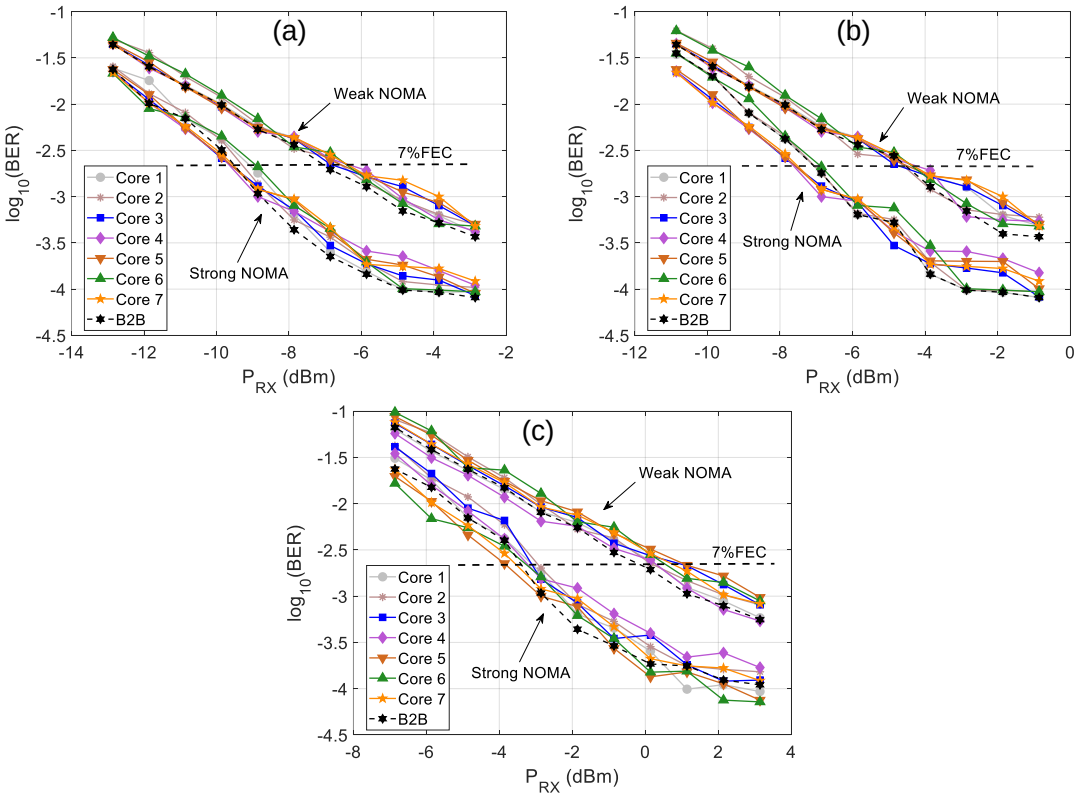

Fig. 6.10. BER vs. received power (PRX) of the weak and strong NOMA levels when the NOMA-CAP signal is transmitted in back-to-back (B2B) configuration and through the 2 km MCF with 7 cores for a total aggregated bit rate per lane of: (a) 50 Gb/s, (b) 70 Gb/s and (c) 90 Gb/s, providing a total aggregated traffic of 350 Gb/s, 490 Gb/s and 690 Gb/s, respectively.

On the other hand, it was presented a technical solution to increase the features of split-cables and H-cables enabling advanced architectures in data centers. The solution comprises the exploitation of space division multiplexing through multi-core fibers and NOMA-CAP as doubler of the link capacity. Particularly, NOMA-CAP has been experimentally measured in an DD system with a PIN-based receiver at different bit rates. The transmission of NOMA-CAP through 2 km of 7-core MCF, providing different total aggregated traffics between 350 Gb/s and 630 Gb/s, has been also demonstrated with negligible transmission penalty. This result pushes forward NOMA-CAP as a strong candidate for future data centers optical interconnects that require split links, high capacity, high granularity and scalability.

Chapter 7. Convergence of Mobile RoF-based Fronthaul and PONs with NOMA-CAP Modulation

7.1 Introduction

Owing to the current exponential growth of the network traffic of cloud and new multimedia streaming services on personal devices, together with the deployment of the "Internet of Things" and massive machine-to-machine communication, the operators expect to provide both broadband wireline and wireless access for end-users through the existing access network infrastructures, minimizing both the network capital expenditure (CAPEX) and the operation expenditure (OPEX) [100]. In this context, deployed passive optical networks (PONs) are already the most competitive solution to serve as mobile fronthaul, especially in cloud access radio network (C-RAN) scenarios where high capacity, low latency and flexibility are required [91]. Moreover, deployed PONs can be cost-effectively upgraded to simultaneously support both wired and wireless services. Common public radio interface (CPRI) and open base station standard initiative (OBSAI) are the current protocols used in fronthaul transmission. Nevertheless, these interfacing techniques are inadequate for upcoming high capacity 5G mobile communication services. Alternatively, radio-over-fiber (RoF) technology has recently sparked more attention [96], [97], [98], [99], not only for simplifying the interfaces, e.g., digitization and format conversion are not required, but also for conserving bandwidth.

In C-RANs, the design of medium-access layer is fundamental to improve the system capacity and to dynamically allocate the available resources. Recently, non-orthogonal multiple access (NOMA) modulation, i.e., multiplexing different users in the power/amplitude domain, has been proposed as an alternative solution for addressing these requirements and to enhance both the capacity and flexibility of the network [86], [89], [90]. Moreover, multi-band orthogonal frequency division multiplexing (MB-OFDM) [188] and multi-band carrierless amplitude phase (MB-CAP) modulation [171] have been proposed as excellent candidates to replace inefficient modulation formats such as impulse radio (IR) and OOK. Although MB-OFDM has shown flexible adaptation to a dynamically

changing wireless medium, MB-CAP allows less complex transceivers [87] and has shown better results [88], [89], achieving large capacities even under difficult channel conditions.

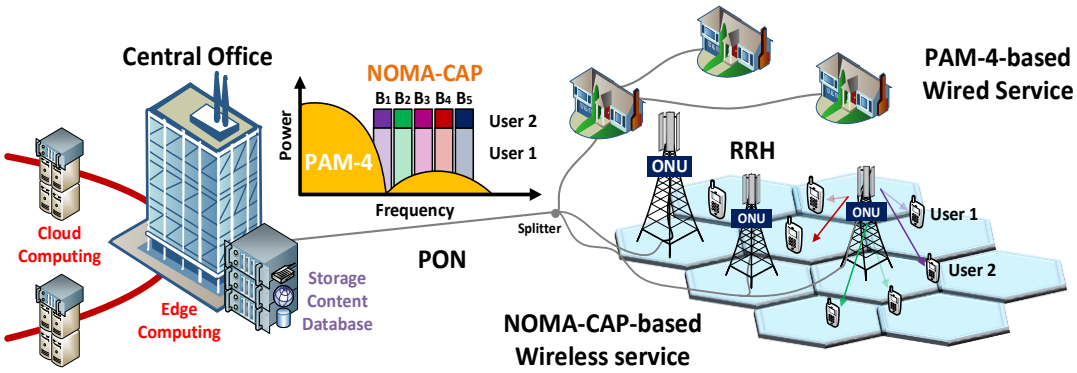

Fig. 7.1. Conceptual diagram of a converged fronthaul and passive optical network (PON). PAM-4 modulation format is used as legacy system and NOMA-CAP is used for future access fronthaul in 5G and beyond.

NOMA and MB-CAP working in tandem have been experimentally validated in [89] as an excellent solution for wireless multi-user provisioning. Although that validation has been performed focusing on the wireless domain, NOMA-CAP modulation format must also be investigated in the optical domain where its suitability for fronthaul transmission and its potential for integration with other converged wireless-wired services must be assessed. NOMA-CAP have been reported for wired services in high-capacity PONs and DC optical interconnects in chapter 6 of this thesis. However, the convergence of NOMA-CAP as a wireless signal in a converged fronthaul and fixed access system has not been studied before. In this chapter, using RoF technology it is demonstrated the downlink transmission of wireless NOMA-CAP waveforms with two power levels per band, converged with a single-carrier wired signal in a PON scenario as shown in Fig. 7.1. Specifically, it is experimentally assessed a wireless-wired converged PON system which utilizes a 10 Gb/s PAM-4 signal as the wired service. PAM-4 was chosen since it has recently gained interest for use in future optical access networks due to its low complexity and compatibility with current intensity modulation-direct detection (IM-DD) deployments, making it a cost-effective solution for future PONs [189], [190]. Moreover, two converged system implementations have been considered. The first one, using electrical frequency division multiplying (FDM) technology, and the second, using hybrid FDM-wavelength division multiplexing (FDM-WDM) technology. While the FDM technology increases the system spectral efficiency, hybrid FDM-WDM technology aims to increase the network capacity without considerably adding complexity [191]. In both cases, the converged system assessment has been performed in terms of bit-error rate (BER)

to determine the potential transmission penalties due to the crosstalk interference and the fiber chromatic dispersion (CD).

The remainder of this chapter is structured as follows. Section 7.2 describes the digital signal processing (DSP) of NOMA-CAP with two power levels and the generation and detection process of PAM-4 signals as well as the implemented optical transmission setup. Section 7.3 shows the measured experimental results for NOMA-CAP and PAM-4 in the proposed converged PON systems. Finally, section 7.4 concludes the chapter and draws the main conclusions.

7.2 Experimental setup description

7.2.1 NOMA-CAP and PAM-4 signal generation and detection

Fig. 7.2(a) shows the transmitter DSP architecture for the converged mobile fronthaul and fixed access system using NOMA-CAP with two NOMA levels per band and PAM-4. For each NOMA-CAP band, the data of both NOMA levels were mapped to quadrature phase shift keying (QPSK) symbols. The two NOMA levels, named "weak NOMA" and "strong NOMA", were power weighted according to the power ratio r_p, and then, both signals were added to conform the NOMA signal of each CAP band. The NOMA signal of each CAP band was upsampled to the ratio between the sampling frequency and the symbol rate. The symbol rate was set at 0.25 GBd to provide a total bit rate of 1 Gb/s per band. After the upsampling process, the resulting complex NOMA signals were split into real and imaginary parts and filtered with a pair of band-specific CAP orthogonal filters [89]. Finally, the NOMA-CAP bands were aggregated to form the transmitted NOMA-CAP signal, $y_{NOMA-CAP}$. In this work, it was established a r_p=7 dB as a good trade-off that optimizes the reception of both NOMA levels. The PAM modulator was configured to work with a uniform four-level constellation, generating the baseband PAM-4 signal to transmit, y_{PAM-4}. For the FDM system implementation, the NOMA-CAP and the PAM-4 signals were digitally added to form the full data transmitted signal, $y_t = y_{NOMA\text{-}CAP} + 10^{\frac{\alpha}{10}} \cdot y_{PAM\text{-}4}$, where PAM-4 signal was amplitude weighted with different values, α={-6.0, -3.0, -1.2} dB, to assess the crosstalk interference between the NOMA-CAP and PAM-4 signals.

The receiver DSP block diagram is shown in Fig. 7.2(b). For the NOMA-CAP demodulator, each MB-CAP band was extracted using the inverted pair of orthogonal filters used at the transmitter side for the band of interest. For the weak NOMA level, it is

necessary to implement successive interference cancellation (SIC) as shown in Fig. 7.2(b), consisting of a decision feedback equalizer (DFE) with 30 forward and 20 backward taps, calculation of the symbol centroid of the strong NOMA level and subtraction from the equalized signal. After SIC, the DFE was applied again to the resulting signal and finally the signal was de-mapped. For the strong NOMA level, only the DFE and the de-mapping were performed. In the case of the PAM demodulator, the received signal was optimally filtered using a low-pass finite impulse response (FIR) filter with a cut-off frequency equal to eighty percent of the PAM symbol rate. The PAM-4 adaptive equalizer was a 13-tap FIR filter and the tap weights were updated with a decision-directed least-mean square (DD-LMS) algorithm [192].

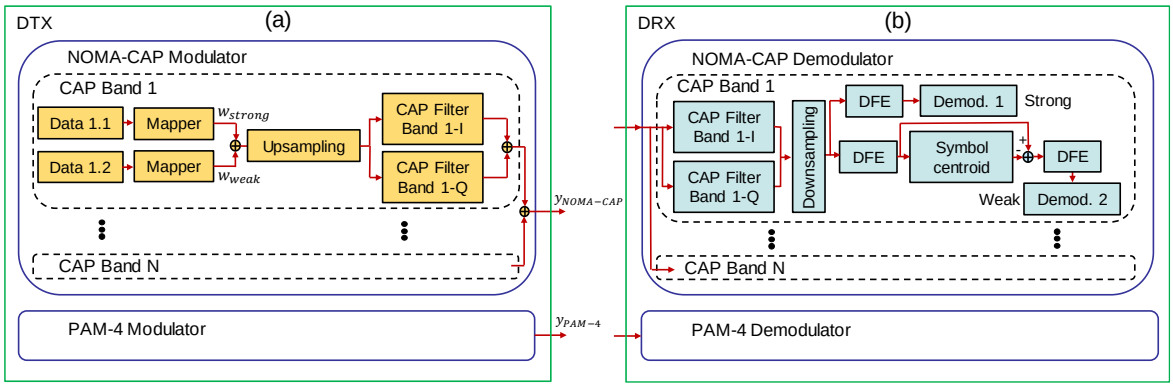

Fig. 7.2. DSP architecture of the converged fronthaul and fixed access system using NOMA-CAP and PAM-4: (a) the digital transmitter (DTX) and (b) digital receiver (DRX).

7.2.2 Converged PON experimental setup

The experimental IM-DD-based setup is depicted in Fig. 7.3(a). The optical transmitter (TX-1) was based on an external cavity laser (ECL) tuned at 1548 nm and modulated with a Mach-Zehnder modulator (MZM) biased at its quadrature point. The MZM was driven with an arbitrary waveform generator (AWG) with 25 GHz 3 dB electrical bandwidth, initially generating the composite NOMA-CAP/PAM-4 signal to be used in the FDM-based converged system implementation. The TX's output was 0 dBm. The optical signal was then launched into a span of 25 km of standard single-mode fiber (SSMF). The optical receiver (RX) was simply based on an avalanche photodetector (APD) combined with a transimpedance amplifier (TIA). A variable optical attenuator (VOA) was used to control the input optical power to the APD. A second transmitter (TX-2), with features similar to the described one, was added to the setup so as to evaluate the converged system performance using the hybrid FDM-WDM implantation. In this case, the second laser was tuned at 1548.2 nm to minimize both the optical beat interference due to unwanted mixing

products generated during the DD process at the receiver side [193], [194], [195] and the optical gap between both lasers. Note that, for this hybrid implementation, although the NOMA-CAP and PAM-4 signals are independently generated by two different transmitters, the FDM technique is conducted as well to avoid the complete overlap of both signal in frequency domain in the DD process. A second VOA was added to the TX-2's output to control the optical power of the interfering signal. Finally, the detected signal was digitized at 25 GSa/s with a real time oscilloscope and processed offline. Fig. 7.3(b) shows an example of the composite electrical spectrum measured at the receiver side, showing a NOMA-CAP signal with fifteen 0.25 GHz CAP bands providing a total aggregated bit rate of 15 Gb/s. The NOMA-CAP bands with ID from 1 to 7 were placed in the spectral gap between the main lobe and the sidelobe of the 10 Gb/s PAM-4 signal, while NOMA-CAP bands with ID from 8 to 15 were accommodated within the frequency range between 8 GHz and 10 GHz. Those locations were chosen to minimize the crosstalk interference between the PAM-4 and NOMA-CAP signals, as it shall be shown in the next section.

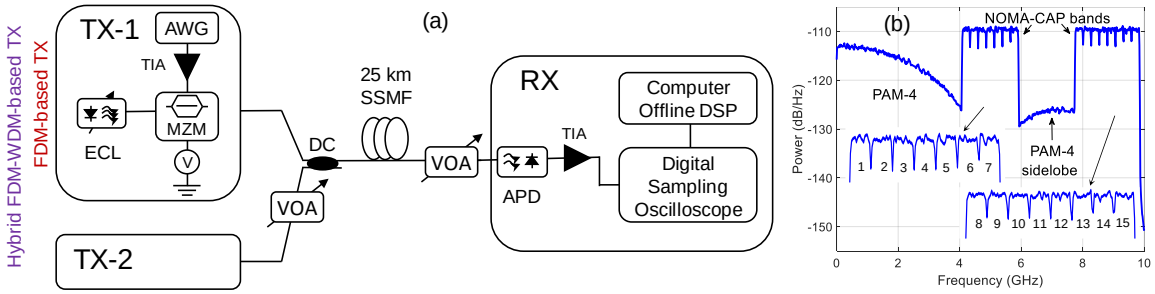

Fig. 7.3. (a) Experimental PON setup. Example of measured spectra of converged NOMA-CAP and PAM-4 services, providing a total bit rate of 25 Gb/s in just 10 GHz of transmission bandwidth.

7.3 Experimental results and discussion

In a converged PON scenario like the one shown in Fig. 7.1, where wired and wireless services can be delivered over a single fiber, the main objective is to find out the best spectral accommodation of the wireless signals minimizing the potential mutual crosstalk interference of/on the adjacent wired services, and simultaneously maximizing the transmission bandwidth utilization of the system.

Fig. 7.4(a) and Fig. 7.4(b) show respectively the converged system crosstalk performance measured in terms of the BER vs. received optical power (P_{RX}) vs. frequency carrier f_{c_i} of a NOMA-CAP signal with just one CAP band of 0.25 GHz when the NOMA-CAP and PAM-4 signals are frequency multiplex and generated using the same transmitter (FDM implementation) and when the two signals are generated using two similar

transmitters with different transmission wavelengths and performing FDM (hybrid FDM-WDM implementation). In all these measurements, f_{c_i} has been swept form 0 GHz to 10 GHz in steps of 125 MHz and the r_p among the two NOMA levels has been fixed to the value of 7 dB. To study the effect of the crosstalk interference, Fig. 7.4(a) also shows the BER curves when the PAM-4 signal has been amplitude weighted to obtain different amplitude relation values, α={-6.0, -3.0, -1.2} dB while, Fig. 7.4(b) shows BER curves for different optical power relation values between the NOMA-CAP and PAM-4 signals, $\beta = P_{NOMA\text{-}CAP}$-$P_{PAM\text{-}4}$={-12.0, -8.0, -4.0, 0.0} dBm. Table 7.1 and Table 7.2 summarize the receiver sensitivities (Ss) of the weak and strong NOMA levels and the 10 Gb/s PAM-4 obtained in the case in which the NOMA-CAP signal is centred in the null point of the PAM-4 signal (in 5 GHz), as well as the ranges of f_{c_i} in which the penalty in the receiver sensitivity (ΔS) due to the crosstalk is lower than 1 dB ($R_{f_{c_i}|\Delta S\leq 1dB}$) shows in Fig. 7.4(a) and Fig. 7.4(b) for all considered values of α and β, respectively. Finally, Table 7.1 and Table 7.2 also show the effective bandwidth (BW_{eff}) of each considered converged system implementations to be used by the wireless transmission, defined as the intersection between $R_{f_{c_i}/\Delta S\leq 1dB}$ of the two MOMA signals and the PAM-4 for a specific α or β value.

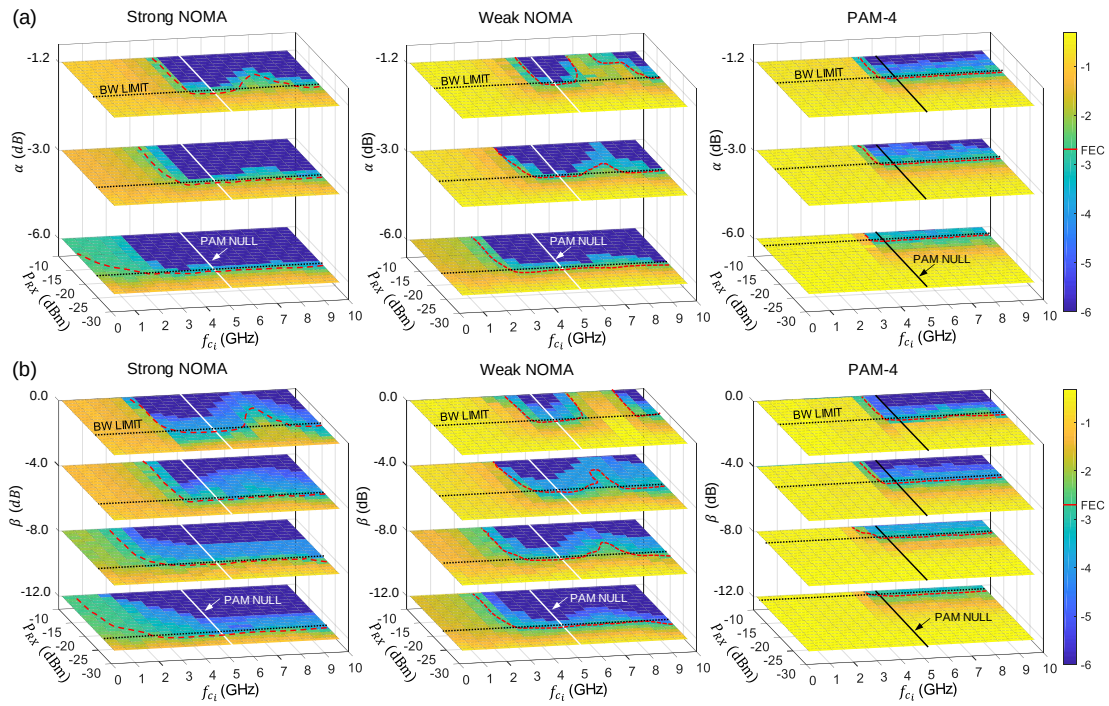

Fig. 7.4. Contour $\log_{10}$(BER) vs. received power (P_{RX}) vs. frequency carrier (f_{c_i}) of a NOMA-CAP signal with just one 0.25 GHz CAP band for the weak and strong NOMA levels and the 10 Gb/s PAM-4 in back-to-back configuration when the NOMA-CAP and PAM-4 signals are generated using: (a) FDM technology and (b) hybrid FDM-WDM technology. Dash red line is the 7% FEC OH limit.

Table 7.1. Summary of receiver sensitivities (Ss) and range of f_{c_i} in which the penalty is less than 1 dB ($\Gamma = R_{f_{c_i}|_{\Delta S \leq 1dB}}$) of the two NOMA-CAP level signals and PAM-4, as well as the effective bandwidth of the system for the wireless transmission (BW_{eff}) of the converged system using FDM technology for α={-6.0, -3.0, -1.2} dB.

α (dB)	-6.0		-3.0		-1.2	
Parameter	S (dBm)	Γ (GHz)	S (dBm)	Γ (GHz)	S (dBm)	Γ (GHz)
Strong NOMA-CAP	-23.2	[2.1, 10]	-23.1	[3.6, 10]	-22.2	[3.8, 6.2], [8.2, 10]
Weak NOMA-CAP	-22.1	[2.9, 10]	-21.2	[3.9, 6.1], [7.6, 10]	-20.2	[4.4, 6], [8.9, 10]
PAM-4	-13.4	[4.5, 10]	-17.2	[4.3, 10]	-18.2	[4.1,10]
BW_{eff} (GHz)	[4.5, 10] → 5.5		[4.3, 6.1], [7.6, 10] → 4.2		[4.4, 6], [8.9, 10] → 2.7	

Table 7.2. Summary of receiver sensitivities (Ss) and range of f_{c_i} in which the penalty is less than 1 dB ($\Gamma = R_{f_{c_i}|_{\Delta S \leq 1dB}}$) of the two NOMA-CAP level signals and PAM-4, as well as the effective bandwidth of the system for the wireless transmission (BW_{eff}) of the converged system hybrid FDM-WDM technology β={-12.0, -8.0, -4.0, 0.0} dB.

β (dB)	-12.0		-8.0		-4.0		0.0	
Parameter	S (dBm)	Γ (GHz)	S (dBm)	Γ (GHz)	S (dBm)	Γ (GHz)	S (dBm)	Γ (GHz)
Strong NOMA-CAP	-26.1	[2.2, 10]	-25.3	[3.0, 10.0]	-24.2	[3.5, 10.0]	-23.5	[3.5, 6.2], [8.3, 10.0]
Weak NOMA-CAP	-23.7	[3.1, 10]	-22.6	[3.6, 6.0], [6.9, 10.0]	-21.8	[4.0, 6.2], [7.7, 10.0]	-20.4	[4.1, 5.9], [9.0, 10.0]
PAM-4	-11.7	[4.8, 10.0]	-14.3	[4.6, 10.0]	-17.8	[4.3, 10.0]	-18.5	[4.4, 10.0]
BW_{eff} (GHz)	[4.8, 10] → 5.2		[4.6, 6.0], [6.9, 10.0] → 4.5		[4.4, 6.2], [7.7, 10] → 4.3		[4.4, 5.9], [9, 10] → 2.5	

As it can be observed in Table 7.1, the effect of changing α over the effective bandwidth of the FDM-based system for the wireless transmission is clear. The higher the α, the lower is the available transmission bandwidth for the NOMA-CAP signal. This is due to the fact that for high α values, the PAM-4 signal power is higher, increasing the crosstalk effect over the NOMA-CAP signal. Note that for α={3.0, 1.2} dB, the frequency range to accommodate the wireless signal is discontinuous due to the higher energy of the PAM-4 side-lobe. In the case of the 10 Gb/s PAM-4, increasing the amplitude relation between the NOMA-CAP and PAM-4 signals corresponds to an improvement of the PAM-4 receiver sensitivity, from -13.4 dBm for α=-6 dB to -18.2 dBm for α=-1.2 dB. From Table 7.2, similar BW_{eff} behaviour can be observed for the converged system based on the hybrid FDM-WDM technology. Thus, for β=-12.0 dB, the crosstalk interference of the PAM-4 signal is lower, consequently leading to higher receiver sensitivities for the two NOMA-CAP levels, hence increasing BW_{eff} up to 5.2 GHz. Nevertheless, the PAM-4 receiver sensitivity is just of -11.4 dBm. On the contrary, for β=0.0 dB, the receiver sensitivity for

PAM-4 is of -18.5 dBm, and the crosstalk over the NOMA-CAP signal is higher, deteriorating the NOMA-CAP receiver sensitivities and reducing BW_{eff} to 2.5 GHz. As a trade-off solution, we consider α=-3 dB and β=-4 dB for the converged system implementation based on the FDM and hybrid FDM-WDM, respectively, both implementations providing and effective bandwidth close to 4.2 GHz where fifteen NOMA-CAP bands of 0.25 GHz can be accommodated as shown in Fig. 7.3(b).

Finally, for back-to-back (B2B) configuration and 25 km SSMF, Fig. 7.5(a, b) and Fig. 7.5(c, d) show the BER vs. P_{RX} curves when the fifteen NOMA-CAP bands providing a total aggregated bit rate of 15 Gb/s and the 10 Gb/s PAM-4 are transmitted simultaneously using FDM and hybrid FDM-WDM technologies considering α=-3.0 dB and β=-4 dB, respectively. From Fig. 7.5(a, b), the receiver sensitivities of the converged system based on FDM technology for the strong and weak NOMA levels are, averaged for all bands, -17.2 dBm and -15.3 dBm respectively, while for 10 Gb/s PAM-4, the receiver sensitivity is -12.8 dBm. In the case in which the converged system is based on hybrid FDM-WDM technology, the receiver sensitivities for the strong NOMA and weak NOMA and, PAM-4 are -20.1 dBm, -18.3 dBm, and 16.1 dBm, see Fig. 7.5(b, c). From Fig. 7.5(a, b) and Fig. 7.5(c, d), no transmission penalty due to CD or any other impairment was observed in the receiver sensitivities after 25 km transmission.

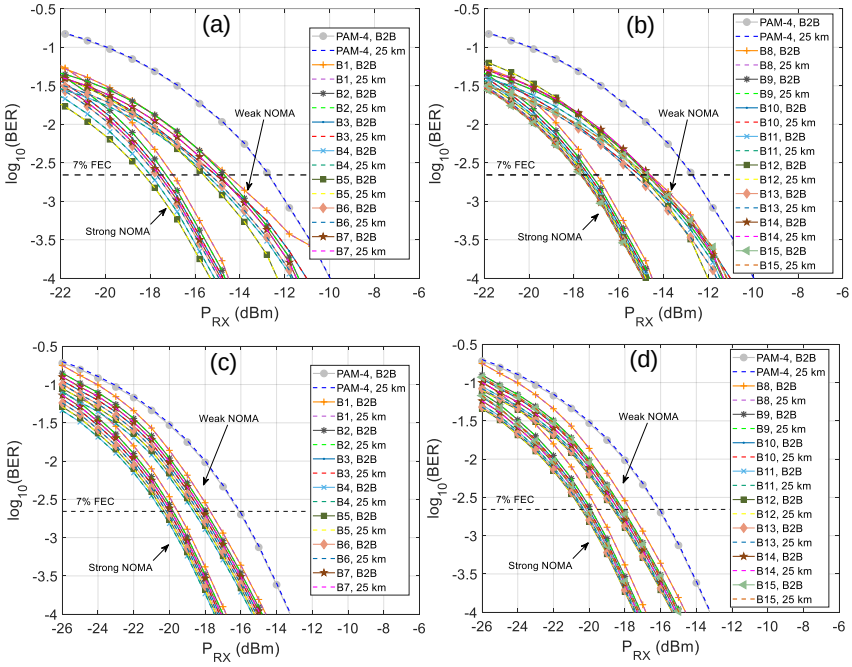

Fig. 7.5. BER vs. received power (P_{RX}) of 10 Gb/s PAM-4 and of each CAP band of a NOMA-CAP signal with two NOMA levels and 15 CAP bands in back-to-back (B2B) configuration and over 25 km of SSMF for: (a) the NOMA-CAP bands with ID from 1 to 7 and, (b) the NOMA-CAP bands with ID from 8 to 15 with FDM technology and; (c) the NOMA-CAP bands with ID from 1 to 7 and, (d) the NOMA-CAP bands with ID from 8 to 15 with hybrid FDM-WDM technology.

7.4 Conclusions

The convergence of NOMA-CAP with PAM-4 within a single-carrier wired service, considered as new 5G and beyond-5G candidate waveform, has been demonstrated in a converged PON scenario. Transmission of fifteen NOMA-CAP bands providing a total aggregated bit rate of 15 Gb/s and 10 Gb/s PAM-4 over 25 km of SSMF has been demonstrated with negligible BER penalty for two different converged system implementations. The first one uses electrical frequency division multiplying (FDM) technology and the second one employs hybrid FDM-wavelength division multiplexing (FDM-WDM) technology. In the first case, the NOMA-CAP bands were aggregated and digitally added to the baseband PAM-4 waveform to form the full data transmitted signal. To evaluate the crosstalk interference between the NOMA-CAP and PAM-4 signals, the PAM-4 modulator's output was amplitude weighted with different values, α={-6.0, -3.0, -1.2} dB. In the second case, NOMA-CAP and PAM-4 signals are generated with two different transmitters, studying the optical crosstalk through the variation of the optical power difference between both signals with a variable optical attenuator, β={-12.0, -8.0, -4.0, 0.0} dB . Both system implementations although offering the same total effective bandwidth for the wireless signal, 4.2 GHz, in term of the receiver sensitivity, the hybrid FDM-WDM technology shows 3 dB gain compared to FDM technology.

Finally, it is considered that the convergence of NOMA-CAP wireless waveform with a 10 Gb/s PAM-4 wired signal, together with the expansion of available wavelengths in future WDM access, represents a straight-forward augmentation of current PON technologies to enable the efficient development of 5G and beyond-5G communication networks.

Chapter 8. Conclusions and Prospects

8.1 General conclusions

This thesis has been focused on providing a new flexible converged metro-access network infrastructure supporting 5G services. New node solutions and modulation formats have been proposed and investigated to satisfy future metro-access networks requirements in terms of network capacity, flexibility, adaptability, energy efficiency and security. The main contributions of this thesis are per chapter summarized as follows:

- Chapter 2 proposed and modelled cost-effective all-optical commutation node solutions (ROADM and OXC) for future SDN-based u-DWDM metro-access networks. Specifically, two different node designs were presented for the ROADM and OXC. The first one, being fully flexible and compacted but far more expensive, was based on wavelength selective switches (WSSs) that could work with frequency slot (FS) granularity. The second one, more cost-effective and modular, worked with DWDM channel granularity. Then, the commutation node functions were applied on a group of FSs at the DWDM channels of the DWDM-based node. Benefits of the nodes based on DWDM technology are the usage of off-the-shelf components, reduced cost (at least 1 order of magnitude lees than WSS-based nodes), modularity (pay-as-you-grow), low response time (<8 ms) and reduced power consumption (5 times less than WSS-based nodes). Finally, a north to south architecture for the network control plane was also proposed. In this, the optical resources could be managed directly from the application level.
- Chapter 3 assessed the performance of the proposed cost-effective DWDM ROADM as a metro-access ring network element for offline and online scenarios. Since a module of the DWDM-based node switches a group of FSs and new modules can be added when they are required, different heuristics to determine an efficient design of the cost-effective DWDM ROADMs of a network were presented. Using proposed heuristics, the obtained performance penalty of a network using DWDM ROADMs, measured against the same network using WSS-based ROADMs with FS granularity, was of 20% for offline scenarios and 35% for online scenarios.

- Chapter 4 evaluated the performance of the proposed cost-effective DWDM OXC and ROADM as metro-access mesh network elements for offline scenarios. A heuristic based on an iterative process to determine an efficient design of the cost-effective DWDM OXCs and ROADMs of a network was presented. Using that heuristic, the network penalty performance was just of 10% regarding the same network using WSS-based nodes working with FS granularity. From all obtained results, it is believed that cost-effective DWDM OXC and ROADM are strong candidate solutions for future u-DWDM-based metro-access networks that require high capacity, high flexibility and scalability.
- Chapter 5 experimentally assessed new 5G multicarrier modulation formats (FBMC, UFMC and GFDM) and OFDM for high-layer split u-DWDM-PON-based fronthaul applications using RoF technology. Both direct and quasi-coherent detection were considered. On the one hand, similar receiver sensitivities were obtained for new 5G multicarrier modulation formats (FBMC, UFMC and GFDM) and OFDM. The direct-detection and quasi-coherent sensitivities were around -14 dBm and -24.2 dBm, respectively. On the other hand, UFMC have been identified as the most appropriated 5G modulation formats for u-DWDM-PON applications since it shows the best spectral localisation, which is reduced by 18.2% regarding OFDM. This is, UFMC could provide an increase of the network's capacity close to 20%.
- Chapter 6 proposed and experimentally assessed NOMA-CAP modulation format for high capacity PON and data center (DC) optical interconnect applications using affordable direct detection. For PON applications, NOMA-CAP, providing a total aggregated capacity ranged between 50 Gb/s and 90 Gb/s, was measured for 25 km of standard single-mode fiber (SSMF). To increase the low available optical power budget of the system, SOA-based amplification at the transmitter and receiver sides was considered. In this case, SOA-based amplification for NOMA-CAP modulation provided optical power budgets of 28.7(23.7) dB and 23.6(18.9) dB at 50(90) Gb/s for the strong and weak NOMA levels, respectively. These achieved power budget levels are aligned with current standards employed in the field. For DC optical interconnect applications, the transmission of 50-90 Gb/s NOMA-CAP through 2 km of 7-core multi-core fiber (MCF), providing different total aggregated traffics between 350 Gb/s and 630 Gb/s, was also demonstrated with negligible transmission penalty. These results push forward NOMA-CAP as a strong candidate for future high-capacity PONs

and CD optical interconnects that require split links, high capacity, high granularity and scalability.

- Chapter 7 demonstrated the transmission of fifteen NOMA-CAP bands providing a total aggregated bit rate of 15 Gb/s and 10 Gb/s PAM-4 over 25 km of SSMF with negligible BER penalty. It is considered that the convergence of NOMA-CAP wireless waveform with a 10 Gb/s PAM-4 wired signal, together with the expansion of available wavelengths in future DWDM access, represents a straight-forward augmentation of current PON technologies to enable the efficient development of 5G and beyond-5G communication networks.

8.2 Future lines

During this Ph. D. thesis, research has been focused on metro-access networks to provide a new flexible optical network infrastructure supporting 5G services through new node solutions and modulation formats. In the following, some future research lines are outlined.

1) The evaluation of the proposed cost-effective DWDM OXC and ROADM as network elements in an online scenario. New heuristics must be proposed to maximize the network performance. Artificial intelligence (AI)-based algorithms can be used for the network design optimization.
2) The experimental assessment of NOMA-CAP using a quasi-coherent receiver to further increase the available power budget for high-capacity PONs.
3) For NOMA-CAP modulation, it can be conducted the optimization of the MB-CAP frequency band size, bit loading and modulation order optimization to increase the aggregated bandwidth through AI-based optimization processes. It is expected substantial gains when optimization processes combine the particular transfer function of the components with the different variables within the NOMA-CAP modulation format.

List of Acronyms

APD	avalanche photodetector
APS	automatic protection switching
BBU	base band unit
BPSK	binary phase shift keying
BVOT	bandwidth-variable optical transceiver
CAP	carrierless amplitude phase modulation
CCDF	complementary cumulative distribution function
CD	chromatic dispersion
CO	central office
CP	cyclic prefix
CPRI	common public radio interface
CWDM	coarse WDM
DC	data center
DD	direct detection
DFB	distributed feedback laser
DFE	decision feedback equalizer
DWDM	dense WDM
EON	elastic optical networking
FBMC	filter bank multicarrier
FC	fiber channel
FFT	fast Fourier transform
FS	Frequency slot

GFDM	generalised frequency division multiplexing
GMPLS	general multiprotocol label switching
HOS	Hybrid optical switching
ISDN	integrated services digital network
ISO	isolator
LO	local oscillator
MCF	multi-core fiber
MPLS	multiprotocol label switching
MZM	Mach-Zehnder modulator
NOMA	non-orthogonal multiple access
NRZ	non-return to zero
OADM	add/drop multiplexer
OAN	optical aggregation node
OCN	optical communication network
OFDM	orthogonal frequency division multiplexing
OLT	optical line termination
OMCN	optical metro-core node
ONU	optical network unit
OOB	out-of-band
OOK	on-off keying
OXC	optical cross-connect
PAM	pulse amplitude modulation
PAPR	peak-to-average power ratio
PB	power budget

PBX	private branch exchange
PCE	path commutation element
PDH	plesiochronous digital hierarchy
PON	passive optical network
PSD	power spectral density
QAM	quadrature amplitude modulation
QCD	quasi-coherent detection
QPSK	quadrature phase shift keying
RA	resource allocation
RAN	radio access network
ROADM	reconfigurable add/drop multiplexer
RoF	radio-over-fiber
RRH	remote radio head
RSA	route and spectrum assignment
RX	receiver
SDH	synchronous digital hierarchy
SDN	software-defined networking
SE	spectral efficiency
SIC	successive interference cancellation
SOA	semiconductor optical amplifier
SONET	synchronous optical network
SSMF	standard single-mode fibers
TDM	time division multiplexing
TX	transmitter

u-DWDM	ultra-DWDM
UFMC	universal filtered multicarrier
VCSEL	vertical cavity surface emitting laser
WDM	wavelength division multiplexing
WSS	wavelength selective switching

Curriculum Vitae

Samael Sarmiento

Samael Sarmiento was born in Las Palmas de Gran Canaria, Spain, in 1991. He received the M.Sc. degree in Telecommunications engineering from the University of Malaga in 2015. In 2016, he joined the Optical Communications Group of the Department of Signal Theory and Communications of the Polytechnic University of Catalonia where he finished his Ph. D. research in 2020. His work was focused on metro-access network convergence and the development of new modulation format for optical communications.

Stays in Foreign Centers

January 2019-April 2019 Photonic Network System Laboratory, National Institute of Information and Communication Technology (NICT), Tokyo, Japan. Study of new modulation formats for optical fiber applications such as 5G mobile fronthaul, passive optical networks and data center interconnect (DCI), supervised by Dr. José Manuel Delgado Mendinueta.

International Journal Papers

1. **Samael Sarmiento**, José Manuel Delgado Mendinueta, José Antonio Altabás, Salvatore Spadaro, Satoshi Shinada, Hideaki Furukawa, Juan José Vegas Olmos, José Antonio Lázaro and Naoya Wada, "Optical Power Budget Enhancement in 50-90 Gb/s IM-DD PONs with NOMA-CAP Modulation and SOA-based Amplification," in *IEEE Photonics Technology Letters*, under review.

2. **Samael Sarmiento**, José Manuel Delgado Mendinueta, José Antonio Altabás, Salvatore Spadaro, Satoshi Shinada, Hideaki Furukawa, Juan José Vegas Olmos, José Antonio Lázaro and Naoya Wada, "Split-enabled 350-630 Gb/s Optical Interconnect with Direct Detection NOMA-CAP and 7-Core Multi-Core Fiber," in *Optics Communications*, vol. 463, pp. 125321, 2020.

3. **Samael Sarmiento,** José. A. Altabás, Salvatore Spadaro and José A. Lázaro, "Experimental Assessment of 10 Gbps 5G Multicarrier Waveforms for High-Layer Split U-DWDM-PON-Based Fronthaul," in *IEEE Journal of Lightwave Technology*, vol. 37, no. 10, pp. 2344-2351, 2019.

4. **Samael Sarmiento**, Salvatore Spadaro, Jose A. Lázaro, "Cost-effective ROADM design to maximize the Traffic Load Capacity of u-DWDM coherent metro-access networks," in *Optical Switching and Networking*, vol. 30, pp. 53-61, 2018.

5. **Samael Sarmiento**, José A. Altabás, David Izquierdo, Ignacio Garcés, Salvatore Spadaro and José A. Lázaro, "Cost-effective DWDM ROADM design for flexible sustainable optical metro-access networks," in *IEEE/OSA Journal of Optical Communications and Networking*, vol. 9, no. 12, pp. 1116-1124, 2017.

International Conferences

1. **Samael Sarmiento**, José Manuel Delgado Mendinueta, José Antonio Altabás, Salvatore Spadaro, Satoshi Shinada, Hideaki Furukawa, Juan José Vegas Olmos, José Antonio Lázaro and Naoya Wada, "Converged RoF-based mobile fronthaul and passive optical network with NOMA-CAP modulation format," in Proc. *SPIE Photonics West, San Francisco, USA, 2020.*

2. **Samael Sarmiento**, José Manuel Delgado Mendinueta, José Antonio Altabás, Salvatore Spadaro, Satoshi Shinada, Hideaki Furukawa, Juan José Vegas Olmos, José Antonio Lázaro and Naoya Wada, "Split-enabled 490 Gb/s optical interconnect with direct detection NOMA-CAP and 7-CORE multi-core fibre," in Proc. *European Conference on Optical Communication (ECOC)*, Dublin, Ireland, 2019.

3. **Samael Sarmiento**, José Manuel Delgado Mendinueta, José Antonio Altabás, Salvatore Spadaro, Satoshi Shinada, Hideaki Furukawa, Juan José Vegas Olmos, José Antonio Lázaro and Naoya Wada, "Optical Power Budget Enhancement in 50 Gb/s IM-DD PONs with NOMA CAP Modulation and SOA-based

Amplification," in Proc. *International Conference of Transparent Optical Network (ICTON)*, Angers, France, 2019.

4. José A. Altabas, David Izquierdo, Jesús Clemente, **Samael Sarmiento**, Guillermo Silva Valdecasa, Michele Squartecchia, Lau F. Suhr, Omar Gallardo, Alicia López, M. Ángeles Losada, Javier Mateo, Jesper B. Jensen, José A. Lázaro, Ignacio Garcés, "Advanced Technologies for Coherent Access Networks" in Proc. *International Conference of Transparent Optical Network (ICTON)*, Angers, France, 2019.

5. **Samael Sarmiento**, José Manuel Delgado Mendinueta, José Antonio Altabás, Salvatore Spadaro, Satoshi Shinada, Hideaki Furukawa, Juan José Vegas Olmos, José Antonio Lázaro and Naoya Wada, "Experimental Investigation of 50-90 Gb/s IM-DD NOMA-CAP Modulation for Short Range Optical Transmission Applications," in Proc. *OptoElectronics and Communications Conference (OECC)/ International Conference on Photonics in Switching and Computing (PSC*), Fukuoka, Japan, 2019.

6. **Samael Sarmiento**, José A. Altabás, Salvatore Spadaro, José A. Lázaro, "From 4.2 Gbps Asymmetrical Clipping (ACO)-OFDM to 8.7 Gbps Layered-ACO-FBMC with Intensity-Modulation Direct-Detection for PONs," in Proc. *Conference on Lasers & Electro-Optics (CLEO)/Europe*, Munich, Germany, 2019.

7. **Samael Sarmiento**, Albert Gran, José A. Altabás, Marco Scalabroni, Salvatore Spadaro, Ignacio Garcés, José A. Lázaro, "Experimental Assessment of 5-10 Gbps 5G Multicarrier Waveforms with Intensity-Modulation Direct-Detection for PONs," in Proc. *Photonics in Switching and Computing (PSC)*, Limassol, Cyprus, 2018.

8. José A. Lázaro, Massiel Coves, **Samael Sarmiento**, José A. Altabás and Adolfo Lerín, "5G Connected Vehicles Supported by Optical Fiber Access," in Proc. *International Conference on Transparent Optical Networks (ICTON)*, Bucharest, Romania, 2018.

9. **Samael Sarmiento**, Salvatore Spadaro and José A. Lázaro, "Cost-effective ROADM architecture for C/DWDM Metro-Access Networks convergence," in

Proc. *International Conference on Transparent Optical Networks (ICTON)*, Girona, Spain, 2017.

10. José A. Altabás, David Izquierdo, Álvaro Pascual, **Samael Sarmiento**, José A. Lázaro, Ignacio Garcés, "Design of flexible udWDM Metro-Access Network Devices assisted by High Resolution Complex Spectroscopy," in Proc. *International Conference on Transparent Optical Networks (ICTON)*, Trento, Italy, 2016.

11. **Samael Sarmiento**, Rafael Montero, José A. Altabás, David Izquierdo, Fernando Agraz, Albert Pagès, Jordi Perelló, Joan Gené, Marc Alonso, Alvaro Pascual, Ignacio Garcés, Salvatore Spadaro and José A. Lázaro, "SDN-enabled flexible optical node designs and transceivers for sustainable metro-access networks convergence," in Proc. *International Conference on Transparent Optical Networks (ICTON)*, Trento, Italy, 2016.

Book Contributions

1. José Altabás, **Samael Sarmiento**, José A. Lázaro, "Passive optical networks: introduction," Wiley Encyclopaedia of Electrical and Electronics Engineering, John Wiley & sons, pp. 1-20, 2018.

References

[1] S. Aleksic, “Towards fifth-generation (5G) optical transport networks,” in *International Conference on Transparent Optical Networks (ICTON)*, Budapest, 2015.

[2] D. Cavendish, “Evolution of optical transport technologies: from SONET/SDH to WDM,” *IEEE Communications Magazine,* vol. 38, no. 6, pp. 164-172, 2000.

[3] P. J. Winzer, “Challenges and evolution of optical transport networks,” in *European Conference and Exhibition on Optical Communication (ECOC)*, Torino, 2010.

[4] J. Berthold, A. A. M. Saleh, L. Blair and J. M. Simmons, “Optical Networking: Past, Present, and Future,” *IEEE Journal of Lightwave Technology,* vol. 26, no. 9, pp. 1104-1118, 2008.

[5] B. Mukherjee, “WDM optical communication networks: progress and challenges,” *IEEE Journal on Selected Areas in Communications,* vol. 18, no. 10, pp. 1810-1824, 2000.

[6] O. Babatunde and S. Mbarouk, “A review of Plesiochronous Digital Hierarchy (PDH) and Synchronous Digital Hierarchy (SDH),” *International Journal of Scientific Research Engineering and Technology (IJSRET)*, vol. 3, no. 3, pp. 1-5, 2014.

[7] K. Voruganti and P. Sarkar, “An analysis of three gigabit networking protocols for storage area networks,” in *IEEE International Performance, Computing, and Communications Conference*, Phoenix, 2001.

[8] D. Rodellar, C. Bungarzeanu, H. Garcia, C. Brisson, A. Kueng and P. A. Robert, “New multichannel Ethernet protocol for passive optical star local area networks using coherent transmission,” in *YBEN-Broadband European Networks and Electronic Image Capture and Publishing*, Zurich, 1998.

[9] D. Johnson and T. Gilfedder, “Evolution of optical core networks,” *BT Technology Journal,* vol. 25, no. 3, pp. 57-64, 2007.

[10] H. Yoshimura, K. Sato and N. Takachio, “Future photonic transport networks based on WDM technologies,” *IEEE Communications Magazine,* vol. 37, no. 2, pp. 74-81, 1999.

[11] J. M. Tang and K. A. Shore, “Wavelength-Routing Capability of Reconfigurable Optical Add/Drop Multiplexers in Dynamic Optical Networks,” *IEEE Journal of Lightwave Technology,* vol. 24, no. 11, pp. 4296-4303, 2006.

[12] A. Tzanakaki, I. Zacharopoulos and I. Tomkos, “Optical add/drop multiplexers and optical cross-connects for wavelength routed networks,” in *International Conference on Transparent Optical Networks (ICTON)*, Warsaw, 2003.

[13] C. F. Lam, Passive optical networks: principles and practice, USA: Academic Press, 2011.

[14] A. Schubert, “G. 709–The optical transport network (OTN),” *JDSU, white paper*, pp. 1-8, 2007.

[15] K. Roberts et al., “High Capacity Transport—100G and Beyond,” *IEEE Journal of Lightwave Technology,* vol. 33, no. 3, pp. 563-57, 2015.

[16] F. Rambach, B. Konrad, L. Dembeck, U. Gebhard, M. Gunkel, “A multilayer cost model for metro/core networks,” *IEEE/OSA Journal of Optical Communications and Networking,* vol. 5, no. 3, pp. 210-225, 2013.

[17] K. S. Kim, “On the evolution of PON-based FTTH solutions,” *Information Sciences,* vol. 149, no. 1, pp. 21-30, 2013.

[18] ITU-T, “G.984.1-Gigabit-capable passive optical networks (GPON): General characteristics,” 2008.

[19] “Media Access Control Parameters, Physical Layers, and Management Parameters for Subscriber Access Networks, IEEE Std 802.3ah-2004,” Institute of Electrical and Electronics Engineers (IEEE), 2004.

[20] ITU-T, “G.987.2-10-Gigabit-capable passive optical networks (XG-PON): Physical media,” 2016.

[21] “Physical Layer Specifications and Management Parameters for 10 Gb/s Passive Optical Networks, IEEE Std 802.3av-2009,” Institute of Electrical and Electronics Engineers (IEEE), 2009.

[22] V. Houtsma, D. van Veen and E. Harstead, “Recent Progress on Standardization of Next-Generation 25, 50, and 100G EPON,” *IEEE Journal of Lightwave Technology,* vol. 35, no. 6, pp. 1228-1234, 2017.

[23] ITU-T, “G.989-40-Gigabit-capable passive optical networks (NG-PON2): Definitions, abbreviations and acronyms,” 2015.

[24] “Cisco Visual Networking Index: Global Mobile Data Traffic Forecast Update, 2017–2022,” Cisco Public, 2019.

[25] M. Ruffini, “Multidimensional Convergence in Future 5G Networks,” *IEEE Journal of Lightwave Technology,* vol. 35, no. 3, pp. 535-549, 2017.

[26] Y. Ji, J. Zhang, Y. Xiao and Z. Liu, "5G flexible optical transport networks with large-capacity, low-latency and high-efficiency," *China Communications,* vol. 16, no. 5, pp. 19-32, 2019.

[27] M. Fiorani, B. Skubic, J. Mårtensson and L. Valcarenghi, "On the design of 5G transport networks," *Photon Network Communications,* vol. 30, no. 1, pp. 403-415, 2015.

[28] X. Liu, N. Deng, M. Zhou, Y. Wang, M. Tao, L. Zhou, S. Li and H. Zeng, "Enabling Technologies for 5G-Oriented Optical Networks," in *Optical Fiber Communications Conference and Exhibition (OFC),* San Diego, 2019.

[29] E. Hugues-Salas et al., "Next generation optical nodes: The vision of the European research project IDEALIST," *IEEE Communications Magazine,* vol. 53, no. 2, pp. 172-181, 2015.

[30] T. J. Xia, H. Fevrier, T. Wang and T. Morioka, "Introduction of spectrally and spatially flexible optical networks," *IEEE Communications Magazine,* vol. 53, no. 2, pp. 24-33, 2015.

[31] S. Yan et al., "Demonstration of Bandwidth Maximization between Flexi/Fixed Grid Optical Networks with Real-Time BVTs," in *European Conference on Optical Communication (ECOC),* Dusseldorf, 2016.

[32] K. Roberts and C. Laperle, "Flexible transceivers," in *European Conference on Optical Communications (ECOC),* Amsterdam, 2012.

[33] D. Hillerkuss and J. Leuthold, "Software-Defined Transceivers in Dynamic Access Networks," *IEEE Journal of Lightwave Technology,* vol. 34, no. 2, pp. 792-797, 2016.

[34] J. Lu, Z. Tan, A. P. T. Lau, S. Fu, M. Tang and Chao Lu, "Modulation format identification assisted by sparse-fast-Fourier-transform for hitless flexible coherent transceivers," *Optics Express,* vol. 27, no. 5, pp. 7072-7086, 2019.

[35] G. Bosco, "Flexible Transceivers and the Rate/Reach Trade-off," in *Optical Fiber Communications Conference and Exposition (OFC),* San Diego, 2018.

[36] G. Bosco, "Advanced Modulation Techniques for Flexible Optical Transceivers: The Rate/Reach Tradeoff," *IEEE Journal of Lightwave Technology,* vol. 37, no. 1, pp. 36-49, 2019.

[37] X. Zhou et al., "Flexible Transceivers: Extracting More Capacity from Elastic Meshed Optical Networks," in *Asia Communications and Photonics Conference (ACP),* Guangzhou, 2017.

[38] J. A. Altabas, D. Izquierdo, J. A. Lazaro and I. Garces, "1Gbps full-duplex 5GHz frequency slots uDWDM flexible Metro/Access Networks based on VCSEL-RSOA

transceiver," in *OptoElectronics and Communications Conference (OECC)/International Conference on Photonics in Switching (PS),* Niigata, 2016.

[39] J. A. Altabas, D. Izquierdo, J. A. Lazaro and I. Garces, "Cost-Effective Transceiver Based on an RSOA and a VCSEL for Flexible uDWDM Networks," *IEEE Photonics Technology Letters,* vol. 28, no. 10, pp. 1111-1114, 2016.

[40] R. Rodes, et al., "All-VCSEL based digital coherent detection link for multi Gbit/s WDM passive optical networks," *Optics Express,* vol. 18, no. 24, pp. 24969-24974, 2010.

[41] P. J. Reyes-Iglesias, A. Ortega-Moñux, and I. Molina-Fernández, "Colorless monolithically integrated 120° downconverter," *Optics Express,* vol. 21, no. 20, pp. 23048-23057, 2013.

[42] J. Clemente et al, "Experimental Demonstration of Colorless Operation of an Integrated 120° Coherent Receiver," in *European Conference on Optical Communication (ECOC),* Rome, 2018.

[43] Jose A. Altabas, David Izquierdo, Jose A. Lazaro, and Ignacio Garces, "Chirp-based direct phase modulation of VCSELs for cost-effective transceivers," *Optics Letters,* vol. 42, no. 3, pp. 583-586, 2017.

[44] Jose A. Altabas, David Izquierdo, Jose A. Lazaro, Adolfo Lerin, Felix Sotelo, and Ignacio Garces, "1Gbps full-duplex links for ultra-dense-WDM 6.25GHz frequency slots in optical metro-access networks," *Optics Express,* vol. 24, no. 1, pp. 555-565, 2016.

[45] M. Nooruzzaman and E. Halima, "Low-cost hybrid ROADM architectures for scalable C/DWDM metro networks," *IEEE Communications Magazine,* vol. 54, no. 8, pp. 153-161, 2016.

[46] M. Nooruzzaman, O. Koyama, M. Yamada and Y. Katsuyama, "Scalable single-fiber CWDM ring networks with stackable ROADMs," *IEEE/OSA Journal of Optical Communications and Networking*, vol. 5, no. 8, pp. 910-920, 2013.

[47] A. Napoli et al., "Next generation elastic optical networks: The vision of the European research project IDEALIST," *IEEE Communications Magazine,* vol. 53, no. 2, pp. 152-162, 2015.

[48] N. Calabretta , W. Miao, K. Mekonnen and K. Prifti, "SOA Based Photonic Integrated WDM Cross-Connects for Optical Metro-Access Networks," *Applied Sciences*, vol. 7, no. 9, p. 865, 2017.

[49] K. I. Sato, "Optical networking and node technologies for creating cost effective bandwidth abundant networks," in *OptoElectronics and Communications Conference (OECC)/International Conference on Photonics in Switching (PS),* Niigata, 2016.

[50] M. Schiano, A. Percelsi and M. Quagliotti, “Flexible Node Architectures for Metro Networks [Invited],” *IEEE Journal of Optical Communications and Networking,* vol. 7, no. 12, pp. B131-B140, 2015.

[51] “1x2 Flexible-grid Wavelength Selective Switch WSS-100,” www.santec.com.

[52] “1x2 Flexgrid Wavelength Selective Switch (WSS),” www.finisar.com.

[53] “Passive Optical Network Components,” www.fs.com.

[54] “Passive Optical Network Components,” www.oequest.com.

[55] D. M. Marom et al., “Survey of photonic switching architectures and technologies in support of spatially and spectrally flexible optical networking,” *IEEE/OSA Journal of Optical Communications and Networking,* vol. 9, no. 1, pp. 1-26, 2017.

[56] A. S. Thyagaturu, A. Mercian, M. P. McGarry, M. Reisslein and W. Kellerer, “Software Defined Optical Networks (SDONs): A Comprehensive Survey,” *IEEE Communications Surveys & Tutorials,* vol. 18, no. 4, pp. 2738-2786, 2016.

[57] E. Kaljic, A. Maric, P. Njemcevic and M. Hadzialic, “A Survey on Data Plane Flexibility and Programmability in Software-Defined Networking,” *IEEE Access,* vol. 7, no. 1, pp. 47804-47840, 2019.

[58] A. Farrel, J. P. Vasseur, and J. Ash, “A Path Computation Element (PCE)-Based Architecture,” IETF RFC 4655, https://www.ietf.org/rfc/rfc4655.txt, 2018.

[59] Y. Ma et al., “Novel CDC ROADM Architecture Utilizing Low Loss WSS and MCS without Necessity of Inline Amplifier and Filter,” in *Optical Fiber Communications Conference and Exhibition (OFC),* San Diego, 2019.

[60] L. Zong, H. Zhao, Z. Feng and Y. Yan, “8x8 Flexible Wavelength Cross-Connect for CDC ROADM Application,” *IEEE Photonics Technology Letters,* vol. 27, no. 4, pp. 2603-2606, 2015.

[61] T. Ishikawa, Y. Mori, H. Hasegawa, S. Subramaniam, K. Sato and O. Moriwaki, “Compact OXC architecture, design and prototype development for flexible waveband routing optical networks,” *Optics Express,* vol. 25, no. 14, pp. 15838-15853, 2017.

[62] B. Collings, “New devices enabling software-defined optical networks,” *IEEE Communications Magazine,* vol. 51, no. 3, pp. 66-71, 2013.

[63] Y. Li, L. Gao, G. Shen and L. Peng, “Impact of ROADM colorless, directionless, and contentionless (CDC) features on optical network performance [Invited],” *IEEE/OSA Journal of Optical Communications and Networking,* vol. 4, no. 11, pp. B58-B67, 2012.

[64] R. A. Jensen, “Optical switch architectures for emerging Colorless/Directionless/Contentionless ROADM networks,” in *Optical Fiber Communication Conference (OFC)*, Los Angeles, 2011.

[65] S. Gringeri, B. Basch, V. Shukla, R. Egorov and T. J. Xia, “Flexible architectures for optical transport nodes and networks,” *IEEE Communications Magazine,* vol. 48, no. 7, pp. 40-50, 2010.

[66] M. S. Erkılınç et al, “Comparison of Low Complexity Coherent Receivers for UDWDM-PONs (λ-to-the-User),” *IEEE Journal of Lightwave Technology,* vol. 36, no. 16, pp. 3453-3464, 2018.

[67] J. Kani, “Enabling Technologies for Future Scalable and Flexible WDM-PON and WDM/TDM-PON Systems,” *IEEE Journal of Selected Topics in Quantum Electronics,* vol. 16, no. 5, pp. 1290-1297, 2010.

[68] S. Pachnicke et al., “Tunable WDM-PON System With Centralized Wavelength Control,” *IEEE Journal of Lightwave Technology,* vol. 34, no. 2, pp. 812-818, 2016.

[69] K. Grobe, M. H. Eiselt, S. Pachnicke and J. Elbers, “Access Networks Based on Tunable Lasers,” *IEEE Journal of Lightwave Technology,* vol. 32, no. 16, pp. 2815-2823, 2014.

[70] M. Luo et al., “Demonstration of 10-Gb/s, 5-GHz Spaced Coherent UDWDM-PON with Digital Signal Processing in Real-Time,” in *Optical Fiber Communications Conference and Exposition (OFC),* San Diego, 2018.

[71] J. Prat et al., “Technologies for Cost-Effective udWDM-PONs,” *IEEE Journal of Lightwave Technology,* vol. 34, no. 2, pp. 783-791, 2016.

[72] H. Rohde, E. Gottwald, A. Teixeira, J. Dias, A. Shahpari, K. Pulverer, and J. Shan Wey, “Coherent Ultra Dense WDM Technology for Next Generation Optical Metro and Access Networks,,” *IEEE Journal of Lightwave Technology,* vol. 32, no. 10, pp. 2041-2052, 2014.

[73] R. M. Ferreira, A. Shahpari, J. D. Reis and A. L. Teixeira, “Coherent UDWDM-PON With Dual-Polarization Transceivers in Real-Time,” *IEEE Photonics Technology Letters,* vol. 29, no. 11, pp. 909-912, 2017.

[74] H. Rohde, S. Smolorz, E. Gottwald and K. Kloppe, “Next generation optical access: 1 Gbit/s for everyon,” in *European Conference on Optical Communication (ECOC),* Vienna, 2009.

[75] J. A. Altabas et al., “Real-time 10Gbps Polarization Independent Quasicoherent Receiver for NG-PON2 Access Networks,” *IEEE Journal of Lightwave Technology,* vol. 37, no. 2, pp. 651-656, 2019.

[76] Vincent Houtsma and Doutje van Veen, “Optical Strategies for Economical Next Generation 50 and 100G PON,” in *Optical Fiber Communications Conference and Exhibition (OFC)*, San Diego, 2019.

[77] R. Bonk, “SOA for future PONs,” in *Optical Fiber Communications Conference and Exposition (OFC)*, San Diego, 2018.

[78] C. Michie, A. Kelly, L. Liu, I. Andonovic and W. Zhong, “Semiconductor optical amplifiers in future passive optical networks,” in *International Conference on Information, Communications and Signal Processing (ICICS)*, Macau, 2009.

[79] V. Bobrovs, S. Spolitis and G. Ivanovs, “Comparison of chromatic dispersion compensation techniques for WDM-PON solution,” in *Baltic Congress on Future Internet Communications*, Vilnius, 2012.

[80] J. A. Lazaro, V. Polo, C. Bock, M. Omella and J. Prat, “Remotely Amplified SARDANA: Single-fibre-tree Advanced Ring-based Dense Access Network Architecture,” in *European Conference on Optical Communications (ECOC)*, Cannes, 2006.

[81] M. Ruffini et al., “Access and metro network convergence for flexible end-to-end network design [invited],” *IEEE/OSA Journal of Optical Communications and Networking*, vol. 9, no. 6, pp. 524-535, 2017.

[82] J. A. Lazaro et al., “SUNSET: Sustainable network infrastructure enabling the future Digital Society,” in *International Conference on Transparent Optical Networks (ICTON)*, Trento, 2016.

[83] W. Shieh, H. Bao and Y. Tang, “Coherent optical OFDM: theory and design,” *Optics Express*, vol. 16, no. 2, pp. 841-859, 2008.

[84] G. L. Stuber, J. R. Barry, S. W. McLaughlin, Ye Li, M. A. Ingram and T. G. Pratt, “Broadband MIMO-OFDM wireless communications,” *Proceedings of the IEEE*, vol. 92, no. 2, pp. 271-294, 2004.

[85] R. Mesleh, H. Elgala and H. Haas, “On the Performance of Different OFDM Based Optical Wireless Communication Systems,” *IEEE/OSA Journal of Optical Communications and Networking*, vol. 3, no. 6, pp. 620-628, 2011.

[86] Y. Cai, Z. Qin, F. Cui, G. Y. Li and J. A. McCann, “Modulation and Multiple Access for 5G Networks,” *IEEE Communications Surveys and Tutorials*, vol. 20, no. 1, pp. 629-646, 2018.

[87] J. L. Wei, J. D. Ingham, D. G. Cunningham, R. V. Penty and I. H. White, “Performance and Power Dissipation Comparisons Between 28 Gb/s NRZ, PAM, CAP and Optical OFDM Systems for Data Communication Applications,” *IEEE Journal of Lightwave Technology*, vol. 30, no. 20, pp. 3273-3280, 2012.

[88] R. Puerta, S. Rommel, J. J. V. Olmos and I. T. Monroy, “Optically generated single side-band radio-over-fiber transmission of 60Gbit/s over 50m at W-band,” in *Optical Fiber Communications Conference and Exhibition (OFC)*, Los Angeles, 2017.

[89] J. A. Altabas et al., “Nonorthogonal Multiple Access and Carrierless Amplitude Phase Modulation for Flexible Multiuser Provisioning in 5G Mobile Networks,” *IEEE Journal of Lightwave Technology,* vol. 35, no. 24, pp. 5456-5463, 2017.

[90] L. Dai, B. Wang, Y. Yuan, S. Han, C. I and Z. Wang, “Non-orthogonal multiple access for 5G: solutions, challenges, opportunities, and future research trends,” *IEEE Communications Magazine,* vol. 53, no. 9, pp. 74-81, 2015.

[91] I. A. Alimi, A. L. Teixeira and P. P. Monteiro, “Toward an Efficient C-RAN Optical Fronthaul for the Future Networks: A Tutorial on Technologies, Requirements, Challenges, and Solutions,” *IEEE Communications Surveys & Tutorials,* vol. 20, no. 1, pp. 708-769, 2018.

[92] A. Pizzinat, P. Chanclou, F. Saliou and T. Diallo, “Things You Should Know About Fronthaul,” *IEEE Journal of Lightwave Technology,* vol. 33, no. 5, pp. 1077-1083, 2015.

[93] CPRI Specification V6.1, “Common Public Radio Interface: Interface Specification,” Online: https://www.cpri.info, 2014.

[94] T. Pfeiffer, “Next generation mobile fronthaul architectures,” in *Optical Fiber Communications Conference and Exhibition (OFC)*, Los Angeles, 2015.

[95] K. Tanaka and A. Agata, “Next-generation optical access networks for C-RAN,” in *Optical Fiber Communications Conference and Exhibition (OFC)*, Los Angeles, 2015.

[96] S. Cho, H. Park, H. S. Chung, K. H. Doo, S. Lee and J. H. Lee, “Cost-effective next generation mobile fronthaul architecture with multi-IF carrier transmission scheme,” in *Optical Fiber Communications Conference and Exhibition (OFC)*, San Francisco, 2014.

[97] Byung Gon Kim, S. H. Bae, H. Kim and Y. C. Chung, “Optical fronthaul technologies for next-generation mobile communications,” in *International Conference on Transparent Optical Networks (ICTON)*, Trento, 2016.

[98] B. G. Kim, H. Kim and Y. C. Chung, “Impact of Multipath Interference on the Performance of RoF-Based Mobile Fronthaul Network Implemented by Using DML,” *IEEE Journal of Lightwave Technology,* vol. 35, no. 2, pp. 145-151, 2017.

[99] H. Kim, “RoF-based Optical Fronthaul Technology for 5G and Beyond,” in *Optical Fiber Communications Conference and Exposition (OFC)*, San Diego, 2018.

[100] A. Marotta, K. Kondepu, D. Cassioli, C. Antonelli, L. M. Correia and L. Valcarenghi, "Software Defined 5G Converged Access as a viable Techno-Economic Solution," in *Optical Fiber Communications Conference and Exposition (OFC)*, San Diego, 2018.

[101] N. Moradpoor, G. Parr, S. McClean, B. Scotney and G. Owusu, "Hybrid optical and wireless technology integrations for next generation broadband access networks," in *IFIP/IEEE International Symposium on Integrated Network Management and Workshops*, Dublin, 2011.

[102] A. Saljoghei, C. Browning and L. P. Barry, "Spectral shaping for hybrid wired/wireless PON with DC balanced encoding," in *Asia-Pacific Microwave Photonics Conference (APMP)*, Sendai, 2014.

[103] X. Hu, C. Ye and K. Zhang, "Converged mobile fronthaul and passive optical network based on hybrid analog-digital transmission scheme," in *Optical Fiber Communications Conference and Exhibition (OFC)*, Anaheim, 2016.

[104] C. Browning et al., "Converged wired and wireless services in next generation optical access networks," in *International Conference on Transparent Optical Networks (ICTON)*, Girona, 2017.

[105] C. Browning et al, "5G wireless and wired convergence in a passive optical network using UF-OFDM and GFDM," in *IEEE International Conference on Communications Workshops (ICC Workshops)*, Paris, 2017.

[106] S. Sakr, A. Liu, D. M. Batista and M. Alomari, "A Survey of Large Scale Data Management Approaches in Cloud Environments," *IEEE Communications Surveys & Tutorials*, vol. 13, no. 3, pp. 311-336, 2011.

[107] Greg Schulz, The Green and Virtual Data Center, New York: Auerbach Publications, 2019.

[108] P. J. Winzer, D. T. Neilson and A. R. Chraplyvy, "Fiber-optic transmission and networking: the previous 20 and the next 20 years [Invited]," *Optics Express*, vol. 26, no. 18, pp. 24190-24239, 2018.

[109] P. J. Winzer, "Spatial multiplexing: The next frontier in network capacity scaling," in *European Conference on Optical Communication (ECOC)*, London, 2013.

[110] T. Hayashi, T. Taru, O. Shimakawa, T. Sasaki and E. Sasaoka, "Design and fabrication of ultra-low crosstalk and low-loss multi-core fiber," *Optics Express*, vol. 19, no. 17, pp. 16576-16592, 2011.

[111] T. Hayashi, T. Taru, O. Shimakawa, T. Sasaki and E. Sasaoka, "Ultra-low-crosstalk multi-core fiber feasible to ultra-long-haul transmission," in *Optical Fiber Communication Conference (OFC)*, Los Angeles, 2011.

[112] Y. Amma, Y. Sasaki, K. Takenaga, S. Matsuo, J. Tu, K. Saitoh and M. Koshiba, "High-density multicore fiber with heterogeneous core arrangement," in *Optical Fiber Communications Conference and Exhibition (OFC)*, Los Angeles, 2015.

[113] Y. Amma, Y. Sasaki, K. Takenaga, S. Matsuo, J. Tu, K. Saitoh, M. Koshiba, T. Morioka and Y. Miyamoto, "109-Tb/s (7×97×172-Gb/s SDM/WDM/PDM) QPSK transmission through 16.8-km homogeneous multi-core fiber," in *2011*, Los Angeles, Optical Fiber Communication Conference (OFC).

[114] B. Zhu, T. F. Taunay, M. F. Yan, J. M. Fini, M. Fishteyn, E. M. Monberg and F. V. Dimarcello, "Seven-core multicore fiber transmissions for passive optical network," *Optics Express,* vol. 18, no. 11, pp. 11117-11122, 2010.

[115] J. M. Galve, I. Gasulla, S. Sales and J. Capmany, "Reconfigurable Radio Access Networks Using Multicore Fibers," *IEEE Journal of Quantum Electronics,* vol. 52, no. 1, pp. 1-7, 2016.

[116] B. Li, Z. Feng, M. Tang, Z. Xu, S. Fu, Q. Wu, L. Deng, W. Tong, S. Liu and P. P. Shum, "Experimental demonstration of large capacity WSDM optical access network with multicore fibers and advanced modulation formats," *Optics Express,* vol. 23, no. 9, pp. 10997-11006, 2015.

[117] Z. Feng et al., "Multicore-Fiber-Enabled WSDM Optical Access Network With Centralized Carrier Delivery and RSOA-Based Adaptive Modulation," *IEEE Photonics Journal,* vol. 7, no. 4, pp. 1-9, 2015.

[118] R. Ryf et al., "Long-Distance Transmission over Coupled-Core Multicore Fiber," in *European Conference on Optical Communication (ECOC),* Dusseldorf, 2016.

[119] Y. Li, N. Hua and X. Zheng, "CapEx advantages of multi-core fiber networks," *Photonic Network Communications,* vol. 31, no. 2, p. 228–238, 2016.

[120] ITU-T, "G.975.1-Forward error correction for high bit-rate DWDM submarine systems," 2004.

[121] Y. Han and G. Li, "Coherent optical communication using polarization multiple-input-multiple-output," *Optics Express,* vol. 13, no. 19, pp. 7527-7534, 2005.

[122] J. A. Altabas et al, "Survey of Faster-Than-Nyquist for Flexible Passive Optical Networks," in *International Conference on Transparent Optical Networks (ICTON),* Budapest, 2015.

[123] T. Muciaccia and V. M. N. Passaro, "Future scenarios for software-defined metro and access networks and software-defined photonics," *Photonics,* vol. 4, no. 1, pp. 1-27, 2017.

[124] P. Pavon-Marino, M. Bueno-Delgado and J. Izquierdo-Zaragoza, "Evaluating internal blocking in noncontentionless flex-grid ROADMs [invited]," *IEEE/OSA*

Journal of Optical Communications and Networking, vol. 7, no. 3, pp. A474-A481, 2015.

[125] Y. Takita, K. Tajima, T. Hashiguchi and T. Katagiri, "Low-cost CD-ROADMs Based Elastic Optical Networks Employing Wavelength Defragmentation," in *European Conference on Optical Communication (ECOC)*, Dusseldorf, 2016.

[126] F. Rambach et al., "A multilayer cost model for metro/core networks," *IEEE/OSA Journal of Optical Communications and Networking*, vol. 5, no. 3, pp. 210-225, 2013.

[127] "Arrayed Waveguide Grating (AWG)," www.ntt-electronics.com.

[128] H. Hasegawa and K. I. Sato, "Large scale optical cross-connect: Architecture, performance analysis, and feasibility demonstration," in *Optical Fiber Communications Conference and Exhibition (OFC)*, Los Angeles, 2015.

[129] J. Wu, S. Subramaniam and H. Hasegawa, "Comparison of OXC Node Architectures for WDM and Flex-Grid Optical Networks," in *International Conference on Computer Communication and Networks (ICCCN)*, Las Vegas, 2015.

[130] JDS Uniphase, "WDM, Filter, 200 GHz, ITU Component DWS Series," www.oequest.com/getproduct/18257/cat/1633/page/1.

[131] "1x32 PLC Fiber Splitter, Splice/Pigtailed ABS Module, 3.0mm, SC/APC," www.fs.com/products/48464.html.

[132] "1x2 Opto-Mechanical Optical Switches," www.fs.com/products/14376.html.

[133] "2x2 Opto-Mechanical Optical Switches," www.fs.com/products/14380.html.

[134] "24-Channel, C-Band 100 GHz Multiplexer," www.oequest.com/getproduct/18697/cat/1337/page/1.

[135] B. Glance, "Polarization independent coherent optical receiver," *IEEE Journal of Lightwave Technology*, vol. 5, no. 2, pp. 274-276, 1987.

[136] N. McKeown et al., "OpenFlow: enabling innovation in campus networks," *ACM SIGCOMM Computer Communication Review*, vol. 38, no. 2, pp. 69-74, 2018.

[137] S. Spadaro, A. Pagès, J. Perelló and F. Agraz, "Virtual Slices Allocation in Multi-tenant Data Centre Architectures Based on Optical technologies and SDN," in *Asia Communications and Photonics Conference*, Hong Kong, 2015.

[138] H. ZANG, et al., "A review of routing and wavelength assignment approaches for wavelength-routed optical WDM networks," *Optical networks magazine*, vol. 1, no. 1, pp. 47-60, 2000.

[139] B. Jaumard, C. Meyer, B. Thiongane and X. Yu, “ILP formulations and optimal solutions for the RWA problem,” in *IEEE Global Telecommunications Conference,* Dallas, 2004.

[140] H. Choo, V. Shakhov and B. Mukherjee, “Routing and wavelength assignment in optical WDM networks with maximum quantity of edge disjoint paths,” *Photonic Network Communications,* vol. 12, no. 2, p. 145–152, 2006.

[141] R. Ramaswami and K. Sivarajan, “Routing and Wavelength Assignment in All-Optical Networks,” *IEEE/ACM Transactions On Networking,* vol. 3, no. 5, pp. 489-500, 1995.

[142] K. Christodoulopoulos, I. Tomkos and E. A. Varvarigos, “Elastic bandwidth allocation in flexible OFDM-based optical networks,” *IEEE Journal of Lightwave Technology,* vol. 29, no. 9, pp. 1354-1366, 2011.

[143] Jin Y. Yen, “Finding the K Shortest Loopless Paths in a Network,” *Management Science,* vol. 17, no. 11, pp. 712-716, 1971.

[144] M. Klinkowski and K. Walkowiak, “Routing and spectrum assignment in spectrum sliced elastic optical path network,” *IEEE Communications Letters,* vol. 15, no. 8, pp. 884-886, 11.

[145] P. P. Marino, Optimization of computer networks: modeling and algorithms: a hands-on approach, John Wiley & Sons, 2016.

[146] K. Christodoulopoulos, I. Tomkos and E. A. Varvarigos, “Elastic Bandwidth Allocation in Flexible OFDM-Based Optical Networks,” *IEEE Journal of Lightwave Technology,* vol. 29, no. 9, pp. 1354-1366, 2011.

[147] M. Klinkowski and K. Walkowiak, “Routing and Spectrum Assignment in Spectrum Sliced Elastic Optical Path Network,” *IEEE Communications Letters,* vol. 15, no. 8, pp. 884-886, 2011.

[148] R. Ramaswami, K. N. Sivarajan, and G. H. Sasaki, Optical networks: a practical perspective, Burlington: Morgan Kaufmann, 2009.

[149] E. Palkopoulou, G. Bosco, A. Carena, D. Klonidis, P. Poggiolini and I. Tomkos, “Nyquist-WDM-Based Flexible Optical Networks: Exploring Physical Layer Design Parameters,” *IEEE Journal of Lightwave Technology,* vol. 31, no. 14, pp. 2332-2339, 2013.

[150] B. C. Chatterjee, S. Ba and E. Oki, “Fragmentation Problems and Management Approaches in Elastic Optical Networks: A Survey,” *IEEE Communications Surveys & Tutorials,* vol. 20, no. 1, pp. 183-210, 2018.

[151] B. C. Chatterjee, S. Ba and E. Oki, “Fragmentation Problems and Management Approaches in Elastic Optical Networks: A Survey,” *IEEE Communications Surveys & Tutorials,* vol. 20, no. 1, pp. 183-210, 2018.

[152] G. Chauvel, “Dispersion in optical fibers,” Anritsu Corporation, 2008.

[153] X. Wang, K. Kuang, S. Wang, S. Xu, H. Liu and G. N. Liu, “Dynamic routing and spectrum allocation in elastic optical networks with mixed line rates,” *IEEE/OSA Journal of Optical Communications and Networking,* vol. 6, no. 112, pp. 1115-1127, 2014.

[154] Seb J. Savory, Giancarlo Gavioli, Robert I. Killey and Polina Bayvel, “Electronic compensation of chromatic dispersion using a digital coherent receive,” *Optics Express,* vol. 15, no. 5, pp. 2120-2126, 2007.

[155] A. Saljoghei, A. Farhang, C. Browning, N. Marchetti, L. E. Doyle and L. Barry, “Investigation of the performance of GFDMA and OFDMA for spectrally efficient broadband PONs,” in *Optical Fiber Communications Conference and Exhibition (OFC),* Los Angeles, 2017.

[156] A. Delmade et al., “Performance analysis of optical front-hauling for 5G Waveforms,” in *Conference on Lasers and Electro-Optics Europe & European Quantum Electronics Conference (CLEO/Europe-EQEC),* Munich, 2017.

[157] J. Zhang et al., “Full-Duplex Quasi-Gapless Carrier Aggregation Using FBMC in Centralized Radio-Over-Fiber Heterogeneous Networks,” *IEEE Journal of Lightwave Technology,* vol. 35, no. 4, pp. 989-996, 2017.

[158] H. J. Cho et al., “Asynchronous Transmission Using Universal Filtered Multicarrier for Multiservice Applications in 5G Fiber-Wireless Integrated Mobile Fronthaul,” in *Optical Fiber Communications Conference and Exposition (OFC),* San Diego, 2017.

[159] Jun-ichi Kani, Jun Terada, Ken-Ichi Suzuki and Akihiro Otaka, “Solutions for Future Mobile Fronthaul and Access-Network Convergence,” *IEEE Journal of Lightwave Technology,* vol. 35, no. 3, pp. 527-534, 2017.

[160] P. Chanclou, L. A. Neto, K. Grzybowski, Z. Tayq, F. Saliou and N. Genay, “Mobile fronthaul architecture and technologies: A RAN equipment assessment [invited],” *IEEE/OSA Journal of Optical Communications and Networking,* vol. 1, no. A1-A7, p. 10, 2018.

[161] M. Bellanger, “Physical layer for future broadband radio systems,” in *IEEE Radio and Wireless Symposium (RWS),* New Orleans, 2010.

[162] frequency spreading, “FS-FBMC: AN alternative scheme for filter bank based multicarrier transmission,” in *International Symposium on Communications Control and Signal Processing (ISCCSP),* Rome, 2012.

[163] R. Gerzaguet, et al, “The 5G candidate waveform race: a comparison of complexity and performance,” *EURASIP Journal on Wireless Communications and Networking,* vol. 2017, no. 1, pp. 1-13, 2017.

[164] V. Vakilian, T. Wild, F. Schaich, S. ten Brink and J. Frigon, “Universal-filtered multi-carrier technique for wireless systems beyond LTE,” in *IEEE Globecom Workshops (GC Wkshps)*, Atlanta, 2013.

[165] Y. Chen, F. Schaich and T. Wild, “Multiple Access and Waveforms for 5G: IDMA and Universal Filtered Multi-Carrier,” in *IEEE Vehicular Technology Conference (VTC Spring)*, Seoul, 2014.

[166] G. Fettweis, M. Krondorf and S. Bittner, “GFDM - Generalized Frequency Division Multiplexing,” in *IEEE Vehicular Technology Conference*, Barcelona, 2009.

[167] F. Barrami, Y. Le Guennec, E. Novakov, J. Duchamp and P. Busson, “A novel FFT/IFFT size efficient technique to generate real time optical OFDM signals compatible with IM/DD systems,” in *European Microwave Conference*, Nuremberg, 2013.

[168] Seung Hee Han and Jae Hong Lee, “An overview of peak-to-average power ratio reduction techniques for multicarrier transmission,” *IEEE Wireless Communications,* vol. 12, no. 2, pp. pp. 56-65, 2015.

[169] J. J. V. Olmos, J. J. Mohr, S. B. Christensen, K. E. Skouby and J. P. Turkiewicz, “400G Interconnects for Data Centres and High-Performance Computing – What is Next?,” in *International Conference on Transparent Optical Networks (ICTON)*, Bucharest, 2018.

[170] W. Bogaerts, “Scaling up silicon photonics: where are the challenges,” in *Optics S. Workshop*, Laussanne, 2017.

[171] M. I. Olmedo et al., “Multiband Carrierless Amplitude Phase Modulation for High Capacity Optical Data Links,” *IEEE Journal of Lightwave Technology,* vol. 32, no. 4, pp. 798-804, 2014.

[172] G. Im et al., “51.84 Mb/s 16-CAP ATM LAN standard,” *IEEE JSAC,* vol. 13, no. 4, pp. 620-632, 1995.

[173] A. Benjebbour et al., “Concept and practical considerations of non-orthogonal multiple access (NOMA) for future radio access,” in *ISISPCS*, Naha, 2013.

[174] H. Kenichi and B. Anass, “Non-orthogonal multiple access (NOMA) with successive interference cancellation for future radio access,” *IEICE TC,* vol. 98, no. 3, pp. 403-414, 2015.

[175] V. Veeravalli and A. Mantravadi, “The coding-spreading tradeoff in CDMA systems,” *IEEE Journal on Selected Areas in Communications,* vol. 20, no. 2, p. 396–408, 2002.

[176] M. Al-Imari, P. Xiao, M. A. Imran and R. Tafazolli, “Uplink non-orthogonal multiple access for 5G wireless networks,” in *Inter. Symp. Wireless Comm. Syst.*, Barcelona, 2014.

[177] P. Morel, P. Chanclou, R. Brenot, T. Motaweh, M. Guegan and A. Sharaiha, "Experimental demonstration of SOAs optical bandwidth widening based on selective filtering," in *IEEE International Semiconductor Laser Conference*, Kyoto, 2010.

[178] R. Brenot et al., "Quantum dots semiconductor optical amplifier with a-3dB bandwidth of up to 120 nm in semi-cooled operation," in *Conference on Optical Fiber Communication (OFC)*, San Diego, 2008.

[179] M. Huang et al., "Cost-effective 25G APD TO-can/ROSA for 100G applications," in *Optical Fiber Communications Conference and Exhibition (OFC)*, Los Angeles, 2017.

[180] J. Zhang, J. S. Wey, J. Yu, Z. Tu, B. Yang, W. Yang, Y. Guo, X. Huang and Z. Ma, "Symmetrical 50-Gb/s/λ PAM-4 TDM-PON in O-band with DSP and Semiconductor Optical Amplifier Supporting PR-30 Link Loss," in *Optical Fiber Communication Conference (OFC)*, San Diego, 2018.

[181] C. Caillaud et al., "Integrated SOA-PIN Detector for High-Speed Short Reach Applications," *IEEE Journal of Lightwave Technology*, vol. 33, no. 8, pp. 1596-1601, 2015.

[182] M. Tao et al., "Improved Dispersion Tolerance for 50G-PON Downstream Transmission via Receiver-Side Equalization," in *Optical Fiber Communications Conference (OFC)*, San Diego, 2019.

[183] X. Miao, M. Bi, J. Yu, L. Li and W. Hu, "SVM-Modified-FFE Enabled Chirp Management for 10G DML-Based 50Gb/s/λ PAM4 IM-DD PON," in *Optical Fiber Communications Conference (OFC)*, San Diego, 2019.

[184] G. Son et al., "High-efficiency broadband light coupling between optical fibers and photonic integrated circuits," *Nanophotonics*, vol. 7, no. 12, pp. 1845-1864, 2018.

[185] D. Rosendo, et al., "A methodology to assess the availability of next-generation data centers," *The Journal of Supercomputing*, pp. 1-25, 2019.

[186] A. J. Zilkie et al., "Multi-Micron Silicon Photonics Platform for Highly Manufacturable and Versatile Photonic Integrated Circuits," *IEEE Journal of Selected Topics in Quantum Electronics*, vol. 25, no. 5, pp. 1-13, 2019.

[187] M. He, et al., "High-performance hybrid silicon and lithium niobate Mach–Zehnder modulators for 100 Gbit/s and beyond," *Nature Photonics*, vol. 13, no. 5, pp. 359-364, 2019.

[188] V. Sipal, J. Gelabert, C. J. Stevens, B. Allen and D. J. Edwards, "Adaptive OFDM for Wireless Interconnect in Confined Enclosures," *IEEE Wireless Communications Letters*, vol. 2, no. 5, pp. 507-510, 2013.

[189] X. Tang, J. Zhou, M. Guo, J. Qi, F. Hu, Y. Qiao, Y. Lu, "40-Gb/s PAM4 with low-complexity equalizers for next-generation PON systems," *Optical Fiber Technology,* vol. 40, pp. 08-113, 2018.

[190] J. Gao, "Demonstration of the first 29dB Power Budget of 25Gb/s 4-PAM System without Optical Amlifier for Next Generation Access Network," in *Optical Fiber Communications Conference (OFC),* Anaheim, 2016.

[191] S. D. Le, A. Lebreton, F. Saliou, Q. Deniel, B. Charbonier and P. Chanclou, "Up to 60 km bidirectional transmission of a 16 channels × 10 Gb/s FDM-WDM PON based on self-seeded reflective semiconductor optical amplifiers," in *Optical Fiber Communication Conference (OFC),* San Francisco, 2014.

[192] David Smalley, "Equalization Concepts: A Tutorial," Application Report," Texas Instruments, 1994.

[193] S. Soerensen, "Optical beat noise suppression and power equalization in subcarrier multiple access passive optical networks by downstream feedback," *IEEE Journal of Lightwave Technology,* vol. 18, no. 10, pp. 1337-1347, 2000.

[194] C. Desem, "Optical interference in subcarrier multiplexed systems with multiple optical carriers," *IEEE Journal on Selected Areas in Communications,* vol. 8, no. 7, pp. 1290-1295, 1990.

[195] C. Chang, "Interference of multiple optical carriers in subcarrier-multiplexed systems," *IEEE Photonics Technology Letters,* vol. 5, no. 7, pp. 848-850, 1993.